Analysis and Mitigation of Asynchronous Interference in Coordinated Multipoint Systems

by

Ahmed Mohamed Hamza Abouelenin

A thesis
presented to the University of Waterloo
in fulfillment of the
thesis requirement for the degree of
Doctor of Philosophy
in
Electrical and Computer Engineering

Waterloo, Ontario, Canada, 2015

I hereby declare that I am the sole author of this thesis. This is a true copy of the thesis, including any required final revisions, as accepted by my examiners.

I understand that my thesis may be made electronically available to the public.

Abstract

Next generation cellular wireless networks need to achieve both high peak and average data rates. Also, they need to improve the fairness by providing more homogenous quality of service distribution over the entire cell area. Base station (BS) cooperation is one of the techniques which is used to achieve these requirements, especially the fairness requirement. It is able not only to mitigate inter-cell interference, but also to exploit this interference and to use it as a useful signal.

Although BS cooperation or what is called coordinated multipoint (CoMP) communications proves that it can achieve high gains in theory, there are some challenges that need to be solved in order for it to be widely deployed. One of the major challenges which prevents the CoMP concept from being widely deployed in new cellular systems is timing synchronization. This problem is particularly challenging when OFDM is employed which is the case in the uplink (UL) and downlink (DL) of WiMAX systems and in the DL of LTE systems. The problem is inherited from the limitations caused by integer time offsets in OFDM systems. In order to achieve the gains promised by CoMP systems, the user equipments' (UEs) signals in UL or the BSs signals in DL should be synchronized such that the time difference of arrivals do not exceed the cyclic prefix length of the transmitted signals.

In this thesis, we first provide a detailed mathematical analysis of the impact of integer time offsets on the performance of single-input-single-output (SISO) OFDM systems. In particular, closed-form expressions for the different types of interference caused by the integer time offset are derived. Furthermore, we derive exact closed-form expressions for the bit error rate (BER) and the symbol error rate (SER) of BPSK, QPSK and 16-QAM modulation for transmission over both AWGN and Rayleigh fading channels. The effect of the fractional carrier frequency offset (CFO) is taken into consideration in the derivations. For OFDM systems with a large number of subcarriers, an approximate method for evaluating the BER/SER is given.

Next, we generalized our expressions to be suitable for the single-input-multiple-output (SIMO) OFDM systems. The derived closed-form expressions for the interference and probability of error enabled us to investigate the timing synchronization problem of UL CoMP systems, where it is not possible for a UE to be synchronized to more than one BS at the same time. This synchronization problem imposes an upper limit on the percentage of cooperation which could occur in an UL CoMP system. By using geometrical and analytical approaches, we define this upper bound. Moreover, an MMSE-based receiver that mitigates the unavoidable asynchronous interference is proposed. Furthermore, a simple joint channel

and delay estimation block is incorporated into the receiver to examine its performance with estimation errors. Finally, an iterative procedure is suggested to reduce the complexity of the proposed mitigation method. Numerical results are provided to show the accuracy of the derived expressions and the robustness of the proposed mitigation method.

Acknowledgements

I am profoundly indebted to my supervisor, Professor Jon W. Mark. There are no words that can express my sincere gratitude to him. I consider myself extremely lucky to have a supervisor who cared so much not only about my work, but also about my personal life. Without his patient guidance and continuous encouragement, I could never finish this work. For me, he is not only a supervisor, but also a lifetime advisor.

I would also like to thank Professor Xuemin (Sherman) Shen, Professor Essam Sourour and Professor Amir Khandani for their continuous help and support throughout the time I spent in my PhD. Special thanks go also to the members of my examining committee, Professor Steven Blostein, Professor En-Hui Yang, Professor Zhou Wang, and Professor Raouf Boutaba for their time, efforts, valuable comments and suggestions.

I am grateful to all the members of the Broadband and Communications Research (BBCR) group for their assistance. My sincere thanks to Samat Shabdanov, Ning Zhang, Ahmed Medra, Hassan Omar, Md Shamsul Alam, Mohamed Ismail, Yujie Tang and Sanaa Taha for their great help and support. Furthermore, I gratefully acknowledge the financial support from Natural Science and Engineering Research Council (NSERC) of Canada and University of Waterloo Graduate Scholarships.

Finally, I would like to thank my parents, my wife, my brother, my sister, my uncle Gaber Metwally and my parents in-law for their unconditional love and support which gave me the strength to complete this work. Also, I would like to thank all my friends in Canada, especially Mostafa Adel, Ahmed Gawish, Hussein Attia, Tamer Mostafa, Usama Shahdah, Ahmed Khairy, Mohamed Abouzahra, Mohamed Yousry, Mohamed Feteiha, Aboelsood Zidan, Ayman Bahgat, Khaled Ammar, Mohamed Galal, Ahmed Kamal, Mohamed Essam, Mohammad Abuleil, and Aijaz Baig, and all my friends in Egypt, especially Ahmed Shalaby, Ahmed Abdelhamid, Mohamed Hanbl, Mostafa Gaber, Ahmed Raafat, Ramy Omar, Ayman Salama, Ashraf El-Antably, Hossam Mahmoud, Yousry Kamal, and Mohamed Zakria.

Dedication

To Allah, the Most Merciful, the Most Compassionate.
To My Parents, Mohamed Hamza and Mahasen Metwally.
To My Wife, Marwa El-Haddad.

Table of Contents

List of Tables

List of Figures

List of Abbreviations

2D	Two-dimensional
ADSL	Asymmetric digital subscriber line
APE	Average probability of error
AWGN	Additive white Gaussian noise
BER	Bit error rate
BPSK	Binary phase-shift keying
BS	Base station
CB	Coordinated beamforming
CFO	Carrier frequency offset
CFR	Channel frequency response
CHF	Characteristic function
CIR	Channel impulse response
CoMP	Coordinated multipoint
CP	Cyclic prefix
CS	Coordinated scheduling
CSI	Channel state information
D2D	Device-to-device
DFT	Discrete Fourier transform
DL	Downlink
DPS	Dynamic point selection
EGC	Equal-gain combining
eICIC	Enhanced inter-cell interference cancelation
FD	Full-dimension
FDD	Frequency-division duplexing
FFT	Fast Fourier transform

GA	Gaussian approximation
GSM	Global system for mobility
HetNets	Heterogeneous networks
IBI	Inter-block interference
ICI	Inter-carrier interference
ISI	Inter-symbol interference
JP	Joint processing
JR	Joint reception
JT	Joint transmission
LTE	Long-Term Evolution
LTE-A	Long-Term Evolution Advanced
M2M	Machine-to-machine
MIMO	Multiple-input-multiple-output
MMSE	Minimum mean square error
MRC	Maximal-ratio combining
MTC	Machine-type communication
MUI	Multiple user interference
NCT	New carrier type
OFDM	Orthogonal frequency-division multiplexing
PDF	Probability density function
PRACH	Physical random access channel
QAM	Quadrature amplitude modulation
QMR	Quasi-minimal residual
QPSK	Quadrature phase-shift keying
RRH	Remote radio head
SER	Symbol error rate
SIMO	Single-input-multiple-output
SINR	Signal-to-interference-plus-noise-ratio
SISO	Single-input-single-output
SNR	Signal-to-noise-ratio
SON	Self-organizing networks
STC	Space-time coding
TA	Time advance

TDD	Time-division duplexing
TDOA	Time difference of arrival
UE	User equipment
UL	Uplink
UTRA	Universal terrestrial radio access
ZC	Zadoff-Chu

List of Symbols

b	BS index
$\boldsymbol{b}$	Vector of all IBI/ISI from all users
B	Number of BSs
c	Speed of light (3×10^8 m/s)
CF	Correction factor
$\boldsymbol{C}_h$	Time-domain channel covariance matrix
$C_K(l)$	ICI coefficients
d_0	Reference distance
$d_{b,u}$	Distance between UE u and BS b
D_s	A square in the complex plane
$\mathbf{e}$	Binary representation of a number where zeros are replaced by -1s.
E_b	Energy per bit
E_s	Energy per symbol.
$f(n)$	ZC samples in time domain
$F(K)$	ZC samples in frequency domain
$\mathbf{F}_L$	First L columns of the unitary FFT matrix
$G_K(l)$	IBI coefficients
$h(l)$	Channel impulse response
I	Identity matrix
$\boldsymbol{J}_N$	Row vector of all ones of size N
K	Subcarrier index
l	Path delay (samples)
L	Number of channel taps
m	Symbol index
n	Sample index

N	Number of OFDM subcarriers
N_0	Noise power spectral density
N_a	Number of used coefficients
N_{CP}	Number of cyclic prefix samples
N_{CS}	Number of samples of the cyclic shift
N_s	ZC sequence length
N_T	Symbol size
P_c	Probability of correct decision
P_e	Bit error rate
P_s	Symbol error rate
$Q(\cdot)$	Q-function
r	ZC root sequence index
$r(n)$	Received samples in time domain
R	Cell Radius
$R(K)$	Received samples in frequency domain
$\mathcal{R}(K)$	Noise-free received signal
S_K	Vector of the concatenated ICI and IBI coefficients
t	Peak index
T_{CP}	CP period
T_s	Sampling Time
u	UE index
U	Number of UEs
$V(K)$	Asynchronous interference samples in frequency domain
$w(n)$	AWGN samples in time domain
$W(K)$	AWGN samples in frequency domain
$\boldsymbol{W}$	Vector of AWGN samples at all the BSs
$x(n)$	Transmitted samples in time domain
$X(K)$	Transmitted samples in frequency domain
$y(n)$	Received OFDM blocks
$\alpha(\theta)$	Attenuation factor that depends on θ
$\delta(\cdot)$	Dirac delta function
ϵ	Normalized frequency offset
η	SNR (dB)

$\bar{\eta}_s$	Average energy per symbol to noise spectral density ratio
$\gamma(n)$	Rectangular window in time domain
$\Gamma(K)$	Rectangular window in frequency domain
$\lambda(K)$	Channel frequency response
$\psi^{b,u}$	Distance-dependent path loss of the link between BS b and UE u
σ^2	AWGN variance
σ_R^2	Variance per dimension
σ_V^2	Asynchronous interference variance
$\sigma_{W,b}^2$	Noise variance at BS b
τ	Maximum delay spread
$(\tau_{\mathbf{max}}^{b,u})$	Maximum delay spread of the link between UE u and BS b
$\tau_{\mathbf{max}}^{\mathbf{exp}}$	Maximum expected delay spread
θ	Integer time offset (samples)
υ	Path loss exponent
φ	Characteristic function
$\Re(\cdot)$	Real part
$\Im(\cdot)$	Imaginary part
$E(\cdot)$	Expectation operation
$\max(\cdot)$	Maximum operation
$\min(\cdot)$	Minimum operation
$(\cdot)_N$	Modulo N operation
$(\cdot)^*$	Complex conjugate operation
$(\cdot)^H$	Hermitian transpose operation
$(\cdot)^T$	Transpose operation
$\otimes$	Circular convolution operation
$\circ$	Hadamard product
$\lvert \cdot \rvert$	Magnitude operation

Chapter 1

Introduction

1.1 Beyond 4G Cellular Networks

There is a huge growth in the mobile traffic volume and data rates that need to be supported by next generation of wireless cellular networks. This growth is driven by the increase of number of users and the evolution of new applications like the internet of things, gigabit wireless connectivity, and tactile internet [1]. Some expectations for this growth are as follows: by 2016, the number of wireless network users in general is expected to be 4 billion [2] and by 2018 the number of 4G cellular network users is expected to be 2 billion [3]. In addition to that, it is anticipated that large number of devices will connect to the wireless networks due to the development of machine-to-machine (M2M) applications, which are expected to be 100 times the number of cellular users [4]. This leads to the prediction of a total of 50 billion connected devices [5] and 1000-fold increase in the traffic volume by 2020 [6].

New technologies are adopted in the current 4G cellular systems to cope with these needs. Examples of these techniques are advanced multiple-input-multiple-output (MIMO) techniques, carrier aggregation, relay nodes, and self-organizing networks (SON) [7,8]. Other techniques which are considered as promising to beyond 4G systems are small-cell deployments, device-to-device (D2D) communication, machine-type communication (MTC), new carrier type (NCT), full-dimension MIMO (FD MIMO), and enhanced inter-cell interference cancelation (eICIC) for heterogeneous networks (HetNets) [2, 9]. Furthermore, working in higher frequency bands is a target for upcoming cellular standards. Fig.1.1 shows some of these technologies which are employed by different releases of LTE and LTE-A standards [2]. These technologies aim to satisfy several requirements such as in-

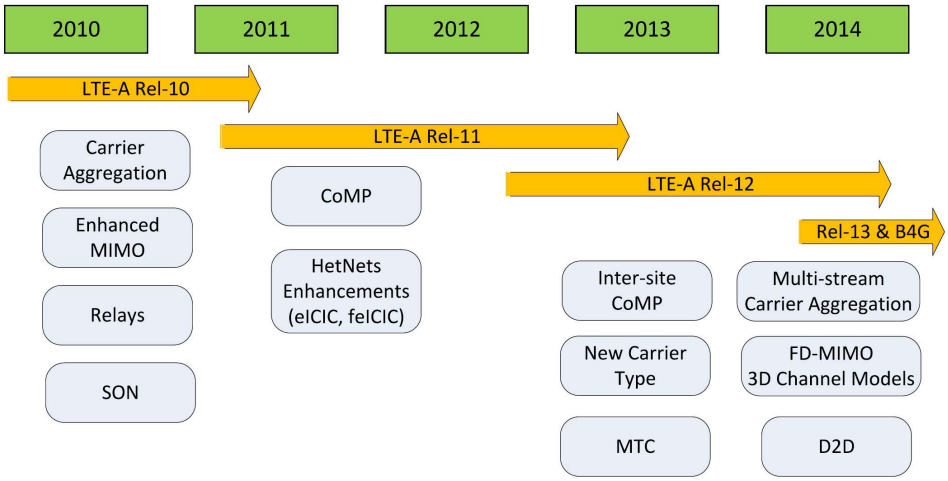

Figure 1.1: Technologies adopted by LTE and LTE-A standards [2].

creasing capacity, decreasing power consumption, supporting different traffic types, and lowering cost [4, 10].

In current cellular networks, interference is the major capacity limiting factor [11] where full frequency reuse is employed. BS cooperation which is referred to in LTE and LTE-A context as coordinated multipoint (CoMP), is a key technology to mitigate this limitation [12,13]. CoMP is a technique where BSs cooperate and/or coordinate to suppress or cancel the inter-cell interference. It is considered as one of the core technologies of 4G systems and it is expected that it will continue as a promising candidate for the next-generation of cellular systems (5G) [14]. The main advantages of CoMP are to enhance coverage, throughput at cell edges, and spectral efficiency [15, 16] where the spectral efficiency of point-to-point links in cellular networks is close to its upper theoretical bound [17].

BS cooperation can be divided, in general, into two categories: interference coordination and joint processing (JP) cooperation [18, 19]. In the former type, the BSs share channel state information (CSI) of the links connecting them to the users in order to coordinate decisions such as scheduling and beamforming, where in JP the BSs share users' data in addition to CSI [20]. JP aims to exploit the interference instead of mitigating it by generalizing the multiple-user MIMO techniques to multiple cells [11]. In doing so, BS cooperation faces numerous practical challenges such as complexity, clustering, channel feedback and backhaul deployments [8, 12, 13].

1.2 Motivation and Research Contributions

1.2.1 Motivation

Although there are great benefits of using CoMP, there are practical challenges that prevent the wide deployment of it and one of these challenges is the timing synchronization requirements [21]. The timing requirement becomes particularly challenging when OFDM is employed, which is the case in the uplink (UL) and downlink (DL) of WiMAX systems and in the DL of LTE systems. Moreover, the timing synchronization requirements need to be satisfied whether in time-division duplexing (TDD) systems such as WiMAX and LTE-TDD or frequency-division duplexing (FDD) systems such as LTE-FDD. In order to achieve the gains promised by CoMP systems, the user equipments' (UEs) signals in UL or the base stations' (BSs) signals in DL should be synchronized such that the time difference of arrivals (TDOAs) do not exceed the cyclic prefix (CP) length of the transmitted signals; otherwise asynchronous interference emerges which degrades the system performance. This limits the areas within a cell which can be covered by cooperation [22]. This motivated us to investigate the limitations imposed by the timing requirements on the CoMP operation.

Conventional methods for timing synchronization and compensation cannot be applied directly to CoMP [19]. For instance, the UEs in an UL CoMP system need to be synchronized to more than one BS. As a result, the common time advance (TA) techniques are not useful, because synchronizing to one BS leads to losing synchronization with others [23]. The problem is more severe in UL than in DL since the CP length in UL should cover TDOAs from larger number of cooperating UEs than the case in DL where the cooperating terminals are BSs [24]. A straightforward solution for this problem is to use CP length that is larger than the expected propagation delays in the system but this will reduce the total throughput of the system. Therefore, this solution is infeasible given that the cell radius can be as large as 100 km in cellular systems [25]. Finding novel processing methods to solve this problem was and still a focus of ongoing research [26]. This motivated us to propose receivers that mitigate the asynchronous interference and solve the timing synchronization problem.

In order to study the effects of asynchronous interference on CoMP operation and to propose new receivers to eliminate it, accurate mathematical model for MIMO OFDM systems with time offsets needs to be derived. The survey in Chapter 2 indicates that there was a gap in this area even for single-input-single-output OFDM systems. For instance, to the best of our knowledge, there is neither exact closed-form mathematical model in frequency domain for single-input-single-output (SISO) OFDM systems with time offset nor exact closed-form expressions for the probability of error for these systems. As a step

to derive the mathematical model required to study the CoMP, this gap needs to be filled first. In addition to that, characterizing the performance of SISO OFDM systems with time offsets helps in evaluating the performance of other systems that suffer from the same synchronization problem such as asymmetric digital subscriber line (ADSL) modems [27]. This motivated us to derive exact closed-form mathematical models and expressions for the probability of error for the SISO, SIMO, and MIMO OFDM systems with time offsets.

1.2.2 Research Contributions

Our research objective was to investigate the unavoidable timing synchronization problem in CoMP systems and to propose solutions to mitigate the asynchronous interference that results from it. This led us to that we need first to characterize the asynchronous interference and to find probability of error expressions for SISO OFDM systems. Therefore, our main contributions are summarized as follows.

- Generalized result for the useful integral of the product of two Gaussian functions over the Rayleigh distribution was derived in Chapter 3 [28]. The main application of this integral is finding the probability of error for quadrature modulations in Rayleigh fading channels [29]. Closed-form solutions for this integral can be found in [29, eq. 5], [30, eq. 6.287.3], and [31, eq. 4]. A detailed derivation of this integral can be found in [29], and a simpler one can be found in [31]. The final results in all these works are not valid in case the arguments of the Q-functions are negative, which sometimes is the case when evaluating the probability of error for OFDM systems with integer time or large frequency offsets in Rayleigh fading channels. In our work, we have provided a new result for the integral which can be used in case the arguments of the Q-functions are positive and/or negative.

- Closed-form mathematical model that fully characterizes the asynchronous interference in frequency domain for transmission over AWGN and Rayleigh fading channels are derived in Chapter 3 and Chapter 4 [32]. This mathematical model was needed to derive the BER/SER expressions and to propose receivers that are able to mitigate this interference. While frequency and fractional timing offsets introduce inter-carrier interference (ICI) only, integer timing offsets introduce, in addition to the ICI, inter-block interference (IBI); in frequency-selective fading channels they also introduce inter-symbol interference (ISI). In our work, we have provided closed-form expressions for these different types of interference.

- Exact expressions for the SER of QPSK and 16-QAM OFDM systems with CFO for transmission over frequency-selective fading channels are derived in Chapter 4 [28]. Also, an extended result for the SER of QPSK OFDM with frequency offset in Rayleigh flat fading channels that is valid for any frequency offset is given. The authors in [33] derived closed-form expressions for the probability of error for BPSK in AWGN, flat and frequency-selective fading channels. Also, they provide expressions for the QPSK but for the AWGN and flat fading channels only. One drawback of the expressions derived in [33] for fading channels is that they are valid only for small normalized frequency offsets.

- Exact expressions for the BER/SER of OFDM systems with integer time offsets are derived in Chapter 3 and Chapter 4 [32]. When evaluating the probability of error for OFDM systems with timing offsets, the existing works either use simulation, approximate expressions, or study only the fractional timing offset case. Therefore, we filled this gap by deriving the exact closed-form expressions for these systems. These expressions can be used to evaluate the performance of systems with insufficient CP or when the time offset is unavoidable like ADSL modems.

- Exact closed-form expressions for the probability of error for SIMO OFDM systems with integer time offsets are derived in Chapter 5 [34]. The expressions are for both equal-gain combining (EGC) and maximal-ratio combining (MRC) receivers. These expressions are needed to investigate the performance limitations of CoMP systems that suffer from timing synchronization problem.

- An upper bound for the percentage of areas that can be covered by BS cooperation in UL is provided through geometrical and analytical approaches in Chapter 5 [34, 35]. The upper bound is general for any number of BSs, and is not limited to symmetrical scenarios where users have the same distances from the corresponding BSs. This upper bound gives an insight about the limitations and constraints imposed by the timing synchronization problem in CoMP systems.

- An MMSE-based receiver that mitigates the asynchronous interference is proposed in Chapter 6 [23, 34]. This receiver is solving the timing problem in CoMP since it does not put any restrictions on the length of cell radius or the range of propagation delays from the UEs to the BSs. Unlike the existing works, the proposed receiver does not need iterative procedure or overlapping fast Fourier transform (FFT) blocks. Also, the effect of imperfect knowledge of delays and CSI on performance is considered. To the best of our knowledge, this is the first time for this effect to be taken into consideration in the open literature.

1.3 Thesis Outline

The rest of this thesis is organized as follows. **Chapter 2** provides a background about CoMP history, categories, challenges, and performance gains. Then a literature review on the general problem of time and frequency offsets in OFDM systems is given. Finally, the chapter discusses the research efforts regarding the timing synchronization problem in CoMP systems and the existing proposed methods to solve it.

In **Chapter 3** and **Chapter 4**, effects of frequency and integer time offsets in SISO OFDM systems are investigated when transmission is over AWGN and Rayleigh fading channels, respectively. The different types of interference that result from these offsets are characterized. Moreover, we derive exact closed-form expressions for the BER/SER of these systems when BPSK, QPSK or 16-QAM modulation is employed. Finally, we propose an approximate method for evaluating the BER/SER when the FFT size is large.

Chapter 5 investigates the limitations and restrictions imposed by the timing synchronization problem in CoMP. Exact BER expressions for SIMO OFDM systems with time offsets are derived. Then using analytical and geometrical approaches, an upper bound to the areas that can benefit from BS cooperation is provided.

In **Chapter 6** an MMSE-based received to mitigate the asynchronous interference in CoMP systems is proposed. Furthermore, the effect of imperfect knowledge of delays and CSI on the performance of proposed receiver is investigated by incorporating a simple joint channel and delay estimation block to the proposed receiver. Moreover, iterative methods to reduce the complexity of the proposed MMSE-based receiver are provided. Finally, numerical results are included to show the exactness of the derived expressions and the robustness of the proposed method.

Chapter 7 summarizes our contributions, draws some concluding remarks from our research and proposes future directions.

Chapter 2

Background and Literature Review

2.1 CoMP

The two building blocks of cooperative cellular networks [36] are cooperative relaying [37] and BS cooperation. In this thesis we focus only on BS cooperation (CoMP). In this section, we provide background about interference management in cellular systems and CoMP history, categories, deployment scenarios, performance gains, and challenges.

2.1.1 CoMP History

The main target of BS cooperation is to mitigate inter-cell interference which has been an obstacle facing cellular communication since its origin. In first cellular generations (2G) such as global system for mobility (GSM), fractional frequency reuse is employed to mitigate this problem, but this led to low spectral utilization [8]. Later, in more recent cellular standards (3G and 4G), full frequency reuse is used to enhance the spectral efficiency [12] but this brings back the inter-cell interference as a limiting factor to the capacity of cellular systems [11]. This was the main motivation behind introducing BS cooperation techniques to new cellular standards.

The concept of BS cooperation originated several decades ago when the macroscopic diversity scheme was used to broadcast the signal of a UE through more than one BS to combat channel fading [11]. Early findings that consider the information-theoretic aspect of uplink BS cooperation [11] can be found in [38, 39] and for DL [40] in [41, 42]. The employment of BS cooperation in cellular standards started by using soft handover in

CDMA cellular communication [43] which can be considered as a basic form of BS cooperation. Simple forms of BS cooperation such as interference randomization, cancelation, and coordination was included in universal terrestrial radio access (UTRA) Release 7 specifications [44]. Also, in releases 8 and 9 which were the official evolution of the LTE standard, there was no advanced interference mitigation schemes and the focus was on interference randomization by scrambling of transmitted signals [3].

It was not until 2008 that advanced schemes of BS cooperation such as joint transmission and reception were suggested to be used in wireless cellular standards [20]. This was part of the efforts towards introducing the LTE-A standard. Nevertheless, this work was not incorporated in the specifications of release 10 of this standard which was completed in 2011 [2]. On the other hand, advanced techniques of BS cooperation were incorporated as an amendment to the WiMAX standard in the same year [45]. Studying advanced techniques of BS cooperation as a part of the LTE-A standard had been resumed in release 11 and it was one of the main work items of this release which had started in September 2011 and finished in December 2012 [18, 46]. The development of these specifications continued in release 12 [2] which was completed in March 2015. New proposals to include more advanced schemes of BS cooperation in future cellular standards (beyond 4G) can be found in [1, 3, 14, 17].

2.1.2 CoMP Categories and Deployment Scenarios

CoMP Categories

BS Cooperation can be classified based on the amount of information that has to be shared among the BSs into the following four categories [11].

- **Interference coordination:** In this category, the BSs share the CSI of links connecting them to the users inside their cells. The sharing of CSI enables the BSs to coordinate their power allocation, beamforming, and scheduling decisions. The data of the users need not to be shared in this mode.
- **MIMO cooperation:** In this category, the BSs share the data of the users in addition to the CSI. The BSs use this information to jointly process the data to and from the users. Instead of just controlling or mitigating the interference in the previous mode (interference coordination), in MIMO cooperation the interference is exploited and used as a useful signal. The disadvantage of this mode is the extra overhead that results from sharing more information among the BSs.

- **Rate-limited MIMO cooperation:** This category is a compromise between the previous two modes. In this category, the CSI is shared first, and then a quantized version of the data of the users is shared. This will decrease the overhead needed for exchanging the information between the BSs, but at the same time, the interference effect will not be eliminated completely.

- **Relay-assisted cooperation:** In this category, relays are used as a part of the backhaul system that connect the BSs. In addition to mitigating the interference, the advantages of using the relays include improving the performance of the direct links between the BSs and users and enlarging the coverage area.

Some of these categories are adopted in cellular standards. For instance, in advanced WiMAX (IEEE 802.16m), two modes are adopted [45]. The first mode is single-BS precoding with multi-BS coordination which includes precoding coordination and interference nulling. This mode corresponds to the interference coordination category mentioned above. The second mode is multi-BS joint processing which includes joint MIMO transmission and/or reception. This mode corresponds to the MIMO cooperation category above. Also, the modes in LTE-A can be categorized as follows [47].

- **Coordinated scheduling/beamforming (CS/CB):** This mode belongs to the interference coordination category. Data transmitted to/from an UE is intended for only the assigned BS but user scheduling, beamforming, and/or precoding decisions are made with coordination with other cooperating BSs.

- **Joint processing (JP):** This mode belongs to the MIMO cooperation category and it is divided into two subcategories

  - Joint transmission/joint reception (JT)/(JR): Data are sent/received simultaneously from multiple cooperating BSs to/from a single or multiple UEs.
  - Dynamic point selection (DPS)/muting: Data is available simultaneously at multiple BSs but it is sent from one BS in a time-frequency resource and this BS can be changed from frame to another.

- **Hybrid category of JP and CS/CB:** Some BSs in the cooperating set use JP while the others use CS/CB.

CoMP Deployment Scenarios

The operation of BS cooperation could be intra-site based or inter-site based. Inter-site cooperation means cooperation among different BSs that are not geographically co-located, while the intra-site is a cooperation among BSs that are geographically co-located such as the cooperation of 3 sectors of one cell. It is clear that inter-site cooperation needs additional backhaul requirements [46]. To evaluate the performance of CoMP within the LTE-A standard, four deployment scenarios are considered as follows [46, 47]. The four scenarios are shown in Fig. 2.1 [18] where eNB is the term used in the LTE standard to refer to a BS.

- **Scenario 1:** Homogeneous network with intra-site CoMP.
- **Scenario 2:** Homogeneous network with inter-site CoMP.
- **Scenario 3:** Heterogeneous network with low power remote radio heads (RRHs) that have different cell IDs (picocells).
- **Scenario 4:** Heterogeneous network with low power RRHs that have the same cell ID.

The second deployment scenario is adopted in our system model for Chapter 5 and Chapter 6.

2.1.3 CoMP Performance Gains

In the standardization efforts of CoMP within the LTE-A, an extensive survey of the performance gains of CoMP is included in [47]. The results focus on the DL since it is harder to evaluate its performance compared to the UL [16]. The evaluation was conducted by more than 20 companies for the 4 deployment scenarios mentioned in the above section [47]. It is worth mentioning that the results reported by different companies indicate some sort of discrepancy in the performance gains due to the different simulations assumptions used to produce each set of results. Assumptions such as modelling of channel estimation errors, scheduling and feedback mechanisms are the main sources of discrepancy [47].

For scenarios 1 and 2 and with BSs with 4 antennas and UEs with 2 antennas, the JT scheme has performance gains in the order of 20-30% and the CS/CB scheme has gain of less than 5% for FDD and approximately 10% for TDD. The performance gains are computed in terms of cell-edge UE spectral efficiency and compared to the single-cell

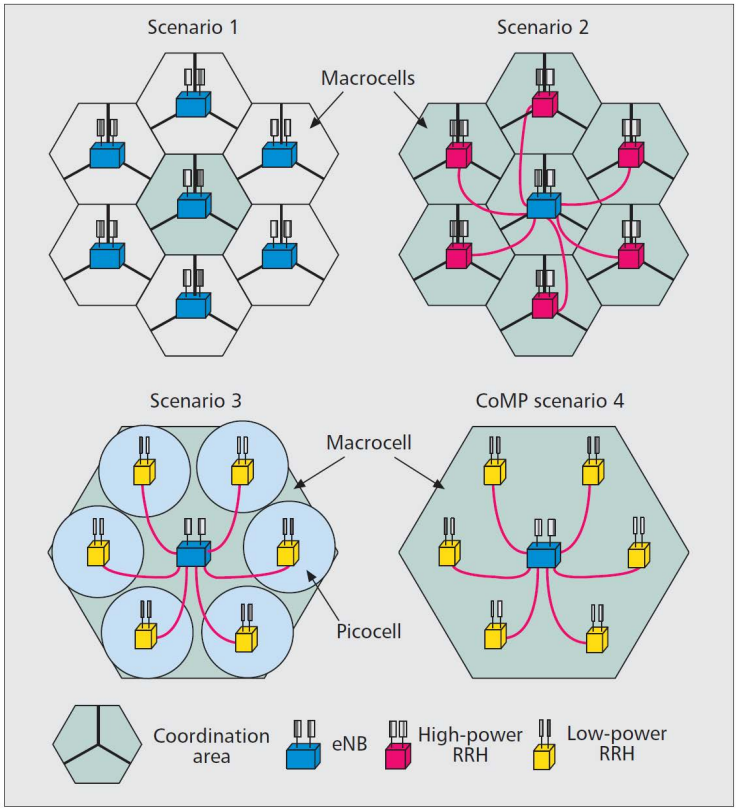

Figure 2.1: CoMP deployment scenarios in LTE-A [18].

multi-user MIMO scheme. For scenarios 3 and 4, both CS/CB and JP schemes have gains in the order of 25-30% compared to the case without interference management [16]. The detailed simulation assumptions and results can be found in [47].

2.1.4 CoMP Challenges

Clustering

To perform multi-cell processing, the BSs must be grouped into clusters and the number of BSs in each cluster must be decided. This number is referred to as the cluster size. This cluster size need to be small due to different reasons [48]. First, the synchronization of users to large number of BSs will be hard. Second, the resources needed to perform multi-cell channel estimation and feedback will increase with increasing the cluster size. Third,

the signaling overhead needed for coordination will increase with increasing the cluster size. On the other hand, large cluster size is better from the perspective of performance, because it reduces the number of cluster-edge users [49]. Therefore, deciding the cluster size is an important factor that needs to be investigated in order to benefit from the multi-cell processing techniques. In [50] and [51] the cluster size is chosen to be in the range of 2 to 7 cells. In [49], simulations results indicate that a small cluster size (about 7 cells) is enough to achieve multi-cell processing gains and at the same time to alleviate the channel feedback overhead. Regardless of the cluster size, there are generally two categories of clustering: fixed clustering and dynamic clustering.

Fixed Clustering In this type, the clusters are predefined according to an easy rule of assignment [48]. In most cases, geographical location is the criteria used to form the clusters [13]. In [52], the authors propose a clustering method based on coordination between a central cell and a number of neighbor rings of cells around this central cell as shown in Fig. 2.2(a). The authors in [53] propose two other methods. The first one is a centralized method, where the cell is divided into 12 sectors and the sectors of the cell are building a cluster and the second one is a distributed method where each cell is divided into 3 sectors and the sectors of 3 neighboring cells are building a cluster as shown in Fig. 2.2(b). The authors in [51] propose a clustering and resource assignment method where each cell is divided into 5 almost equally-sized areas and the resource blocks are also split into 5 equally-sized blocks. The resource blocks are assigned to users according to their location, as illustrated in Fig. 2.2(c). A more robust method is proposed in [49] where users are classified into cluster-interior users that are served by intra-cluster coordination and cluster-edge users which are served by inter-cluster coordination. This method reduces the inter-cluster interference and improves the overall performance.

Dynamic Clustering In this type, the BSs that form a cluster are changing according to change in parameters such as the UE locations or the channel conditions [13]. The performance of this type is better than fixed clustering but this comes at the price of added signaling among the BSs. This signaling is needed to update the clusters [48]. Example of dynamic clustering is the work in [50], where the authors prove that the performance of a dynamic clustering with cluster size equal to two is better than the performance of a fixed clustering with larger cluster sizes (4 to 7 cells). One challenge of dynamic clustering is the cluster size determination problem. Another one is the selection of the cost function that is used to decide which BSs are better to cooperate.

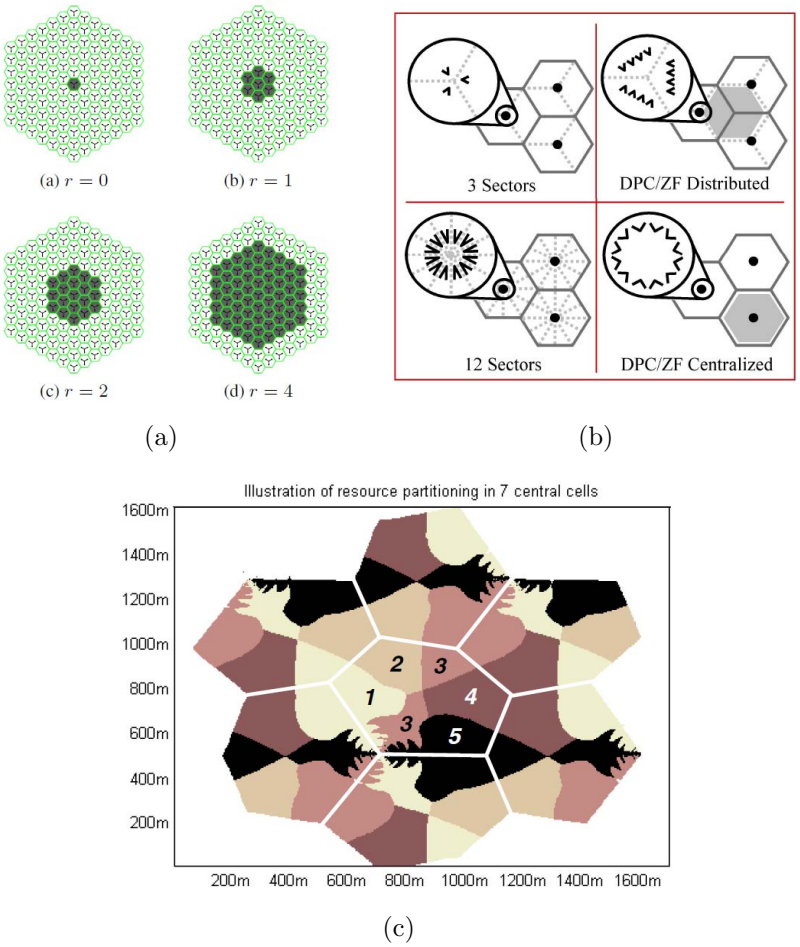

(a) (b)

(c)

Figure 2.2: (a) Cluster of rings [52]; (b) cluster of sectors [53]; (c) cluster of almost equal-size areas [51].

Synchronization

This is another challenge associated with using the multi-cell processing techniques. The cooperating BSs need to be synchronized in time and frequency to avoid ISI and ICI. In the following, we will provide an overview of the existing literature related to the frequency synchronization. The timing synchronization challenge is described in detail in Section 2.3.2.

Frequency Synchronization A frequency synchronization problem takes place in the DL of COMP systems where the BSs jointly cooperate to transmit signals to the mobile stations. The base stations use a precoding matrix which is sent by all the BSs. Due to CFOs between the base stations, the received signals at the UEs suffer from independent time continuous phase shifts which cause performance degradation [54]. This performance becomes worse when the delay of CSI feedback to base stations become larger. This problem can be solved by using expensive oscillators stabilized by GPS signals at the BSs [55]. Another alternative solution proposed in [56] is to perform a preliminary estimation of the BSs' CFOs at the UEs and feedback these estimates to the BSs which use this information in addition to the average channel signal-to-noise ratios in order to final estimate and correct the CFOs at the BSs themselves.

Channel Estimation and Feedback

The next challenge that faces the multi-cell processing techniques is the channel estimation and feedback. The problem associated with channel estimation is threefold problem. First, the multi-cell processing techniques need robust channel estimation methods since the interference cancelation for cell edge users is sensitive to channel estimation errors [13]. Second, it is reported in [57] that the delay between channel estimation and precoding at BSs causes performance degradation. Third, the overhead is large due to increasing the number of used pilots which are needed to perform robust channel estimation.

The channel feedback problem is closely related to the channel estimation problem since increasing the number of channel gains that need to be fed back from the UEs to the BSs due to CoMP operation is consuming more power which is a valuable resource for UEs. Examples of solutions to this problem are that, instead of full feedback of CSI from the UEs to BSs, each UE just feedbacks the precoder index to its assigned BS or the UE feeds back an index representing the closest channel gain to the one it already has been estimated [13]. For more information about the works done to investigate and solve the channel estimation and feedback problem, refer to [48] and the references therein.

Scheduling

The aim of scheduling is to assign system resources efficiently to UEs in order to maximize the performance. Therefore, the multi-cell processing scheduler tasks are resource allocation, decision of which multi-cell processing schemes should be used, power control, choice of precoders and link adaptation [13]. The challenges associated with scheduling are also

threefold [48]. First, the multi-cell processing scheduler should decide when to perform cooperation and when to use conventional transmission (without cooperation) and to be able to perform its functionality in both modes. Second, the scheduler decision must use the least amount of CSI to avoid extra overhead from signaling full CSI. Third, scheduling complexity in CoMP is high so new algorithms should be proposed to minimize the complexity without sacrificing the performance.

Backhaul

The backhaul is the connection between the cooperating BSs and is responsible for exchanging the data, CSI, and control signals among BSs. The backhaul load depends on the cluster size and the used multi-cell processing schemes, and varies from few Mbit/s to a few Gbit/s [13]. The backhaul can be a serious problem if centralized decoding is applied. Therefore, using adaptive centralized/decentralized approach can be a solution [12]. Another problem associated with the backhaul is the latency requirement of multi-cell processing schemes. For example, if CoMP needs to be applied in LTE system, backhaul latency should not exceed 1 ms because of fixed HARQ timing [13]. Also, the performance degradation due to outdated CSI put another latency requirement on the backhaul connection used [12].

2.2 Time and Frequency Offsets in SISO OFDM Systems

Consider an OFDM system with N subcarriers and N_{CP} samples of CP. Let $x_m(n)$ denote the n-th sample of the transmitted OFDM symbol m, where $-N_{CP} \leq n \leq N-1$. The received signal in time domain can be expressed as

$$r(n) = e^{j2\pi\epsilon n/N} \sum_{m} \sum_{l=1}^{L} (h(l) \cdot x_m(n - l - \theta - mN_T)) + w(n), \tag{2.1}$$

where $N_T = N + N_{CP}$ is the OFDM symbol size, ϵ denotes the normalized frequency offset (normalized to the subcarrier spacing), and θ denotes the time offset in samples. $w(n)$ is the AWGN samples and $h(l)$ is the channel impulse response (CIR) with l denotes the path delay in samples and L is the total number of channel taps.

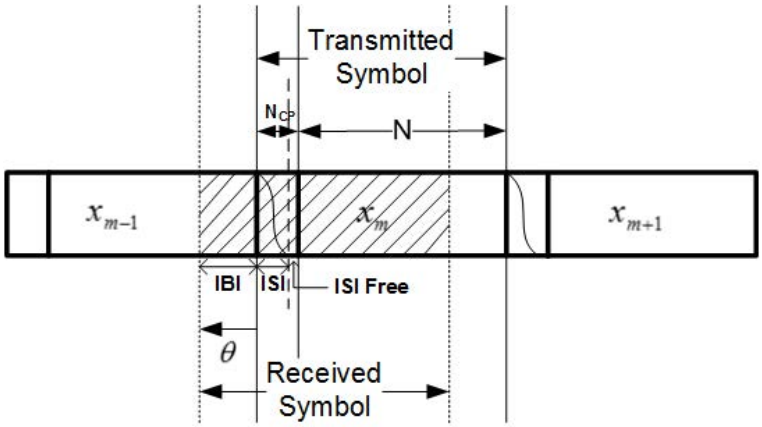

Figure 2.3: Integer time offset in OFDM systems.

2.2.1 Effect of Time Offset in OFDM Systems

Time offsets in OFDM systems could be due to misdetection of the beginning of frame, drifts between the sampling clocks of the transmitter and the receiver, or when the channel delay spread is larger than the CP. There are two types of time offsets: fractional time offset and integer time offset. In this thesis, we will focus only on integer time offset (i.e., it is assumed that the fractional time offset is equal to 0) since many works in the open literature deal with the effect of the fractional time offset.

In this section, the effect of integer time offset, when it is to the left as shown in Fig. 2.3, is considered. We will follow the same convention adopted in [58, 59] and consider that the delay in this case has a negative polarity. In order to study the effect of the time offset, we have to distinguish between three different cases. First case is when the time offset does not exceed the free region which is not affected by inter-symbol interference (ISI) ($-N_{CP} + L - 1 \leq \theta \leq 0$). In this case and assuming $\epsilon = 0$, the received signal in frequency domain is given by

$$R_m(K) = X_m(K)\lambda(K)e^{\frac{j2\pi K\theta}{N}} + W_m(K), \tag{2.2}$$

where $X_m(K)$ is the K-th sample of the Discrete Fourier Transform (DFT) of $x_m(n)$ and $W_m(K)$ is the K-th sample of the DFT of $w_m(n)$, which is the AWGN samples overlapping with OFDM symbol m. $\lambda(K)$ is the channel frequency response (CFR). It can be seen from (2.2) that the timing error is translated into phase shift in frequency domain which can be compensated by channel equalizer [60].

The second case is when the time offset exceeds the free ISI region but still less than the CP length ($-N_{CP} \leq \theta \leq -N_{CP}+L-2$). In this case, the received signal is affected by ISI which results from mixing the successive symbols due to the convolution with the channel. Also, this leads to that the subcarriers lose orthogonality and the signal is affected by ICI as well. The last case is when the time offset is larger than the CP length ($\theta < -N_{CP}$). In this case, in addition to the ISI and ICI, the received signal suffers from IBI which results from that the DFT window includes samples from the previous OFDM symbol. In both the second and third cases, the received signal in frequency domain can be expressed as [60]

$$R_m(K) = \alpha(\theta)\lambda(K) \cdot X_m(K) \cdot e^{\frac{j2\pi K\theta}{N}} + V_m(K) + W_m(K), \tag{2.3}$$

where $\alpha(\theta)$ is an attenuation factor and $V_m(K)$ is an interference term that accounts for the ISI, IBI, and ICI. The attenuation of the symbols can be approximated as shown in (2.4) and the interference term can be modeled as Gaussian noise with power σ_V^2 as shown in (2.5) [61].

$$\alpha(\theta) = \sum_{l=0}^{L-1} |h(l)|^2 \frac{N-\theta_l}{N}. \tag{2.4}$$

$$\sigma_V^2 = \sum_{l=0}^{L-1} |h(l)|^2 \left(2\frac{\theta_l}{N} - \left(\frac{\theta_l}{N}\right)^2\right), \tag{2.5}$$

where

$$\theta_l = \begin{cases} \theta - l, & \theta > l \\ l - N_{CP} - \theta, & 0 < \theta < -(N_{CP} - l) \\ 0, & else. \end{cases} \tag{2.6}$$

From (2.4), it can be concluded that in OFDM systems with large N, the attenuation factor can be neglected. Another note from (2.4) and (2.5) is that both the attenuation factor and the interference term not only depend on the timing error but also they depend on the channel delay profile.

2.2.2 Effect of Frequency Offset in OFDM Systems

Frequency offsets in OFDM systems are usually caused by Doppler shifts due to mobility and/or drifts between the oscillators generating the carrier frequency of the transmitter

and the receiver [33]. There are two types of frequency offset: fractional and integer offsets. In this thesis, only fractional frequency offsets are considered since integer frequency offsets can be estimated and compensated in the acquisition phase of the synchronization task [61].

OFDM has a high spectral efficiency due to subcarriers overlapping in frequency domain, but this causes the OFDM systems to be very sensitive to frequency offsets. Fig.2.4 shows 8 subcarriers of an OFDM symbol with carrier frequency 10 MHz and subcarrier spacing 1 MHz [62]. If the system is perfectly synchronized ($\epsilon = 0$) the zero crossings of the frequency domain sinc pulses coincide and there is no interference (i.e., ICI) among subcarriers. On the other hand, if the frequency offset ($\epsilon > 0$), ICI emerges and the received signal in frequency domain (assuming $\theta = 0$) can be expressed as [63]

$$\begin{aligned} R_m(K) &= \lambda(K) X_m(K) C(0) \\ &\quad + \sum_{u=0, u\neq K}^{N-1} C((u-K)_N) \lambda(u) X_m(u) + W_m(K), \end{aligned} \tag{2.7}$$

where $(\cdot)_N$ is modulo N operation and $C(K)$ are the ICI coefficients which are given by [64]

$$C(K) = \frac{\sin(\pi[K+\epsilon])}{N \sin\left(\frac{\pi[K+\epsilon]}{N}\right)} \exp\{j\pi(1-\frac{1}{N})(K+\epsilon)\}. \tag{2.8}$$

2.2.3 Evaluation Methodologies

In general, two approaches can be used to evaluate the degradation that results from time and/or frequency offsets in OFDM systems. The first approach is to use the loss in signal-to-noise-ratio (SNR) as a measure of this degradation [58–61, 65–67]. For instance, the authors in [59] derived exact signal-to-interference ratio expressions for OFDM systems with time offset. The second approach, which gives different useful insight, is to use the probability of error as the criterion to evaluate this degradation, and this can be found in [28, 33, 64, 68–73].

For OFDM systems with frequency offset, the authors in [74] use Gaussian approximation of the ICI to evaluate the probability of error and they conclude that this approximation is valid only at low SNRs. Also, the authors in [63] use the Gaussian approximation of ICI but for evaluating the performance in multi-path fading channels. A more accurate method that uses the characteristic function and the Beaulieu series to obtain exact analysis for the probability of error is derived in [64] but this method needs the computation

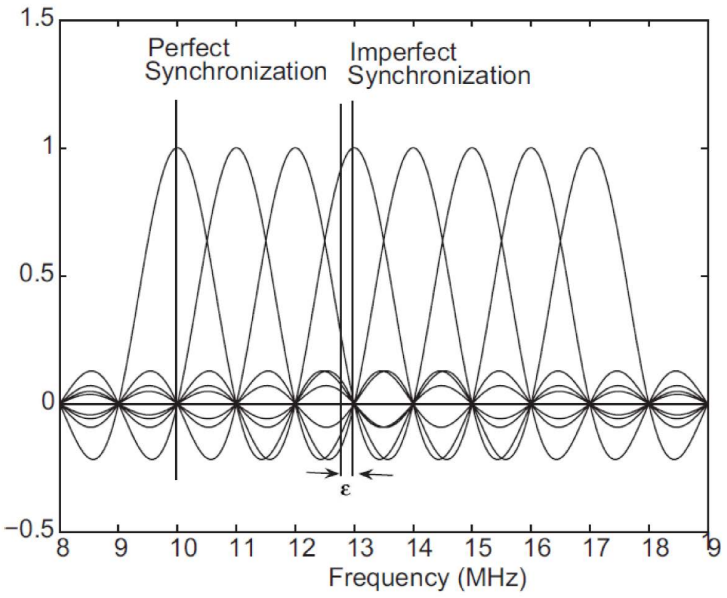

Figure 2.4: Fractional frequency offset in OFDM systems [62].

of infinite series. Exact closed-form expressions for the probability of error are derived recently in [33]. The authors give expressions for the probability of error for BPSK in AWGN, flat and frequency-selective fading channels. Also, they provide expressions for the QPSK but for the AWGN and flat fading channels only. One drawback of the expressions derived in [33] for fading channels is that they are valid only for small normalized frequency offsets. The authors in [70] extended the results in [33] for the BPSK case to be valid for any frequency offset. Also, the authors in [75] provide expression for evaluating the probability of error for 16-QAM modulation for transmission over AWGN. Therefore, exact closed-form expressions for evaluating the SER of QPSK and 16-QAM OFDM in Rayleigh frequency-selective fading channels need to be derived. Moreover, the expression in [33] for QPSK in Rayleigh flat fading channels need to be generalized in order to be valid for any frequency offset.

On the other hand, for OFDM systems with time offset, a simulation study is provided in [71] to investigate the BER performance degradation due to time synchronization errors. Probability of error for OFDM systems with fractional time offsets is studied in [72] and [73]. For instance, the authors in [73] derive an exact closed-form expression for the BER of OFDM systems with residual time offsets. In [76], the authors give an approximate expression for the BER of uplink OFDMA systems with integer time offsets

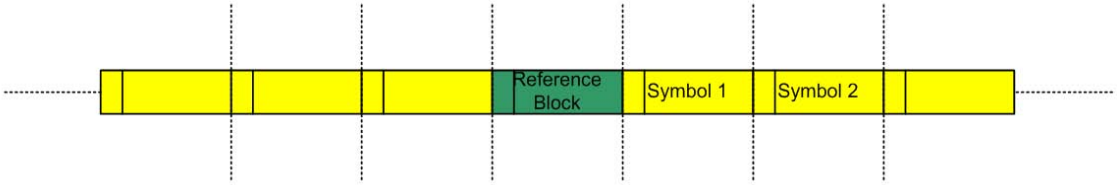

Figure 2.5: Initial timing synchronization by searching for a reference block inside the frame.

in Rician fading channels. Also, the authors in [69] evaluate the effect of integer time offsets in OFDM systems using test statistics and employing approximate expressions for the BER by considering the interference component as a Gaussian random variable. Several studies have shown that approximating the interference as a Gaussian random variable is inaccurate [74, 77, 78], especially at high SNRs. In a nutshell, when evaluating the probability of error for OFDM systems with time offset, the existing works either use simulation, approximate expressions, or study only the fractional time offset case.

2.3 Timing Synchronization in Cellular and CoMP Systems

2.3.1 Timing Synchronization in Cellular Systems

In cellular communications, the normal way of synchronizing UEs to BSs is a two-stage process. In the first step, the BS broadcasts the DL sub-frame to all the UEs in the cell and each UE tries to find the start of the DL sub-frame to be able to synchronize to the BS. Usually this step is accomplished in new wireless standards as shown in Fig. 2.5 by searching for a special pattern (reference block) in the transmitted frame like the preamble in WiMAX or synchronization signals in LTE. This step is implemented once at the beginning of the connection and it is called the initial timing synchronization. The other task of initial synchronization is a rough estimation of the start of OFDM symbols in order to be able to feed them into the FFT processing block to perform the DFT operation which is needed by subsequent blocks such as channel estimation and equalization.

In the second stage, and after knowing the start of the DL sub-frame in the first stage, the UEs start sending their UL sub-frames after the end of reception of the DL sub-frame. The BS will receive these UL sub-frames and send a TA command to each UE to adjust

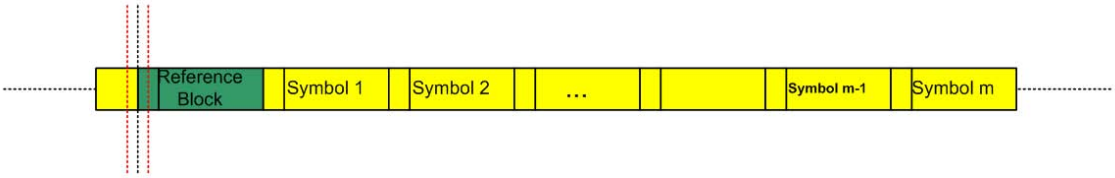

Figure 2.6: Fine timing synchronization to track small time offsets.

its transmission time in order to be received at the expected time. The UE will keep synchronized to the BS by fine tracking the changes of the arrival of the start of the frame; this process is referred to as fine timing synchronization as shown in Fig. 2.6. These slight changes in the arrival of the start of the frame may occur due to mobility or difference between sampling clocks in the transmitter and the receiver.

2.3.2 Timing Synchronization in OFDM CoMP Systems

To illustrate the synchronization problem in CoMP, let us assume that BS1 and BS2 in Fig. 2.7 cooperate to jointly decode the UEs' signals in their cells. The two BSs are synchronized and they begin to transmit their DL signals at exactly the same time. The DL signal of BS1 will arrive at UE1 after a delay equal to $d_{1,1}/c$, where $c = 3 \times 10^8$ m/s is the speed of light and $d_{b,u}$ is the distance between UE u and BS b. Consequently, and before any time adjustment [23]:

- The UL signal of UE1 will arrive at BS1 after delay $2d_{1,1}/c$.
- The UL signal of UE1 will arrive at BS2 after delay $d_{1,1}/c + d_{2,1}/c$.

UE1 is served by BS1, so a time advance (TA) order is sent by BS1 to UE1 to instruct it to send earlier, by $2d_{1,1}/c$, in order for the UL signal to be received at BS1 at the expected time. Consequently, and after BS1 time adjustment:

- The UL signal of UE1 will arrive at BS1 at the expected time.
- The UL signal of UE1 will arrive at BS2 after delay $d_{1,1}/c + d_{2,1}/c - 2d_{1,1}/c = d_{2,1}/c - d_{1,1}/c$.

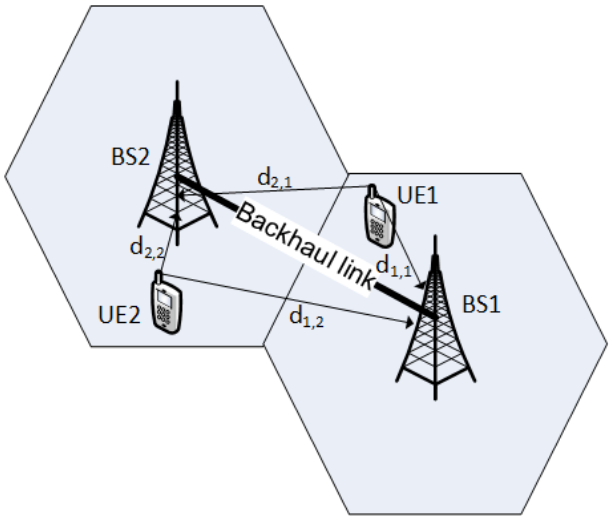

Figure 2.7: UL CoMP scenario with two BSs and two users.

Fig. 2.8 shows the received signals at BS2. The signal of UE2 is synchronized since this UE is at the same cell as BS2. In order to recover UE1's signal by JP of BS1 and BS2, the delay of the signal at BS2 must be less than T_{CP} minus the maximum delay spread of the link between UE1 and BS2 ($\tau_{\max}^{2,1}$), as shown in (2.9). Otherwise, ISI occurs and the orthogonality between subcarriers is lost, leading to ICI [60].

$$0 \leq (d_{2,1} - d_{1,1})/c \leq T_{CP} - (\tau_{\max}^{2,1} \cdot T_s), \tag{2.9}$$

where T_s is the sampling time. Therefore, if the signal arrival time is as indicated in position 'a', this leads to that UE1 can be part of CoMP operation because the signals of both UEs can be recovered in this case. On the other hand, if the signal arrival time is as indicated in position 'b', UE1 cannot be part of CoMP operation.

Although a TDD system is used in this section to describe the timing synchronization problem in CoMP, FDD systems suffer from the same problem. While in FDD systems the UL and DL streams use different frequency bands, the TA mechanism is still needed to maintain orthogonality among different UL streams [79]. Therefore, the limitation that each UE cannot be synchronized to more than one BS is the same as in TDD systems. As a result, UL signals coming from UEs outside the cell covered by the serving BS may not arrive within the CP period causing the same problem.

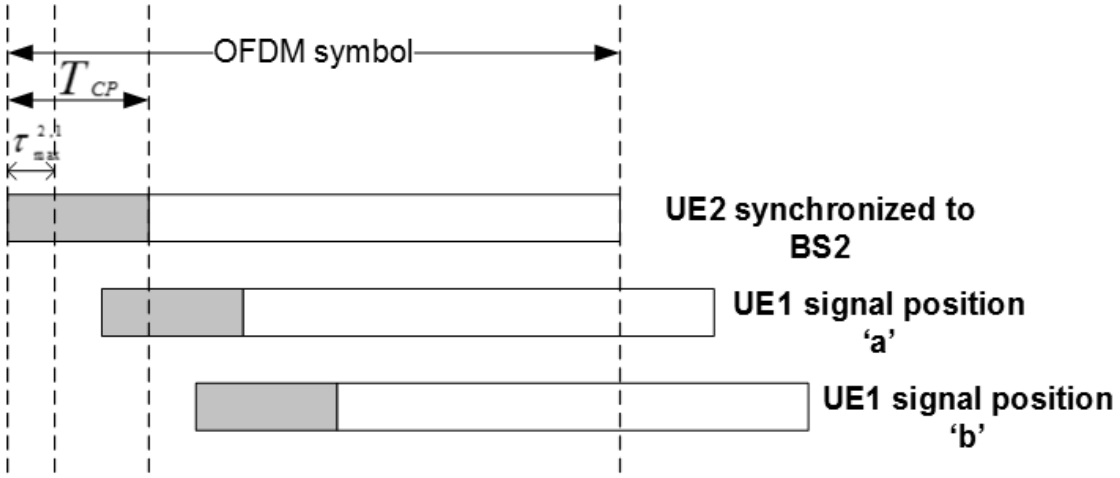

Figure 2.8: Signals' arrival times at BS2.

2.3.3 Related Work

The impact of time offset on cooperative MIMO OFDM systems like CoMP is studied in [80]. It was shown that time offsets limit the achievable signal-to-interference-plus-noise-ratio (SINR) in these systems. Also, the limitations that timing requirements in CoMP impose have been investigated in [81] where the authors performed an analysis to find the radius of the cooperation area among 3 cells for a symmetrical mobile configuration scenario. Using system level simulations, the authors in [24] showed that the timing synchronization problem in JP UL is more severe than JT DL. As for the compensation methods that aim to mitigate or reduce the effect of this problem, many methods have been proposed to solve the problem in the DL path [26, 82–84]. These methods cannot be applied directly to the UL path, since in the DL case, the BSs can cooperate and/or coordinate (e.g., using joint precoding or space-time coding (STC)) to compensate for the delays in the transmission side (BSs). The same principle does not apply to the UEs in the UL, so there is a need for novel processing methods to solve the timing synchronization problem in UL OFDM CoMP systems. A low-complexity method is proposed in [85] to mitigate the asynchronous interference in DL. The same technique can be used for UL systems but for small propagation delays.

Relatively few methods have been proposed in the open literature to solve the timing synchronization problem in UL OFDM CoMP systems. In [86], the authors outlined a method for suppressing the asynchronous interference in single carrier systems by overlapping the received FFT blocks. In [87], the authors offered another method but for

multi-carrier systems, using an iterative receiver with soft processing, to reduce the effect of asynchronous interference. Both works [86,87] assumed perfect knowledge of delays and CSI. In fact, the estimation of these parameters in CoMP systems is not an easy task. In addition, imperfect knowledge of these parameters can cause significant performance degradation [21].

Chapter 3

OFDM Systems with Integer Time and Frequency Offsets in AWGN and Flat Fading Channels

3.1 Effect of the Integer Time and Frequency Offsets for Transmission over AWGN and Rayleigh Flat Fading Channels

Consider an OFDM system with N subcarriers and N_{CP} samples of cyclic prefix. Let $x_m(n)$, $-N_{CP} \leq n \leq N-1$ denote the n-th sample of the transmitted OFDM symbol m. Assuming that the integer time offset equals θ samples and the normalized frequency offset (normalized to the subcarrier spacing) equals ϵ, two cases are considered. The first one, as shown in Fig. 3.1, is when the time offset is to the right. The received symbol in this case consists of the samples (assuming $\epsilon = 0$) $[x_m(\theta), x_m(\theta+1), ..., x_m(N-1), x_{m+1}(-N_{CP}), x_{m+1}(-N_{CP}+1), ..., x_{m+1}(-N_{CP}+\theta-1)]$. Therefore, this case can be considered as the positive time offset case as indicated in [58] and [59]. The second case is when the time offset is to the left of the OFDM symbol (negative time offset), which implies that the interference is from the preceding OFDM symbol and the received symbol's samples (assuming $\epsilon = 0$) are $[x_{m-1}(N-\theta-N_{CP}), x_{m-1}(N-\theta-N_{CP}+1), ..., x_{m-1}(N-1), x_m(-N_{CP}), x_m(-N_{CP}+1), ..., x_m(0), x_m(1), ..., x_m(N+\theta-1)]$. In this case, the CP helps in reducing the degradation effect of the time offset.

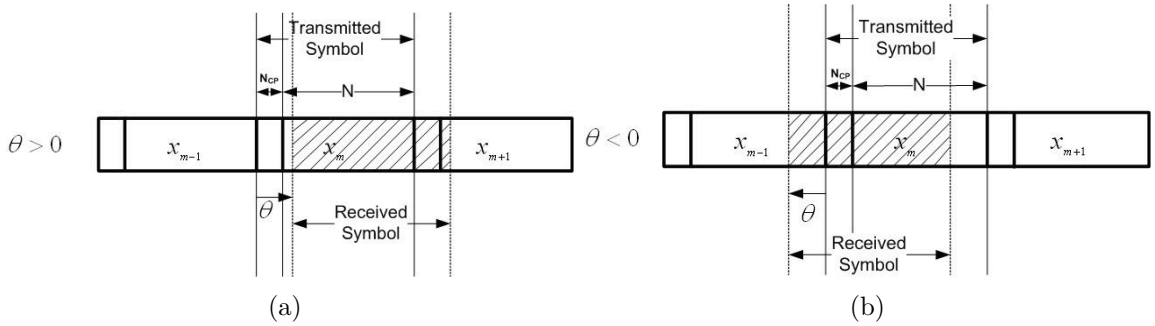

Figure 3.1: (a) Time offset to the right ($\theta > 0$); (b) time offset to the left ($\theta < 0$).

3.1.1 Positive Integer Time Offset ($\theta > 0$)

The received signal in the frequency domain after removing the CP is given by

$$
\begin{aligned}
R_m(K) &= \sum_{n=0}^{N-\theta-1} x_m(n+\theta) e^{\frac{j2\pi(\epsilon-K)n}{N}} + \sum_{n=N-\theta}^{N-1} x_{m+1}(n-N-N_{CP}+\theta) e^{\frac{j2\pi(\epsilon-K)n}{N}} + W_m(K) \\
&= \sum_{n=0}^{N-1} x_m(n+\theta)\gamma_{1P}(n) e^{\frac{j2\pi(\epsilon-K)n}{N}} + \sum_{n=0}^{N-1} x_{m+1}(n-N-N_{CP}+\theta)\gamma_{2P}(n) e^{\frac{j2\pi(\epsilon-K)n}{N}} + W_m(K) \\
&= \frac{1}{N}((X_m(K) e^{\frac{j2\pi K\theta}{N}}) \otimes \Gamma_{1P}(K)) + \frac{1}{N}((X_{m+1}(K) e^{\frac{j2\pi K(-N-N_{CP}+\theta)}{N}}) \otimes \Gamma_{2P}(K)) + W_m(K) \\
&= \frac{1}{N}\sum_{u=0}^{N-1} X_m((K-u)_N) e^{\frac{j2\pi\theta(K-u)}{N}} \Gamma_{1P}(u) + \frac{1}{N}\sum_{u=0}^{N-1} X_{m+1}((K-u)_N) e^{\frac{j2\pi(\theta-N_{CP})(K-u)}{N}} \Gamma_{2P}(u) \\
&\quad + W_m(K), \qquad (3.1)
\end{aligned}
$$

where $\otimes$ denotes the circular convolution operation. $X_m(K)$ and $X_{m+1}(K)$ are the samples of the DFTs of $x_m(n)$ and $x_{m+1}(n)$, respectively, $W_m(K)$ is K-th sample of the DFT of $w_m(n)$ which is the AWGN samples overlapping with OFDM symbol m with zero mean and variance σ^2, and $\gamma_{1P}(n)$ and $\gamma_{2P}(n)$ are two rectangular windows defined as follows:

$$
\gamma_{1P}(n) = \begin{cases} 1, & 0 \le n \le N-\theta-1 \\ 0, & otherwise \end{cases}, \text{ and } \quad \gamma_{2P}(n) = \begin{cases} 1, & N-\theta \le n \le N-1 \\ 0, & otherwise \end{cases}.
$$

$\Gamma_{1P}(u)$ and $\Gamma_{2P}(u)$ are the samples of the DFTs of $\gamma_{1P}(n) \cdot e^{\frac{j2\pi\epsilon n}{N}}$ and $\gamma_{2P}(n) \cdot e^{\frac{j2\pi\epsilon n}{N}}$ as computed in (3.2) and (3.3).

$$\Gamma_{1P}(u) = \begin{cases} N-\theta, & u = \epsilon \\ \frac{(1-e^{j2\pi(\epsilon-u)(N-\theta)/N})}{(1-e^{j2\pi(\epsilon-u)/N})}, & u \neq \epsilon \end{cases} \tag{3.2}$$

$$\Gamma_{2P}(u) = \begin{cases} \theta, & u = \epsilon \\ \frac{(e^{-j2\pi(\epsilon-u)\theta/N}-1)}{(1-e^{j2\pi(\epsilon-u)/N})} \cdot e^{j2\pi(\epsilon-u)}, & u \neq \epsilon \end{cases} \tag{3.3}$$

Finally, separating the desired signal from the ICI component results in (3.4):

$$\begin{aligned} R_m(K) = \frac{\Gamma_{1P}(0)}{N} X_m(K) e^{\frac{j2\pi K\theta}{N}} + \frac{1}{N}\sum_{u=1}^{N-1} X_m((K-u)_N) e^{\frac{j2\pi\theta(K-u)}{N}} \cdot \Gamma_{1P}(u) \\ + \frac{1}{N}\sum_{u=0}^{N-1} X_{m+1}((K-u)_N) e^{\frac{j2\pi(\theta-N_{CP})(K-u)}{N}} \cdot \Gamma_{2P}(u) + W_m(K) \end{aligned} \tag{3.4}$$

3.1.2 Negative Integer Time Offset ($\theta \leq 0$)

The same analysis can be applied by replacing θ with $\theta_{CP} = \max(-\theta - N_{CP}, 0)$. Therefore, the received signal in the frequency domain after removing the CP is given by

$$\begin{aligned} R_m(K) &= \sum_{n=0}^{\theta_{CP}-1} x_{m-1}(n+N-\theta_{CP}) e^{\frac{j2\pi(\epsilon-K)n}{N}} + \sum_{n=\theta_{CP}}^{N-1} x_m(n-N_{CP}-\theta_{CP}) e^{\frac{j2\pi(\epsilon-K)n}{N}} \\ &\quad + W_m(K) \\ &= \sum_{n=0}^{N-1} x_{m-1}(n+N+\theta+N_{CP})\gamma_{2N}(n) e^{\frac{j2\pi(\epsilon-K)n}{N}} + \sum_{n=0}^{N-1} x_m(n+\theta)\gamma_{1N}(n) e^{\frac{j2\pi(\epsilon-K)n}{N}} \\ &\quad + W_m(K) \\ &= \frac{1}{N}((X_{m-1}(K) e^{\frac{j2\pi K(\theta+N_{CP})}{N}}) \otimes \Gamma_{2N}(K)) + \frac{1}{N}((X_m(K) e^{\frac{j2\pi K\theta}{N}}) \otimes \Gamma_{1N}(K)) + W_m(K) \\ &= \frac{1}{N}\sum_{u=0}^{N-1} X_{m-1}((K-u)_N) e^{\frac{j2\pi(\theta+N_{CP})(K-u)}{N}} \Gamma_{2N}(u) + \frac{1}{N}\sum_{u=0}^{N-1} X_m((K-u)_N) e^{\frac{j2\pi\theta(K-u)}{N}} \Gamma_{1N}(u) \\ &\quad + W_m(K), \end{aligned} \tag{3.5}$$

where

$$\gamma_{1N}(n) = \begin{cases} 1, & \theta_{CP} \leq n \leq N-1 \\ 0, & otherwise \end{cases}, \text{ and } \quad \gamma_{2N}(n) = \begin{cases} 1, & 0 \leq n \leq \theta_{CP}-1 \\ 0, & otherwise \end{cases}.$$

$\Gamma_{1N}(u)$ and $\Gamma_{2N}(u)$ are the samples of the DFTs of $\gamma_{1N}(n) \cdot e^{\frac{j2\pi\epsilon n}{N}}$ and $\gamma_{2N}(n) \cdot e^{\frac{j2\pi\epsilon n}{N}}$ as computed in (3.6) and (3.7), respectively.

$$\Gamma_{1N}(u) = \begin{cases} N-\theta_{CP}, & u = \epsilon \\ \frac{(1-e^{j2\pi(\epsilon-u)(N-\theta_{CP})/N})}{(1-e^{j2\pi(\epsilon-u)/N})} \cdot e^{j2\pi(\epsilon-u)\theta_{CP}/N}, & u \neq \epsilon \end{cases} \tag{3.6}$$

$$\Gamma_{2N}(u) = \begin{cases} \theta_{CP}, & u = \epsilon \\ \frac{(1-e^{j2\pi(\epsilon-u)\theta_{CP}/N})}{(1-e^{j2\pi(\epsilon-u)/N})}, & u \neq \epsilon \end{cases}. \tag{3.7}$$

Separating the desired signal from the ICI component results in (3.8):

$$\begin{aligned} R_m(K) = \frac{\Gamma_{1N}(0)}{N} X_m(K) e^{\frac{j2\pi K\theta}{N}} + \frac{1}{N}\sum_{u=1}^{N-1} X_m((K-u)_N) e^{\frac{j2\pi\theta(K-u)}{N}} \cdot \Gamma_{1N}(u) \\ + \frac{1}{N}\sum_{u=0}^{N-1} X_{m-1}((K-u)_N) e^{\frac{j2\pi(\theta+N_{CP})(K-u)}{N}} \cdot \Gamma_{2N}(u) + W_m(K). \end{aligned} \tag{3.8}$$

Both (3.4) and (3.8) can be put in the form

$$\begin{aligned} R_m(K) = \lambda C_K(0) X_m(K) + \lambda \sum_{u=1}^{N-1} C_K(u) X_m((K-u)_N) \\ + \lambda \sum_{u=0}^{N-1} G_K(u) X_{m\pm1}((K-u)_N) + W_m(K), \end{aligned} \tag{3.9}$$

where λ is deterministic and equals 1 in the case of AWGN. In the case of flat fading, λ is a complex Gaussian random variable with zero mean and variance ($\sigma_R^2 = 0.5$) per dimension and its magnitude has the density $f(|\lambda|) = \frac{|\lambda|}{\sigma_R^2} e^{-|\lambda|^2/2\sigma_R^2}$. Note that the first term in (3.9) is the desired signal multiplied by an attenuation factor, the second term is the ICI, and the third term is the IBI. Also note that in (3.8) when the time offset is less than or equal to the CP length ($\theta_{CP} = 0$), there is no IBI and the ICI is due to the CFO only.

3.2 BER/SER of OFDM with Integer Time and Frequency Offsets in AWGN and Rayleigh Flat Fading Channels

In this section, we derive exact closed-form expressions for the BER/SER of OFDM systems with integer time and frequency offsets for the case of BPSK, QPSK and 16-QAM modulations and for both AWGN and Rayleigh flat fading channels.

3.2.1 BPSK Modulation

AWGN Channel

In order to derive the exact BER expressions for OFDM systems with integer time and frequency offsets, we follow procedure similar to the ones adopted in [33] and [64] for OFDM systems with frequency offset. Assuming BPSK modulation, i.e., $X_m(K) \in \{-1, 1\}$, without loss of generality, we will assume that the transmitted symbol on the desired subcarrier K is equal to 1 ($X_m(K) = 1$). It is also assumed that the phase shift that is multiplied by the desired subcarrier in (3.4) and (3.8) is compensated for. This can be justified by the fact that, in OFDM systems, this phase shift is compensated for automatically by channel equalization, which cannot differentiate between phase shifts introduced by the channel and those caused by time and frequency offsets [60]. Based on these assumptions, the received signal in subcarrier K can be expressed as shown in (3.10) and (3.11).

For $\theta > 0$:

$$R_m(K) = \frac{\Gamma_{1P}(0)}{N} + \frac{1}{N}\sum_{u=1}^{N-1} X_m((K-u)_N) e^{\frac{-j2\pi\theta u}{N}} \cdot \Gamma_{1P}(u) + \frac{1}{N}\sum_{u=0}^{N-1} X_{m+1}((K-u)_N) e^{\frac{-j2\pi(N_{CP}K+(\theta-N_{CP})u)}{N}} \cdot \Gamma_{2P}(u) + W_m(K). \tag{3.10}$$

For $\theta \leq 0$:

$$R_m(K) = \frac{\Gamma_{1N}(0)}{N} + \frac{1}{N}\sum_{u=1}^{N-1} X_m((K-u)_N) e^{\frac{-j2\pi\theta u}{N}} \cdot \Gamma_{1N}(u) + \frac{1}{N}\sum_{u=0}^{N-1} X_{m-1}((K-u)_N) e^{\frac{j2\pi(N_{CP}K-(\theta+N_{CP})u)}{N}} \cdot \Gamma_{2N}(u) + W_m(K). \tag{3.11}$$

Since $X_m(K)$, $X_{m+1}(K)$ in (3.10) and $X_m(K)$, $X_{m-1}(K)$ in (3.11) (where $K = 0, 1, ..., N-1$) are independent random variables and $R_m(K)$ is a summation of these random variables with weighting factors, the characteristic function (CHF) of $R_m(K)$ will be the product of their individual CHFs. Moreover, since the modulation scheme is BPSK, it is sufficient to consider only the real part of $R_m(K)$; then the CHF is given by [64]

$$\varphi_{\Re(R_m(K))}(\omega) = e^{j\omega\Re(S_K(0))-\omega^2\sigma^2/2} \cdot \prod_{l=1}^{M} \cos(\omega\Re(S_K(l))), \tag{3.12}$$

where $\varphi_{\Re(R_m(K))}(\omega)$ is the CHF of the real part of $R_m(K)$, $M = 2N-1$ and

$$S_K(l) = \begin{cases} C_K(l) & 0 \le l \le N-1 \\ G_K(l-N) & N \le l \le M. \end{cases} \tag{3.13}$$

For $\theta > 0$:

$$\begin{aligned} C_K(u) &= \frac{1}{N} \cdot e^{\frac{-j2\pi\theta u}{N}} \cdot \Gamma_{1P}(u), \quad 0 \le u \le N-1, \\ G_K(u) &= \frac{1}{N} \cdot e^{\frac{-j2\pi(N_{CP}K+(\theta-N_{CP})u)}{N}} \cdot \Gamma_{2P}(u), \quad 0 \le u \le N-1. \end{aligned} \tag{3.14}$$

For $\theta \le 0$:

$$\begin{aligned} C_K(u) &= \frac{1}{N} \cdot e^{\frac{-j2\pi\theta u}{N}} \cdot \Gamma_{1N}(u), \quad 0 \le u \le N-1, \\ G_K(u) &= \frac{1}{N} \cdot e^{\frac{j2\pi(N_{CP}K-(\theta+N_{CP})u)}{N}} \cdot \Gamma_{2N}(u), \quad 0 \le u \le N-1. \end{aligned} \tag{3.15}$$

The product of cosines in (3.12) can be rewritten as a sum of cosines by applying the standard product-to-sum trigonometric identity recursively [33]. Then (3.12) can be expressed as

$$\varphi_{\Re(R_m(K))}(\omega) = \frac{1}{2^M} \sum_{i=1}^{2^{M-1}} (e^{j\omega\alpha_{i,K}-\omega^2\sigma^2/2} + e^{j\omega\beta_{i,K}-\omega^2\sigma^2/2}), \tag{3.16}$$

where

$$\alpha_{i,K} = \Re(S_K(0) + \mathbf{S}_K^T\mathbf{e}_i), \quad \beta_{i,K} = \Re(S_K(0) - \mathbf{S}_K^T\mathbf{e}_i), \tag{3.17}$$

and $\mathbf{S}_K$ is the vector $[S_K(1)\ S_K(2)\ S_K(3)...S_K(M)]^T$. $\mathbf{e}_i$ is a vector of length M consisting of the binary representation of the number $(2^M - i)$, where zeros are replaced by -1s.

It can be noted from (3.16) that the CHF of $R_m(K)$ depends on the subcarrier K and is not constant for all subcarriers. Thus, in OFDM systems with integer time offset, the performance of different subcarriers is not identical. This discrepancy in subcarrier performance is due to the existence of the CP. For instance, when the CP length and the CFO equal zero in (3.14) and (3.15), the ICI and the IBI coefficients will be symmetric around the y-axis. On the other hand, when there is CP, this symmetry does not exist and the subcarriers are divided into groups; each group has different performance as will be shown later in the numerical results section.

Noting that (3.16) is a sum of the CHFs of different Gaussian random variables [33] and that evaluating the performance of OFDM systems with integer time offsets requires averaging over the performance of all the subcarriers, the exact BER can be computed as

$$P_e = \frac{1}{N(2^M)} \sum_{K=0}^{N-1} \sum_{i=1}^{2^{M-1}} Q(\sqrt{2\eta}\alpha_{i,K}) + Q(\sqrt{2\eta}\beta_{i,K}), \tag{3.18}$$

where $Q(\cdot)$ denotes the Q-function and $\eta = E_b/N_0$ is the SNR assuming unit energy per bit E_b and that the noise power spectral density σ^2 equals $N_0/2$.

Rayleigh Flat Fading Channel

The bit error probability conditioned on the magnitude of the channel gain is given by

$$P_{e|\lambda} = \frac{1}{N(2^M)} \sum_{K=0}^{N-1} \sum_{i=1}^{2^{M-1}} Q(\sqrt{2\eta}\alpha_{i,K}|\lambda|) + Q(\sqrt{2\eta}\beta_{i,K}|\lambda|). \tag{3.19}$$

Then the probability of error is obtained by integrating the conditional error probability over the fading distribution as follows:

$$\bar{P}_e = \int_0^\infty P_{e|\lambda} f(|\lambda|) d|\lambda|. \tag{3.20}$$

Evaluating this integral using the identity in [88, eq. 2.8.5.9], the probability of error for an OFDM system using BPSK with integer time and frequency offsets in a Rayleigh flat fading channel can be expressed as

$$\bar{P}_e = \frac{1}{2} - \frac{1}{N2^{M+1}} \sum_{K=0}^{N-1} \sum_{i=1}^{2^{M-1}} \alpha_{i,K} \sqrt{\frac{2\eta\sigma_R^2}{1+2\eta\alpha_{i,K}^2\sigma_R^2}} + \beta_{i,K} \sqrt{\frac{2\eta\sigma_R^2}{1+2\eta\beta_{i,K}^2\sigma_R^2}}. \tag{3.21}$$

3.2.2 QPSK Modulation

AWGN Channel

By following the same procedure as in the previous section, and by employing the result obtained in [33] for OFDM systems with frequency offset, the SER for OFDM systems employing QPSK with integer time and frequency offsets for transmission over the AWGN channel can be expressed as

$$P_s = 1 - \frac{1}{N2^{2M}} \sum_{K=0}^{N-1} \sum_{i1=1}^{2^{M-1}} \sum_{i2=1}^{2^{M-1}} \sum_{m=1}^{4} Q(-\sqrt{2\eta}\psi_{i1,i2,K}[1,m]) \times Q(-\sqrt{2\eta}\psi_{i1,i2,K}[2,m]), \quad (3.22)$$

where

$$\begin{aligned}
[\mathbf{\Psi}_{i1,i2,K}]_{2\times 4} &= (\mathbf{C1}_{i1,i2,K}\ \mathbf{C2}_{i1,i2,K}\ \mathbf{C3}_{i1,i2,K}\ \mathbf{C4}_{i1,i2,K}), \\
[\mathbf{C1}_{i1,i2,K}]_{2\times 1} &= \mathbf{A}_K^0 - \mathbf{D}_K^0 + \mathbf{A}_K\mathbf{e}_{i1} + \mathbf{D}_K\mathbf{e}_{i2}, \\
[\mathbf{C2}_{i1,i2,K}]_{2\times 1} &= \mathbf{A}_K^0 - \mathbf{D}_K^0 - \mathbf{A}_K\mathbf{e}_{i1} - \mathbf{D}_K\mathbf{e}_{i2}, \\
[\mathbf{C3}_{i1,i2,K}]_{2\times 1} &= \mathbf{A}_K^0 - \mathbf{D}_K^0 + \mathbf{A}_K\mathbf{e}_{i1} - \mathbf{D}_K\mathbf{e}_{i2}, \\
[\mathbf{C4}_{i1,i2,K}]_{2\times 1} &= \mathbf{A}_K^0 - \mathbf{D}_K^0 - \mathbf{A}_K\mathbf{e}_{i1} + \mathbf{D}_K\mathbf{e}_{i2}, \\
[\mathbf{A}_K^l]_{2\times 1} &= (\Re(S_K(l))\ \Im(S_K(l)))^T, \\
[\mathbf{D}_K^l]_{2\times 1} &= (\Im(S_K(l))\ -\Re(S_K(l)))^T, \\
[\mathbf{A}_K]_{2\times M} &= (\mathbf{A}_K^1\ \mathbf{A}_K^2\ \mathbf{A}_K^3\ \cdots \mathbf{A}_K^M), \text{and} \\
[\mathbf{D}_K]_{2\times M} &= (\mathbf{D}_K^1\ \mathbf{D}_K^2\ \mathbf{D}_K^3\ \cdots \mathbf{D}_K^M).
\end{aligned} \quad (3.23)$$

S_K are the interference coefficients given in (3.13) and $\eta = E_s/2N_0$ where E_s is the energy per symbol.

Rayleigh Flat Fading Channel

The symbol error probability conditioned on the magnitude of the channel gain is given by

$$P_{s|\lambda} = 1 - \frac{1}{N2^{2M}} \sum_{K=0}^{N-1} \sum_{i1=1}^{2^{M-1}} \sum_{i2=1}^{2^{M-1}} \sum_{m=1}^{4} Q(-\sqrt{2\eta}\psi_{i1,i2,K}[1,m]|\lambda|) \times Q(-\sqrt{2\eta}\psi_{i1,i2,K}[2,m]|\lambda|). \quad (3.24)$$

To evaluate the average SER, the conditional SER in (3.24) needs to be averaged over the Rayleigh fading distribution:

$$\bar{P}_s = \int_0^\infty P_{s|\lambda} f(|\lambda|) d|\lambda|. \tag{3.25}$$

From (3.24) and (3.25), it is clear that this averaging involves an integral of the form

$$I = \int_0^\infty f(r) Q(rA_1) Q(rA_2) dr, \tag{3.26}$$

which is a common integral for finding the SER in quadrature modulation formats [29]. Closed-form expressions for this integral can be found in [29–31]. The problem in these results is that they are not valid when the arguments A_1 and/or A_2 in (3.26) are negative, which is the case in OFDM systems with integer time offsets. A new result for this integral is derived in Appendix A [28]. The new result is valid for any polarity of A_1 and/or A_2 and is shown below:

$$\begin{aligned} I = \frac{1}{4} &+ \frac{A_1\sigma_R}{\sqrt{A_1^2\sigma_R^2+1}}\left(-\frac{1}{4} + \frac{1}{2\pi}\arctan\left\{\frac{A_2\sigma_R}{\sqrt{A_1^2\sigma_R^2+1}}\right\}\right) \\ &+ \frac{A_2\sigma_R}{\sqrt{A_2^2\sigma_R^2+1}}\left(-\frac{1}{4} + \frac{1}{2\pi}\arctan\left\{\frac{A_1\sigma_R}{\sqrt{A_2^2\sigma_R^2+1}}\right\}\right). \end{aligned} \tag{3.27}$$

By employing this new modified result, the SER for transmission over the Rayleigh flat fading channel can be expressed as

$$\begin{aligned} \bar{P}_s = \frac{3}{4} - \frac{1}{N2^{2M+1}} \sum_{K=0}^{N-1} \sum_{i1=1}^{2^{M-1}} \sum_{i2=1}^{2^{M-1}} \sum_{m=1}^{4} &\delta_1 \cdot \psi_{i1,i2,K}[1,m]\left(\frac{1}{2} + \frac{1}{\pi}\arctan\left\{\delta_1 \cdot \psi_{i1,i2,K}[2,m]\right\}\right) \\ &+ \delta_2 \cdot \psi_{i1,i2,K}[2,m]\left(\frac{1}{2} + \frac{1}{\pi}\arctan\left\{\delta_2 \cdot \psi_{i1,i2,K}[1,m]\right\}\right), \end{aligned} \tag{3.28}$$

where

$$\delta_1 = \sqrt{\frac{2\sigma_R^2\eta}{1+2\sigma_R^2\eta\psi_{i1,i2,K}^2[1,m]}},$$

and

$$\delta_2 = \sqrt{\frac{2\sigma_R^2\eta}{1+2\sigma_R^2\eta\psi_{i1,i2,K}^2[2,m]}}.$$

3.2.3 16-QAM Modulation

AWGN Channel

In this modulation scheme, first the total probability of correct decision P_c given that the transmitted symbol belongs to the first quadrant of the complex plane is evaluated. Then the average probability of error is given by ($P_s = 1 - P_c$). In order to evaluate P_c, let us first assume that the transmitted symbol is ($X_m(K) = 1 + j$), then the conditional probability of correct decision can be expressed as [64]

$$\begin{aligned} &P_{c1}(\mathcal{R}_m(K) + W_m(K) \in D_{s1} | X_m(K) = 1 + j, \mathcal{R}_m(K)) \\ &\quad = \chi(0,0) - \chi(0,2) - \chi(2,0) + \chi(2,2), \end{aligned} \tag{3.29}$$

where $\mathcal{R}_m(K)$ denotes the noise-free received signal, D_{s1} is a square in the complex plane with vertices $(0,0)$, $(0,2)$, $(2,0)$, and $(2,2)$ defining the correct decision region when the transmitted symbol equals ($X_m(K) = 1 + j$), and $\chi(a,b)$ is defined as follows:

$$\chi(a,b) = Q(\frac{a - \Re(\mathcal{R}_m(K))}{\sigma}) Q(\frac{b - \Im(\mathcal{R}_m(K))}{\sigma}). \tag{3.30}$$

Following the procedure in [75], the two-dimensional probability density function (2D-PDF) of $\mathcal{R}_m(K)$ given that the transmitted symbol is ($X_m(K) = 1 + j$) is given by

$$\begin{aligned} P\{\Re(\mathcal{R}_m(K)), \Im(\mathcal{R}_m(K)) | X_m(K) = 1 + j\} = \frac{1}{4 \times 2^{4M}} \sum_{i1=1}^{2^{M-1}} \sum_{i2=1}^{2^{M-1}} \sum_{i3=1}^{2^{M-1}} \sum_{i4=1}^{2^{M-1}} \sum_{d=1}^{16} \\ \delta\{\Re(\mathcal{R}_m(K)) - C^1_{i1,i2,i3,i4,K}[1,d]\} \times \delta\{\Im(\mathcal{R}_m(K)) - C^1_{i1,i2,i3,i4,K}[2,d]\}, \end{aligned} \tag{3.31}$$

where $[\mathbf{C}^1_{i1,i2,i3,i4,K}]_{2\times 1} = \mathbf{A}^0_K - \mathbf{D}^0_K + \mathbf{C}_K \mathbf{e}_d$ and $\delta(\cdot)$ is the Dirac delta function. $\mathbf{C}_K = (\mathbf{A}_K \mathbf{e}_{i1} \;\; 2\mathbf{A}_K \mathbf{e}_{i2} \;\; \mathbf{D}_K \mathbf{e}_{i3} \;\; 2\mathbf{D}_K \mathbf{e}_{i4})$ and $\mathbf{e}_d (d = 1, 2, ..., 2^4)$ is the d-th column of a 4×2^4 matrix, which is a vector of length 4 consisting of the binary representation of the number $2^4 - d$, where zeros are replaced by -1s. Then the probability of correct decision is given by averaging (3.29) over the distribution in (3.31) as computed in (3.32).

$$\begin{aligned} P_{c1,av} = \frac{1}{4N \times 2^{4M}} \sum_{K=0}^{N-1} \sum_{i1=1}^{2^{M-1}} \sum_{i2=1}^{2^{M-1}} \sum_{i3=1}^{2^{M-1}} \sum_{i4=1}^{2^{M-1}} \sum_{d=1}^{16} \\ Q(-\sqrt{\bar{\eta}_s/5}\; C^1_{i1,i2,i3,i4,K}[1,d]) \times Q(-\sqrt{\bar{\eta}_s/5}\; C^1_{i1,i2,i3,i4,K}[2,d]) \\ - Q(-\sqrt{\bar{\eta}_s/5}\; C^1_{i1,i2,i3,i4,K}[1,d]) \times Q(-\sqrt{\bar{\eta}_s/5}\; (C^1_{i1,i2,i3,i4,K}[2,d] - 2)) \\ - Q(-\sqrt{\bar{\eta}_s/5}\; (C^1_{i1,i2,i3,i4,K}[1,d] - 2)) \times Q(-\sqrt{\bar{\eta}_s/5}\; C^1_{i1,i2,i3,i4,K}[2,d]) \\ + Q(-\sqrt{\bar{\eta}_s/5}\; (C^1_{i1,i2,i3,i4,K}[1,d] - 2)) \times Q(-\sqrt{\bar{\eta}_s/5}\; (C^1_{i1,i2,i3,i4,K}[2,d] - 2)), \end{aligned} \tag{3.32}$$

where $\bar{\eta}_s = E_s/N_0$ is the average energy per symbol to noise spectral density ratio. Similarly, the probability of correct decision for the other three points in the first quadrant can be evaluated given that the conditional probability of error for each of them can be expressed as [75]

$$\begin{aligned}
&P_{c2}(\mathcal{R}_m(K) + W_m(K) \in D_{s2} | X_m(K) = 1 + 3j, \mathcal{R}_m(K)) = \chi(0,2) - \chi(2,2), \\
&P_{c3}(\mathcal{R}_m(K) + W_m(K) \in D_{s3} | X_m(K) = 3 + j, \mathcal{R}_m(K)) = \chi(2,0) - \chi(2,2), \text{and} \\
&P_{c4}(\mathcal{R}_m(K) + W_m(K) \in D_{s4} | X_m(K) = 3 + 3j, \mathcal{R}_m(K)) = \chi(2,2). \qquad (3.33)
\end{aligned}$$

The corresponding 2D-PDFs can take the same form as in (3.31) but with replacing $\mathbf{C}^1_{i1,i2,i3,i4,K}$ by $(\mathbf{C}^2_{i1,i2,i3,i4,K} = \mathbf{A}^0_K - 3\mathbf{D}^0_K + \mathbf{C}_K\mathbf{e}_d)$, $(\mathbf{C}^3_{i1,i2,i3,i4,K} = 3\mathbf{A}^0_K - \mathbf{D}^0_K + \mathbf{C}_K\mathbf{e}_d)$, and $(\mathbf{C}^4_{i1,i2,i3,i4,K} = 3\mathbf{A}^0_K - 3\mathbf{D}^0_K + \mathbf{C}_K\mathbf{e}_d)$, respectively. Summing the probability of correct decision of the four points results in P_c. Therefore, the SER for OFDM systems employing 16-QAM with integer time and frequency offsets for transmission over the AWGN channel can be expressed as

$$\begin{aligned}
P_s = 1 - \frac{1}{4N \times 2^{4M}} &\sum_{K=0}^{N-1} \sum_{i1=1}^{2^{M-1}} \sum_{i2=1}^{2^{M-1}} \sum_{i3=1}^{2^{M-1}} \sum_{i4=1}^{2^{M-1}} \sum_{d=1}^{16} \\
&\{Q(-\sqrt{\bar{\eta}_s/5}\ C^1_1(0)) \times Q(-\sqrt{\bar{\eta}_s/5}\ C^1_2(0))\} - \{Q(-\sqrt{\bar{\eta}_s/5}\ C^1_1(0)) \times Q(-\sqrt{\bar{\eta}_s/5}\ C^1_2(2))\} \\
&- \{Q(-\sqrt{\bar{\eta}_s/5}\ C^1_1(2)) \times Q(-\sqrt{\bar{\eta}_s/5}\ C^1_2(0))\} + \{Q(-\sqrt{\bar{\eta}_s/5}\ C^1_1(2)) \times Q(-\sqrt{\bar{\eta}_s/5}\ C^1_2(2))\} \\
&+ \{Q(-\sqrt{\bar{\eta}_s/5}\ C^2_1(0)) \times Q(-\sqrt{\bar{\eta}_s/5}\ C^2_2(2))\} - \{Q(-\sqrt{\bar{\eta}_s/5}\ C^2_1(2)) \times Q(-\sqrt{\bar{\eta}_s/5}\ C^2_2(2))\} \\
&+ \{Q(-\sqrt{\bar{\eta}_s/5}\ C^3_1(2)) \times Q(-\sqrt{\bar{\eta}_s/5}\ C^3_2(0))\} - \{Q(-\sqrt{\bar{\eta}_s/5}\ C^3_1(2)) \times Q(-\sqrt{\bar{\eta}_s/5}\ C^3_2(2))\} \\
&+ \{Q(-\sqrt{\bar{\eta}_s/5}\ C^4_1(2)) \times Q(-\sqrt{\bar{\eta}_s/5}\ C^4_2(2))\}, \qquad (3.34)
\end{aligned}$$

where $C^i_1(a)$ and $C^i_2(a)$ denote $C^i_{i1,i2,i3,i4,K}[1,d] - a$ and $C^i_2 = C^i_{i1,i2,i3,i4,K}[2,d] - a$, respectively.

Rayleigh Flat Fading Channel

Following the same procedure as in the BPSK and QPSK cases, and using (3.27), the SER for OFDM systems employing 16-QAM over the Rayleigh flat fading channel can be

expressed as

$$\bar{P}_s = \frac{3}{4} - \frac{1}{4N \times 2^{4M+1}} \sum_{K=0}^{N-1} \sum_{i1=1}^{2^{M-1}} \sum_{i2=1}^{2^{M-1}} \sum_{i3=1}^{2^{M-1}} \sum_{i4=1}^{2^{M-1}} \sum_{d=1}^{16}$$
$$\left\{\delta_1^1(0) \cdot C_1^1(0) \cdot g(\delta_1^1(0) \cdot C_2^1(0)) + \delta_2^1(0) \cdot C_2^1(0) \cdot g(\delta_2^1(0) \cdot C_1^1(0))\right\}$$
$$- \left\{\delta_1^1(0) \cdot C_1^1(0) \cdot g(\delta_1^1(0) \cdot C_2^1(2)) + \delta_2^1(2) \cdot C_2^1(2) \cdot g(\delta_2^1(2) \cdot C_1^1(0))\right\}$$
$$- \left\{\delta_1^1(2) \cdot C_1^1(2) \cdot g(\delta_1^1(2) \cdot C_2^1(0)) + \delta_2^1(0) \cdot C_2^1(0) \cdot g(\delta_2^1(0) \cdot C_1^1(2))\right\}$$
$$+ \left\{\delta_1^1(2) \cdot C_1^1(2) \cdot g(\delta_1^1(2) \cdot C_2^1(2)) + \delta_2^1(2) \cdot C_2^1(2) \cdot g(\delta_2^1(2) \cdot C_1^1(2))\right\}$$
$$+ \left\{\delta_1^2(0) \cdot C_1^2(0) \cdot g(\delta_1^2(0) \cdot C_2^2(2)) + \delta_2^2(2) \cdot C_2^2(2) \cdot g(\delta_2^2(2) \cdot C_1^2(0))\right\}$$
$$- \left\{\delta_1^2(2) \cdot C_1^2(2) \cdot g(\delta_1^2(2) \cdot C_2^1(2)) + \delta_2^2(2) \cdot C_2^2(2) \cdot g(\delta_2^2(2) \cdot C_1^2(2))\right\}$$
$$+ \left\{\delta_1^3(2) \cdot C_1^3(2) \cdot g(\delta_1^3(2) \cdot C_2^3(0)) + \delta_2^3(0) \cdot C_2^3(0) \cdot g(\delta_2^3(0) \cdot C_1^3(2))\right\}$$
$$- \left\{\delta_1^3(2) \cdot C_1^3(2) \cdot g(\delta_1^3(2) \cdot C_2^3(2)) + \delta_2^3(2) \cdot C_2^3(2) \cdot g(\delta_2^3(2) \cdot C_1^3(2))\right\}$$
$$+ \left\{\delta_1^4(2) \cdot C_1^4(2) \cdot g(\delta_1^4(2) \cdot C_2^4(2)) + \delta_2^4(2) \cdot C_2^4(2) \cdot g(\delta_2^4(2) \cdot C_1^4(2))\right\}, \tag{3.35}$$

where $g(x) = \frac{1}{2} + \frac{1}{\pi}\arctan(x)$ and

$$\delta_1^i(a) = \sqrt{\frac{\sigma_R^2 \bar{\eta}_s/5}{1 + \sigma_R^2 \bar{\eta}_s (C_1^i(a))^2/5}},$$

and

$$\delta_2^i(a) = \sqrt{\frac{\sigma_R^2 \bar{\eta}_s/5}{1 + \sigma_R^2 \bar{\eta}_s (C_2^i(a))^2/5}}.$$

3.3 Approximate Method for BER/SER Evaluation in AWGN and Rayleigh Flat Fading Channels

As can be seen from (3.18), (3.22), and (3.34) the complexity of evaluating the BER/SER expressions increases exponentially with $M = 2N - 1$ in the case of BPSK, with $2M$ in the case of QPSK and with $4M$ in the case of 16-QAM because of the large number of summations involved in the computation of the BER/SER. Thus, for large FFT sizes, the complexity of the BER/SER evaluation becomes high, and an approximate method is desirable. Our method is based on reducing the number of summations needed to evaluate

the probability of error by truncating the number of the interference coefficients that are used from M to N_a (i.e., the coefficients with the most significant contribution are retained, while the remaining coefficients are discarded and replaced by a Gaussian approximation).

For instance, in order to select the coefficients that are for BPSK modulation in AWGN and flat fading channels we sort the coefficients based on their relevance to the computation of the probability of error, which can be inferred from the product in (3.12). Noting that the smaller the real value of the interfering coefficient is, the closer the value of its cosine to one will, and hence the smaller contribution from this coefficient to the product of cosines in (3.12) and in turn the less relevance to the probability of error computation. The rest of the coefficients (the discarded ones) are approximated by a Gaussian random variable with its power is added to the power of the Gaussian noise. The exact same procedure can be used for QPSK and 16-QAM modulation albeit by adjusting the metric used for sorting to conform with the CHF of them.

It is clear that choosing the number of used coefficients N_a involves a tradeoff between complexity and accuracy of the performance evaluation. The fewer the used coefficients are, the less accurate the results will be. The lower bound corresponds to approximating all the interference by one Gaussian random variable instead of the mixture of Gaussian densities that appears in (3.16). We list the steps of the approximate method to evaluate the BER/SER for any FFT of large size in the following computational algorithm.

Computational Algorithm:

- Compute the following function for each of the coefficients $S_K(l)$, $(l = 1, 2, ..., M)$:
  For BPSK: $F_1(l) = \cos(\Re(S_K(l)))$
  For QPSK: $F_1(l) = \cos\{\Re(S_K(l)) + \Im(S_K(l))\} \times \cos\{\Im(S_K(l)) - \Re(S_K(l))\}$
  For 16-QAM: $F_1(l) = \cos\{\Re(S_K(l)) + \Im(S_K(l))\} \times \cos\{2(\Re(S_K(l)) + \Im(S_K(l)))\} \times \cos\{\Im(S_K(l)) - \Re(S_K(l))\} \times \cos\{2(\Im(S_K(l)) - \Re(S_K(l)))\}$.

- Sort the coefficients $S_K(l)$ in ascending order according to the value of $F_1(l)$:
  $S_K(l) \rightarrow \widehat{S}_K(l)$, where $\widehat{S}_K(l)$ are the sorted coefficients.

- Determine the number of coefficients that will be used in the evaluation of the BER/SER (N_a).

- For the discarded coefficients $\widehat{S}_K(l)$, $(l = N_a + 1, N_a + 2, ..., M)$ compute the variance $(\sigma_I^2 = \sum_{N_a+1}^{M} |\widehat{S}_K(l)|^2)$.

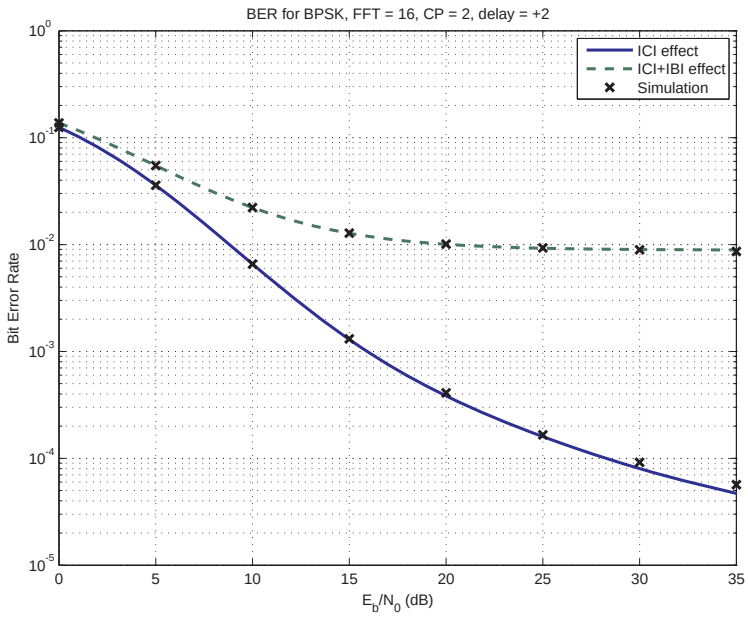

Figure 3.2: Effect of ICI and IBI on the probability of error.

- Then the BER can be computed from (3.18), (3.21), and (3.34) and the SER from (3.22), (3.28), and (3.35) by replacing M with N_a, $S_K(l)$ with $\widehat{S}_K(l)$, $(l = 1, 2, ..., N_a)$ and by replacing σ^2 with $(\sigma^2 + \sigma_I^2)$.

3.4 Numerical Results

First, the effect of integer time offset only in the absence of frequency offset is studied. We consider BPSK OFDM with $N = 16$, $N_{CP} = 2$, and for transmission over AWGN channel. The time offset equal to 2 samples to the right. Fig. 3.2 shows the effect of both ICI and IBI on the probability of error. The effect of ICI alone can be obtained theoretically by substituting in (3.13) with the ICI coefficients only ($G_K = 0$) and by simulation by setting the value of the interfering symbol samples to zero. The additional degradation caused by IBI can be noted easily.

In Fig. 3.3, the performance of different subcarriers is shown for BPSK OFDM with $N = 16$, $N_{CP} = 0$ and 2 and time offset equal to 4 samples to the right. The transmission is over the AWGN channel. It can be seen that when $(N_{CP} = 2)$ the subcarriers are divided

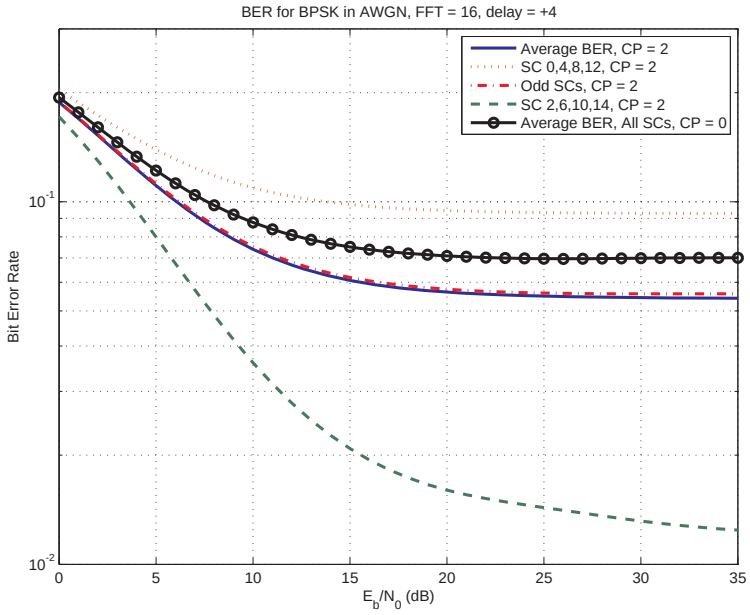

Figure 3.3: Performance of different subcarriers.

into groups with different performance, as expected. On the other hand, all subcarriers have the same performance when there is no CP ($N_{CP} = 0$).

Next, we examine the performance when the time offset is negative (to the left) in AWGN channel. Generally, it can be seen that in the negative time offsets, the CP alleviate the degradation in the performance. Fig. 3.4 shows the performance when the time offset is equal to the CP length. In this case, there is neither ICI nor IBI, and the performance (with phase shift compensation) is the same as there is no time offset. The degradation in performance starts when the time offset exceeds the CP length as can be seen from the figure.

In Fig. 3.5, the performance when the time offset is negative and equal 3 samples to the left, with normalized frequency offset equal 0.1. Also, the performance for transmission over flat fading channel ($L = 1$) is investigated. Moreover, we show performance results when Gaussian approximation (GA) similar to the one adopted in [69] is used to compute the probability of error. The probability of error using GA can be computed by $P_{e,GA} = Q(\sqrt{2\eta_{GA}})$ [69] where η_{GA} is the signal-to-interference-plus-noise-ratio assuming that the interference terms can be approximated by one Gaussian random variable with its power added to the noise power. First, it can be seen that the results from our derived expressions agree with the simulations ones. On the other hand, the GA results are similar to the

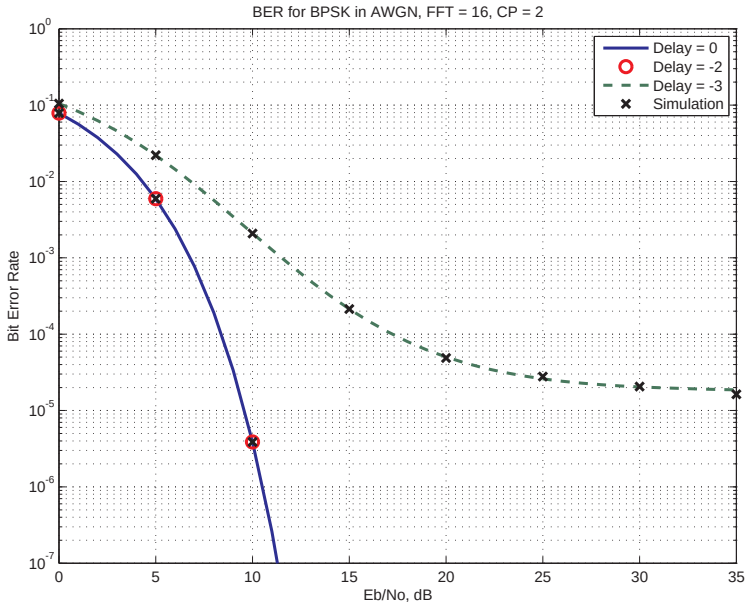

Figure 3.4: Exact BER performance of BPSK OFDM in AWGN channel when time offset is negative.

simulation results in the low SNRs but start to deviate at high SNRs. These remarks are similar to the ones in [74] which showed that the GA is not accurate at high SNRs.

Fig. 3.6 shows the approximate SER for QPSK and 16-QAM OFDM when $N = 256$ for AWGN and flat fading channels when the time offset equals one sample to the right. The results are obtained using the proposed method for approximating the performance with a smaller number of coefficients ($N_a = 7$ for QPSK and $N_a = 4$ for 16-QAM). It can be seen that if the time offset is larger than zero, even if it is less than the CP length, there is degradation in performance compared to the case when there is no time offset. It can also be seen that the results from the proposed method approximated very well the simulation results.

Finally, we investigate the performance of OFDM systems with CFO only. This can be done by setting the value of the integer time offset in the derived expressions to zero. Fig. 3.7 shows the performance of QPSK OFDM systems for transmission over flat fading channel ($L = 1$). When the frequency offset is small $\epsilon = 0.01, 0.1$, our results coincide with the results from the expression in [33] and the simulation results. On the other hand, in high frequency offsets $\epsilon = 0.15, 0.2$, it is clear that our analytical results are similar to the simulation results, while the results obtained from the expression in [33] are not. Lastly,

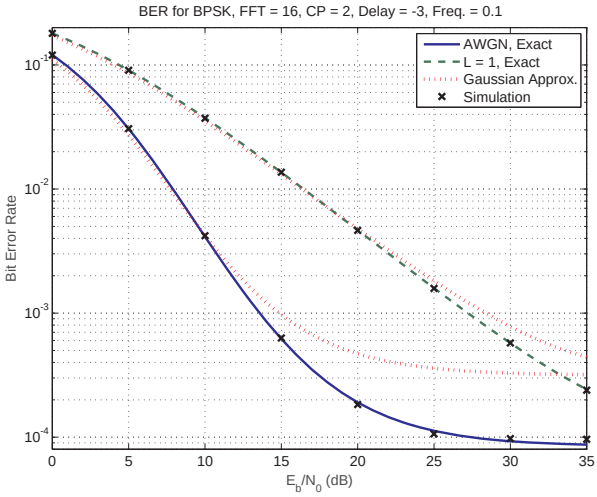

Figure 3.5: BER performance of BPSK OFDM with frequency and negative integer time offsets.

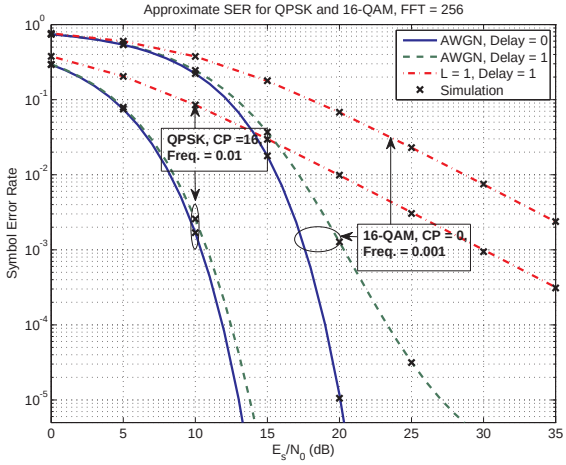

Figure 3.6: Approximate SER performance of QPSK and 16-QAM OFDM for AWGN and flat fading channels when time offset is positive.

Fig. 3.8 shows the SER of 16-QAM OFDM systems with CFO only. The performance is investigated for transmission over Rayleigh flat fading channel since no exact closed-form expressions can be found in the open literature for this case. It can be seen that the analytical and simulation results are matching.

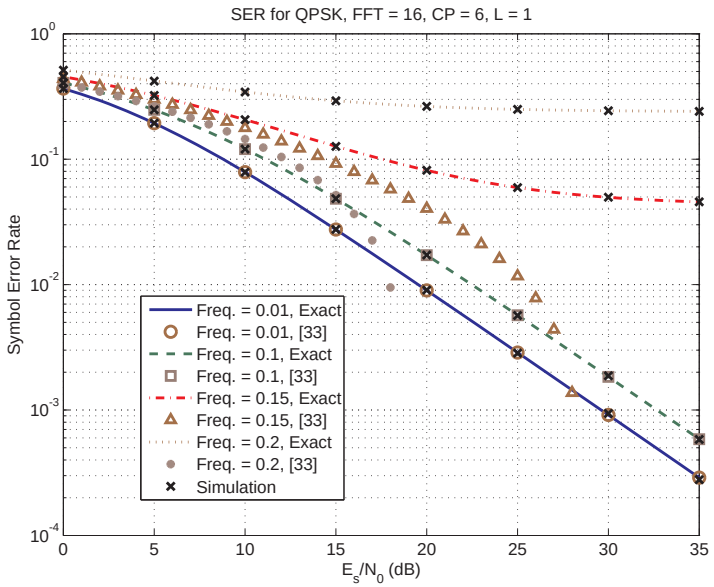

Figure 3.7: SER performance of QPSK OFDM with frequency offset only in Rayleigh flat fading channel.

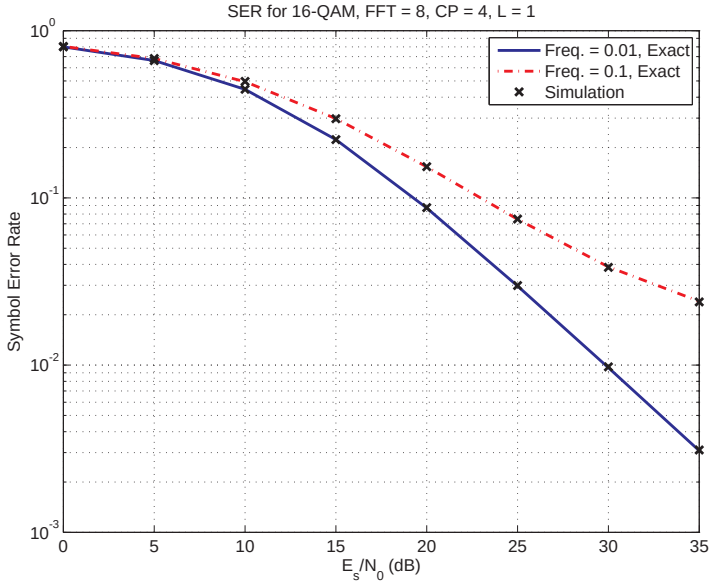

Figure 3.8: SER performance of 16-QAM OFDM with frequency offset only in Rayleigh flat fading channel.

Chapter 4

OFDM Systems with Integer Time and Frequency Offsets in Frequency-Selective Fading Channels

4.1 Effect of the Integer Time and Frequency Offsets for Transmission over Frequency-Selective Rayleigh Fading Channels

In this section, we assume a slow fading quasi-static channel where the channel coherence time is larger than the duration of the OFDM symbol. The channel is modeled by a tapped delay line where the gains of its taps $h(l), l = 0, 1, 2, ..., L-1$, are complex Gaussian random variables with zero mean and uniform power delay profile with $\sigma_h^2(l) = 2\sigma_{R(l)}^2$, where $\sigma_{R(l)}^2$ is the variance per dimension and $\tau = L - 1$ is the maximum delay spread. Therefore, the received signal in the time domain is given by

$$r(n) = \sum_{m} \sum_{l=0}^{L-1} h(l) x_m(n - l - mN_T) + w(n), \tag{4.1}$$

where $N_T = N + N_{CP}$ is the OFDM symbol size and $w(n)$ are the AWGN samples. Then the received signal is divided into blocks y_m of size N_T corresponding to the the transmitted symbols x_m. In case of the frequency-selective fading channels and for OFDM systems with integer time offset that is larger than the CP length, the successive symbols

are mixed together resulting in ISI. In order to evaluate the performance for transmission over these channels using the CHF and following the same procedure as in the AWGN case, the received signal in the frequency domain should be put in the form of (4.2) where the contribution from the desired OFDM symbol to the ISI should be separated from the contribution from the interfering (previous or next) OFDM symbol.

$$R_m(K) = (\boldsymbol{H}_{\text{des}}\boldsymbol{\lambda})^T \boldsymbol{X}_m + (\boldsymbol{H}_{\text{int}}\boldsymbol{\lambda})^T \boldsymbol{X}_{m\pm1} + W_m(K), \tag{4.2}$$

where $\boldsymbol{X}_m = (X_m(0)\ X_m(1)\ ...\ X_m(N-1))^T$ and the two vectors ($\boldsymbol{X}_m$ and $\boldsymbol{X}_{m\pm1}$) are statistically independent. $\boldsymbol{\lambda}$ is the CFR and equals $\mathbf{F}_L\mathbf{h}$ where $\mathbf{h} = (h(0)\ h(1)\ ...\ h(L-1))^T$ and $\mathbf{F}_L$ are the first L columns of the unitary FFT matrix given by $F_L(K,n) = \exp\{-j2\pi Kn/N\}, K, n = 0, 1, ..., N-1$. $\boldsymbol{H}_{\text{des}}$ and $\boldsymbol{H}_{\text{int}}$ are two matrices which include the interference coefficients that depend on the desired OFDM symbol and on the interfering (previous or next) OFDM symbol, respectively. In the rest of this section we will characterize the received signal in the frequency domain for OFDM systems with both positive and negative integer time offsets in a form similar to the one in (4.2).

4.1.1 Positive Integer Time Offset ($\theta > 0$)

When the time offset is to the right, the received signal on subcarrier K in OFDM symbol m in the frequency domain is given by

$$R_m(K) = \sum_{n=0}^{N-\theta-1} y_m(n+\theta) e^{\frac{j2\pi(\epsilon-K)n}{N}} + \sum_{n=N-\theta}^{N-1} y_{m+1}(n-N-N_{CP}+\theta) e^{\frac{j2\pi(\epsilon-K)n}{N}} + W_m(K). \tag{4.3}$$

Due to ISI, the first $\tau = L-1$ samples (maximum delay spread) of y_{m+1} are corrupted and are given by

$$\begin{aligned} z(n) &= z_s(n) + z_p(n) \\ &= t_m(n+N+N_{CP}) + t_{m+1}(n), \quad 0 \le n < \tau \end{aligned} \tag{4.4}$$

where

$$t_m(n) = \sum_{l=0}^{\tau} h(n-l)x_m(n). \tag{4.5}$$

$z_s(n)$ is the contribution to the ISI from the desired OFDM symbol $x_m(n)$ and $z_p(n)$ is the contribution from the next OFDM symbol $x_{m+1}(n)$. Therefore, the received signal in (4.3) can be expressed as

$$\begin{aligned} R_m(K) &= \sum_{n=0}^{N-\theta-1} y_m(n+\theta) e^{\frac{j2\pi(\epsilon-K)n}{N}} + \sum_{n=N-\theta}^{N-\theta+\theta_{\tau p}-1} z(n-N+\theta) e^{\frac{j2\pi(\epsilon-K)n}{N}} \\ &+ \sum_{n=N-\theta+\theta_{\tau p}}^{N-1} y_{m+1}(n-N-N_{CP}+\theta) e^{\frac{j2\pi(\epsilon-K)n}{N}} + W_m(K), \\ &= I_1(K) + I_2(K) + I_3(K) + W_m(K), \end{aligned} \tag{4.6}$$

where $\theta_{\tau p} = \min(\theta, \tau)$ with the assumption that $(\tau < \theta + N_{CP} - 1)$. With some straightforward mathematical manipulations, it can be shown that $I_1(K)$ and $I_3(K)$ can be expressed as follows:

$$\begin{aligned} I_1(K) &= \sum_{n=0}^{N-\theta-1} y_m(n+\theta) e^{\frac{j2\pi(\epsilon-K)n}{N}} \\ &= \frac{1}{N} \sum_{u=0}^{N-1} X_m(u)\lambda(u) e^{\frac{j2\pi\theta u}{N}} \cdot \Gamma_{1P}((K-u)_N), \end{aligned} \tag{4.7}$$

and

$$\begin{aligned} I_3(K) &= \sum_{n=N-\theta+\theta_{\tau p}}^{N-1} y_{m+1}(n-N-N_{CP}+\theta) e^{\frac{j2\pi(\epsilon-K)n}{N}} \\ &= \frac{1}{N} \sum_{u=0}^{N-1} X_{m+1}(u)\lambda(u) e^{\frac{j2\pi(\theta-N_{CP})u}{N}} \cdot \Gamma_{2P_f}((K-u)_N) \end{aligned} \tag{4.8}$$

where $\lambda(u)$ is the u-th element of the vector $\boldsymbol{\lambda}$. Also, $\Gamma_{1P}(u)$ as defined in (3.2) and

$$\Gamma_{2P_f}(u) = \begin{cases} \theta - \theta_{\tau p}, & u = \epsilon \\ \frac{(e^{-j2\pi(\epsilon-u)(\theta-\theta_{\tau p})/N} - 1)}{(1-e^{j2\pi(\epsilon-u)/N})} \cdot e^{j2\pi(\epsilon-u)}, & u \neq \epsilon \end{cases} \tag{4.9}$$

Finally, the ISI effect in the frequency domain can be obtained as

$$I_2(K) = I_s(K) + I_p(K), \tag{4.10}$$

where

$$
\begin{aligned}
I_s(K) &= \sum_{n=N-\theta}^{N-\theta+\theta_{\tau p}-1} z_s(n-N+\theta)e^{\frac{j2\pi(\epsilon-K)n}{N}} \\
&= e^{\frac{j2\pi(\epsilon-K)(N-\theta)}{N}} \sum_{n=0}^{N-1} z_s(n)\gamma_{Ptr}(n)e^{\frac{j2\pi(\epsilon-K)n}{N}} \\
&= \frac{1}{N}e^{\frac{j2\pi(\epsilon-K)(N-\theta)}{N}}[(\lambda(K)\sum_{n=0}^{N-1} x_m(n)\gamma_s(n)e^{\frac{-j2\pi Kn}{N}}) \otimes \Gamma_{Ptr}(K)] \\
&= \frac{1}{N^2}e^{\frac{j2\pi(\epsilon-K)(N-\theta)}{N}}[(\lambda(K)(X_m(K) \otimes \Gamma_s(K))) \otimes \Gamma_{Ptr}(K)] \\
&= \frac{1}{N^2}e^{\frac{j2\pi(\epsilon-K)(N-\theta)}{N}}[\sum_{u_1=0}^{N-1} \Gamma_{Ptr}((K-u_1))_N\lambda(u_1)\sum_{u_2=0}^{N-1} \Gamma_s((u_1-u_2))_N X_m(u_2)], \quad (4.11)
\end{aligned}
$$

and

$$
\begin{aligned}
I_p(K) &= \sum_{n=N-\theta}^{N-\theta+\theta_{\tau p}-1} z_p(n-N+\theta)e^{\frac{j2\pi(\epsilon-K)n}{N}} \\
&= e^{\frac{j2\pi(\epsilon-K)(N-\theta)}{N}} \sum_{n=0}^{N-1} z_p(n)\gamma_{Ptr}(n)e^{\frac{j2\pi(\epsilon-K)n}{N}} \\
&= \frac{1}{N}e^{\frac{j2\pi(\epsilon-K)(N-\theta)}{N}}[(\lambda(K)\sum_{n=0}^{N-1} x_{m+1}(n-N_{CP})\gamma_p(n)e^{\frac{-j2\pi Kn}{N}}) \otimes \Gamma_{Ptr}(K)] \\
&= \frac{1}{N^2}e^{\frac{j2\pi(\epsilon-K)(N-\theta)}{N}}[(\lambda(K)(X_{m+1}(K)e^{\frac{-j2\pi KN_{CP}}{N}} \otimes \Gamma_p(K))) \otimes \Gamma_{Ptr}(K)] \\
&= \frac{1}{N^2}e^{\frac{j2\pi(\epsilon-K)(N-\theta)}{N}}\cdot \\
&\quad [\sum_{u_1=0}^{N-1} \Gamma_{Ptr}((K-u_1))_N\lambda(u_1)\sum_{u_2=0}^{N-1} \Gamma_p((u_1-u_2))_N X_{m+1}(u_2)e^{\frac{-j2\pi u_2 N_{CP}}{N}}]. \quad (4.12)
\end{aligned}
$$

$\gamma_s(n)$, $\gamma_p(n)$, and $\gamma_{Ptr}(n)$ are three rectangular windows defined as follows:

$$
\gamma_s(n) = \begin{cases} 1, & N-\tau \le n \le N-1 \\ 0, & otherwise \end{cases}, \quad \gamma_p(n) = \begin{cases} 1, & 0 \le n \le \tau-1 \\ 0, & otherwise \end{cases},
$$

$$
\gamma_{Ptr}(n) = \begin{cases} 1, & 0 \le n \le \theta_{\tau p}-1 \\ 0, & otherwise \end{cases}.
$$

$\Gamma_s(u)$ and $\Gamma_p(u)$ are the samples of the DFTs of $\gamma_s(n)$ and $\gamma_p(n)$ as computed in (4.13) and (4.14), respectively, and $\Gamma_{Ptr}(u)$ are the samples of the DFT of $\gamma_{Ptr}(n) \cdot e^{\frac{j2\pi\epsilon n}{N}}$ as computed in (4.15).

$$\Gamma_s(u) = \begin{cases} \tau, & u = 0 \\ \frac{(e^{j2\pi u\tau/N}-1)}{(1-e^{-j2\pi u/N})}, & u \neq 0 \end{cases}, \tag{4.13}$$

$$\Gamma_p(u) = \Gamma_s(u) e^{-j2\pi u\tau/N}, \tag{4.14}$$

$$\Gamma_{Ptr}(u) = \begin{cases} \theta_{\tau p}, & u = \epsilon \\ \frac{(1-e^{j2\pi(\epsilon-u)\theta_{\tau p}/N})}{(1-e^{j2\pi(\epsilon-u)/N})}, & u \neq \epsilon \end{cases}. \tag{4.15}$$

Combining (4.7), (4.8), (4.11), and (4.12) and putting the equations in a matrix form, the received signal on subcarrier K can be expressed as

$$\begin{aligned} R_m(K) = {} & \boldsymbol{C}_{P,K}(\boldsymbol{\lambda} \circ \boldsymbol{X}_m) + \boldsymbol{Z}_{P,K}(\boldsymbol{\lambda} \circ (\boldsymbol{T}_s\ \boldsymbol{X}_m)) \\ & + \boldsymbol{B}_{P,K}(\boldsymbol{\lambda} \circ \boldsymbol{X}_{m+1}) + \boldsymbol{Z}_{P,K}(\boldsymbol{\lambda} \circ (\boldsymbol{T}_p\ \boldsymbol{X}_{m+1})) + W_m(K), \end{aligned} \tag{4.16}$$

where $\circ$ denotes the Hadamard product. $\boldsymbol{C}_{P,K}$, $\boldsymbol{B}_{P,K}$, and $\boldsymbol{Z}_{P,K}$ are the K-th rows of the matrices $\boldsymbol{C}_P$, $\boldsymbol{B}_P$, and $\boldsymbol{Z}_P$, respectively, which are defined in (4.17). Also, $\boldsymbol{T}_s$ and $\boldsymbol{T}_p$ are defined in (4.17).

$$\begin{aligned} [C_P]_{K,u} &= \frac{1}{N}\Gamma_{1P}((K-u)_N) e^{j2\pi\theta u/N}, \\ [B_P]_{K,u} &= \frac{1}{N}\Gamma_{2P_f}((K-u)_N) e^{j2\pi(\theta-N_{CP})u/N}, \\ [Z_P]_{K,u_1} &= \frac{1}{N^2}\Gamma_{Ptr}((K-u_1)_N) e^{\frac{j2\pi(\epsilon-K)(N-\theta)}{N}}, \\ [T_p]_{u_1,u_2} &= \frac{1}{N}\Gamma_p((u_1-u_2)_N) e^{-j2\pi N_{CP}u_2/N}, \text{and} \\ [T_s]_{u_1,u_2} &= \frac{1}{N}\Gamma_s((u_1-u_2)_N). \end{aligned} \tag{4.17}$$

Finally, by rearranging the terms in (4.16), the received signal on subcarrier K can be expressed as

$$R_m(K) = (\boldsymbol{H}_{\text{des}}\boldsymbol{\lambda})^T \boldsymbol{X}_m + (\boldsymbol{H}_{\text{int}}\boldsymbol{\lambda})^T \boldsymbol{X}_{m+1} + W_m(K), \tag{4.18}$$

where

$$\begin{aligned} \boldsymbol{H}_{\text{des}} &= \boldsymbol{H}_{\text{ICI},K} + \boldsymbol{H}_{\text{ISI}_s,K}, \\ \boldsymbol{H}_{\text{int}} &= \boldsymbol{H}_{\text{IBI},K} + \boldsymbol{H}_{\text{ISI}_p,K}, \end{aligned} \tag{4.19}$$

and $\boldsymbol{H}_{\text{ICI},K} = \text{diag}(\boldsymbol{C}_{P,K})$, $\boldsymbol{H}_{\text{IBI},K} = \text{diag}(\boldsymbol{B}_{P,K})$, $\boldsymbol{H}_{\text{ISI}_s,K} = (\boldsymbol{Z}_{P,K}^T \boldsymbol{J}_N)^T \circ \boldsymbol{T}_s^T$, and $\boldsymbol{H}_{\text{ISI}_p,K} = (\boldsymbol{Z}_{P,K}^T \boldsymbol{J}_N)^T \circ \boldsymbol{T}_p^T$, where $\boldsymbol{J}_N$ is a row vector of all ones of size N.

4.1.2 Negative Integer Time Offset ($\theta \leq 0$)

When the time offset is to the left, the received signal on subcarrier K in OFDM symbol m in the frequency domain is given by

$$\begin{aligned} R_m(K) = &\sum_{n=0}^{\theta_{CP}-1} y_{m-1}(n+N-\theta_{CP}) e^{\frac{j2\pi(\epsilon-K)n}{N}} + \sum_{n=\theta_{CP}}^{\theta_{CP}+\theta_{\tau n}-1} z(n-\theta_{CP}) e^{\frac{j2\pi(\epsilon-K)n}{N}} \\ &+ \sum_{n=\theta_{CP}+\theta_{\tau n}}^{N-1} y_m(n-N_{CP}-\theta_{CP}) e^{\frac{j2\pi(\epsilon-K)n}{N}} + W_m(K), \end{aligned} \tag{4.20}$$

where $\theta_{\tau n} = L - 1 + \theta_{CP_m}$ and $\theta_{CP_m} = \min(-\theta - N_{CP}, 0)$. Again, $z(n)$ are the ISI samples that can be decomposed into two parts,

$$\begin{aligned} z(n) &= z_s(n) + z_p(n) \\ &= t_{m-1}(n+N+N_{CP}) + t_m(n), \quad 0 \leq n < \tau \end{aligned} \tag{4.21}$$

where $z_s(n)$ is the contribution from the previous OFDM symbol to the ISI, $z_p(n)$ is the contribution from the desired OFDM symbol and t_m is as defined in (4.5).

Following the same procedure as in the previous section, the received signal on subcarrier K can be expressed as

$$R_m(K) = (\boldsymbol{H}_{\text{des}} \boldsymbol{\lambda})^T \boldsymbol{X}_m + (\boldsymbol{H}_{\text{int}} \boldsymbol{\lambda})^T \boldsymbol{X}_{m-1} + W_m(K), \tag{4.22}$$

where

$$\begin{aligned} \boldsymbol{H}_{\text{des}} &= \boldsymbol{H}_{\text{ICI},K} + \boldsymbol{H}_{\text{ISI}_p,K} \\ \boldsymbol{H}_{\text{int}} &= \boldsymbol{H}_{\text{IBI},K} + \boldsymbol{H}_{\text{ISI}_s,K}, \end{aligned} \tag{4.23}$$

$\boldsymbol{H}_{\text{ICI},K} = \text{diag}(\boldsymbol{C}_{N,K})$, $\boldsymbol{H}_{\text{IBI},K} = \text{diag}(\boldsymbol{B}_{N,K})$, $\boldsymbol{H}_{\text{ISI}_s,K} = (\boldsymbol{Z}_{N,K}^T \boldsymbol{J}_N)^T \circ \boldsymbol{T}_s^T$, and $\boldsymbol{H}_{\text{ISI}_p,K} = (\boldsymbol{Z}_{N,K}^T \boldsymbol{J}_N)^T \circ \boldsymbol{T}_p^T$, where $\boldsymbol{T}_s$, $\boldsymbol{T}_p$ are defined in (4.17). $\boldsymbol{C}_{N,K}$, $\boldsymbol{B}_{N,K}$, and $\boldsymbol{Z}_{N,K}$ are the K-th rows of the matrices $\boldsymbol{C}_N$, $\boldsymbol{B}_N$, and $\boldsymbol{Z}_N$, respectively, which are given by

$$\begin{aligned}
[C_N]_{K,u} &= \frac{1}{N}\Gamma_{1N_f}((K-u)_N)e^{j2\pi\theta u/N}, \\
[B_N]_{K,u} &= \frac{1}{N}\Gamma_{2N}((K-u)_N)e^{j2\pi(\theta+N_{CP})u/N}, \text{and} \\
[Z_N]_{K,u_1} &= \frac{1}{N^2}\Gamma_{ntr}((K-u_1)_N)e^{j2\pi(\epsilon-K)(\theta_{CP}+\theta_{CP_m})K/N},
\end{aligned} \tag{4.24}$$

where

$$\Gamma_{1N_f}(u) = \begin{cases} N-(\theta_{CP}+\theta_{\tau n}), & u=\epsilon \\ \frac{(1-e^{j2\pi(\epsilon-u)(N-(\theta_{CP}+\theta_{\tau n}))/N})}{(1-e^{j2\pi(\epsilon-u)/N})} \cdot e^{j2\pi(\epsilon-u)(\theta_{CP}+\theta_{\tau n})/N}, & u\neq\epsilon \end{cases},$$

$$\Gamma_{ntr}(u) = \begin{cases} \theta_{\tau n}, & u=\epsilon \\ \frac{(1-e^{j2\pi(\epsilon-u)\theta_{\tau n}/N})}{(1-e^{j2\pi(\epsilon-u)/N})}, & u\neq\epsilon \end{cases},$$

and $\Gamma_{2N}(u)$ is as defined in (3.7). It can be noted from (4.18) and (4.22) that in the absence of ISI, or in the case of AWGN or flat fading channels the two matrices $\boldsymbol{H}_{\text{des}}$ and $\boldsymbol{H}_{\text{int}}$ are diagonal and the ICI and the IBI coefficients are their diagonal entries, respectively.

4.2 BER/SER of OFDM with Integer Time and Frequency Offsets in Frequency-Selective Rayleigh Fading Channels

Now, both (4.18) and (4.22) can be put in the form of (4.2). Let $\boldsymbol{V} = \boldsymbol{H}\boldsymbol{\lambda}$, where $[H]_{m,n}$ is the (m,n)-th element of the matrix $\boldsymbol{H}$, which is defined as:

$$\begin{aligned}
[H]_{m,n} &= [H_{\text{des}}]_{m,n} \\
[H]_{m+N,n} &= [H_{\text{int}}]_{m,n} \quad 0 \le m,n \le N-1.
\end{aligned} \tag{4.25}$$

Then the received signal on subcarrier K after equalization is given by

$$V^*(K)R_m(K) = |V(K)|^2 X_m(K) + V^*(K)\bar{\boldsymbol{V}}^T\bar{\boldsymbol{X}} + V^*(K)W_m(K), \tag{4.26}$$

where $(\cdot)^*$ denotes the complex conjugate operation. $\bar{\boldsymbol{V}} = [V]_{n,n\neq K}$ and $\bar{\boldsymbol{X}} = [X]_{n,n\neq K}, 0 \leq n \leq 2N-1$ where $[V]_n$ is the n-th element of the vector $\boldsymbol{V}$ and $[X]_n$ is the n-th element of the vector $\boldsymbol{X}$, which is defined as

$$[X]_K = [X_m]_K, \quad [X]_{K+N} = [X_{m\pm1}]_K, \quad 0 \leq K \leq N-1. \tag{4.27}$$

BPSK Modulation

Without loss of generality, we assume that the value of the transmitted symbol on the desired subcarrier K is equal to 1 ($X_m(K) = 1$) and, since the modulation is BPSK, only the real part of the received signal is considered:

$$\Re(V^*(K)R_m(K)) = |V(K)|^2 + \Re(V^*(K)\bar{\boldsymbol{V}}^T)\bar{\boldsymbol{X}} + \Re(V^*(K)W_m(K)), \tag{4.28}$$

and its conditional CHF is given by

$$\varphi_{\Re(V^*(K)R_m(K))}(\omega) = \frac{1}{2^M}\sum_{i=1}^{2^{M-1}}(e^{j\omega[|V(K)|^2+z_{i,K}]-\omega^2\sigma_v^2/2} + e^{j\omega[|V(K)|^2-z_{i,K}]-\omega^2\sigma_v^2/2}), \tag{4.29}$$

where $z_{i,K} = \Re(V^*(K)\bar{\boldsymbol{V}}\boldsymbol{e}_i)$ and $\sigma_v = |V(K)|\sigma$. Following the same procedure as in the AWGN case, the conditional BER given $\bar{\boldsymbol{V}}$ and $V(K)$ can be expressed as

$$P_{e|\bar{\boldsymbol{V}},V(K)} = \frac{1}{N(2^M)}\sum_{K=0}^{N-1}\sum_{i=1}^{2^{M-1}} Q\Big(\frac{|V(K)|^2 + z_{i,K}}{\sigma_v}\Big) + Q\Big(\frac{|V(K)|^2 - z_{i,K}}{\sigma_v}\Big). \tag{4.30}$$

Following [63], and since the linear transformation of a multivariate complex Gaussian random variable is another multivariate complex Gaussian random variable, the conditional distribution $f_{\bar{\boldsymbol{V}}|V(K)}(\bar{\boldsymbol{V}}|V(K))$ is Gaussian with mean and covariance given by [89].

$$\begin{aligned} E(\bar{\boldsymbol{V}}|V(K)) &= V(K)C^{-1}_{V(K)V(K)}\boldsymbol{C}_{\bar{\boldsymbol{V}}V(K)}, \\ \boldsymbol{C}_{\bar{\boldsymbol{V}}|V(K)} &= \boldsymbol{C}_{\bar{\boldsymbol{V}}\bar{\boldsymbol{V}}} - C^{-1}_{V(K)V(K)}\boldsymbol{C}_{\bar{\boldsymbol{V}}V(K)}\boldsymbol{C}^H_{\bar{\boldsymbol{V}}V(K)}. \end{aligned} \tag{4.31}$$

$E(\cdot)$ denotes the expectation operation and

$$\boldsymbol{C}_V = E\{\boldsymbol{V}\boldsymbol{V}^H\} = (\boldsymbol{H}\mathbf{F}_L)\boldsymbol{C}_h(\boldsymbol{H}\mathbf{F}_L)^H, \tag{4.32}$$

where $(\cdot)^H$ denotes the Hermitian transpose operation and $\boldsymbol{C}_h$ is the time-domain channel covariance matrix.

Following [33], and by defining the random variable $(z_{i,K}|V(K))$, which is Gaussian with mean $|V(K)|^2\mu_{i,K}$ and variance $\frac{1}{2}|V(K)|^2\nu_{i,K}$, which can be computed from (4.31) where $\mu_{i,K} = C^{-1}_{V(K)V(K)}\Re(\boldsymbol{C}_{\bar{\boldsymbol{V}}V(K)}\boldsymbol{e}_i)$ and $\nu_{i,K} = \boldsymbol{e}_i\boldsymbol{C}_{\bar{\boldsymbol{V}}|V(K)}\boldsymbol{e}_i^T$, the conditional BER given $V(K)$ can be expressed as

$$P_{e|V(K)} = \frac{1}{N(2^M)}\sum_{K=0}^{N-1}\sum_{i=1}^{2^{M-1}} Q\Big(\frac{|V(K)|(1+\mu_{i,K})}{\sigma\sqrt{1+\frac{\nu_{i,K}}{2\sigma^2}}}\Big) + Q\Big(\frac{|V(K)|(1-\mu_{i,K})}{\sigma\sqrt{1+\frac{\nu_{i,K}}{2\sigma^2}}}\Big). \tag{4.33}$$

Using the identity in [88, eq. 2.8.5.9], the BER can be evaluated by integrating the conditional distribution in (4.33) over the Rayleigh distribution with $\sigma_R^2 = C_{V(K)V(K)}/2$. Therefore, the BER can be obtained as

$$\begin{aligned}\bar{P}_e = \frac{1}{2} - \frac{1}{N2^{M+1}}\sum_{K=0}^{N-1}\sum_{i=1}^{2^{M-1}} &(1+\mu_{i,K})\sqrt{\frac{2\sigma_R^2\eta}{1+2\sigma_R^2\eta[1+\mu_{i,K}]^2+\nu_{i,K}}} \\ &+ (1-\mu_{i,K})\sqrt{\frac{2\sigma_R^2\eta}{1+2\sigma_R^2\eta[1-\mu_{i,K}]^2+\nu_{i,K}}}.\end{aligned} \tag{4.34}$$

QPSK Modulation

Following the same procedure as in the previous section and using (3.22) and (4.30), the conditional SER given $\bar{\boldsymbol{V}}$ and $V(K)$ can be obtained as

$$\begin{aligned}P_{s|\bar{\boldsymbol{V}},V(K)} = 1 - \frac{1}{N2^{2M}}&\sum_{K=0}^{N-1}\sum_{i1=1}^{2^{M-1}}\sum_{i2=1}^{2^{M-1}}\sum_{m=1}^{4} \\ &Q\left\{\frac{-\Big(|V(K)|^2 + z_{i1,i2,K}[1,m]\Big)}{\sigma_v}\right\} \times Q\left\{\frac{-\Big(|V(K)|^2 + z_{i1,i2,K}[2,m]\Big)}{\sigma_v}\right\}\end{aligned} \tag{4.35}$$

where $z_{i1,i2,K}[n,m]$ is the (n,m)-th element of the 2x4 matrix $\mathbf{Z}_K$, which is defined as $\mathbf{Z}_K = \big((\mathbf{Z}_{A,K}+\mathbf{Z}_{B,K})\ (-\mathbf{Z}_{A,K}-\mathbf{Z}_{B,K})\ (\mathbf{Z}_{A,K}-\mathbf{Z}_{B,K})\ (-\mathbf{Z}_{A,K}+\mathbf{Z}_{B,K})\big)$, and

$$\begin{aligned}[\mathbf{Z}_{A,K}] = &\quad (\Re(V^*(K)\mathbf{e}_{i1}^T\bar{\boldsymbol{V}}) \quad \Im(V^*(K)\mathbf{e}_{i1}^T\bar{\boldsymbol{V}}))^T, \\ [\mathbf{Z}_{B,K}] = &\ (\Im(V^*(K)\mathbf{e}_{i2}^T\bar{\boldsymbol{V}}) \quad -\Re(V^*(K)\mathbf{e}_{i2}^T\bar{\boldsymbol{V}}))^T.\end{aligned}$$

As in the previous section, the conditional SER given $V(K)$ can be expressed as

$$P_{s|V(K)} = 1 - \frac{1}{N2^{2M}} \sum_{K=0}^{N-1} \sum_{i1=1}^{2^{M-1}} \sum_{i2=1}^{2^{M-1}} \sum_{m=1}^{4} Q\left\{ \frac{-\Big(|V(K)|\big[1+\mu_{i1,i2,K}[1,m]\big]\Big)}{\sigma\sqrt{1+\frac{\nu_{i1,i2,K}[m]}{2\sigma^2}}} \right\} \times Q\left\{ \frac{-\Big(|V(K)|\big[1+\mu_{i1,i2,K}[2,m]\big]\Big)}{\sigma\sqrt{1+\frac{\nu_{i1,i2,K}[m]}{2\sigma^2}}} \right\}, \tag{4.36}$$

where $\mu_{i1,i2,K}[n,m]$ is the (n,m)-th element of the 2x4 matrix $\mathbf{M}_K = \big((\mathbf{M}_{A,K}+\mathbf{M}_{B,K})\ (-\mathbf{M}_{A,K}-\mathbf{M}_{B,K})\ (\mathbf{M}_{A,K}-\mathbf{M}_{B,K})\ (-\mathbf{M}_{A,K}+\mathbf{M}_{B,K})\big)$,

$$[\mathbf{M}_{A,K}] = C^{-1}_{V(K)V(K)} \left(\Re(\mathbf{e}_{i1}^T \mathbf{C}_{\bar{\boldsymbol{V}}V(K)})\ \Im(\mathbf{e}_{i1}^T \mathbf{C}_{\bar{\boldsymbol{V}}V(K)})\right)^T,$$
$$[\mathbf{M}_{B,K}] = C^{-1}_{V(K)V(K)} \left(\Im(\mathbf{e}_{i2}^T \mathbf{C}_{\bar{\boldsymbol{V}}V(K)})\ -\Re(\mathbf{e}_{i2}^T \mathbf{C}_{\bar{\boldsymbol{V}}V(K)})\right)^T,$$

and $\nu_{i1,i2,K}[m]$ is the m-th element of the 1x4 vector $\boldsymbol{V}_K = (\boldsymbol{V1}_K\ \boldsymbol{V2}_K\ \boldsymbol{V3}_K\ \boldsymbol{V4}_K)$, where

$$\begin{aligned}
\boldsymbol{V1}_K &= (\mathbf{e}_{i1}+\mathbf{e}_{i2})\boldsymbol{C}_{\bar{\boldsymbol{V}}|V(K)}(\mathbf{e}_{i1}+\mathbf{e}_{i2})^T,\\
\boldsymbol{V2}_K &= (-\mathbf{e}_{i1}-\mathbf{e}_{i2})\boldsymbol{C}_{\bar{\boldsymbol{V}}|V(K)}(-\mathbf{e}_{i1}-\mathbf{e}_{i2})^T,\\
\boldsymbol{V3}_K &= (\mathbf{e}_{i1}-\mathbf{e}_{i2})\boldsymbol{C}_{\bar{\boldsymbol{V}}|V(K)}(\mathbf{e}_{i1}-\mathbf{e}_{i2})^T, \text{and}\\
\boldsymbol{V4}_K &= (-\mathbf{e}_{i1}+\mathbf{e}_{i2})\boldsymbol{C}_{\bar{\boldsymbol{V}}|V(K)}(-\mathbf{e}_{i1}+\mathbf{e}_{i2})^T.
\end{aligned} \tag{4.37}$$

Finally, the SER can be evaluated by averaging (4.36) using (3.27) with $\sigma_R^2 = C_{V(K)V(K)}/2$. Therefore, the SER of OFDM systems employing QPSK for transmission over frequency-selective Rayleigh fading channels can be obtained as

$$\begin{aligned}
\bar{P}_s = \frac{3}{4} - \frac{1}{N2^{2M+1}} \sum_{K=0}^{N-1} \sum_{i1=1}^{2^{M-1}} \sum_{i2=1}^{2^{M-1}} \sum_{m=1}^{4} &\Delta_1 \cdot \psi_{i1,i2,K}[1,m]\big(\frac{1}{2}+\frac{1}{\pi}\arctan\{\Delta_1 \cdot \psi_{i1,i2,K}[2,m]\}\big)\\
&+ \Delta_2 \cdot \psi_{i1,i2,K}[2,m]\big(\frac{1}{2}+\frac{1}{\pi}\arctan\{\Delta_2 \cdot \psi_{i1,i2,K}[1,m]\}\big),
\end{aligned} \tag{4.38}$$

where

$$\Delta_1 = \sqrt{\frac{2\sigma_R^2\eta}{1+\eta\nu_{i1,i2,K}[m]+2\sigma_R^2\eta\psi^2_{i1,i2,K}[1,m]}}, \Delta_2 = \sqrt{\frac{2\sigma_R^2\eta}{1+\eta\nu_{i1,i2,K}[m]+2\sigma_R^2\eta\psi^2_{i1,i2,K}[2,m]}}$$

$\psi_{i1,i2,K}[n,m]$ is the (n,m)-th element of the 2x4 matrix $\Psi_K = \mathbf{D} + \mathbf{M}_K$ and $\boldsymbol{D} = (1\ \ 1)^T$.

16-QAM Modulation

Following the same procedure as in the BPSK and QPSK cases, the conditional SER given $V(K)$ can be expressed as

$$P_{s|V(K)} = 1 - \frac{1}{4N \times 2^{4M}} \sum_{K=0}^{N-1} \sum_{i1=1}^{2^{M-1}} \sum_{i2=1}^{2^{M-1}} \sum_{i3=1}^{2^{M-1}} \sum_{i4=1}^{2^{M-1}} \sum_{d=1}^{4}$$
$$\{Q(-\kappa_1^1(0)) \times Q(-\kappa_2^1(0))\} - \{Q(-\kappa_1^1(0)) \times Q(-\kappa_2^1(2))\} - \{Q(-\kappa_1^1(2)) \times Q(-\kappa_2^1(0))\}$$
$$+ \{Q(-\kappa_1^1(2)) \times Q(-\kappa_2^1(2))\} + \{Q(-\kappa_1^2(0)) \times Q(-\kappa_2^2(2))\} - \{Q(-\kappa_1^2(2)) \times Q(-\kappa_2^2(2))\}$$
$$+ \{Q(-\kappa_1^3(2)) \times Q(-\kappa_2^3(0))\} - \{Q(-\kappa_1^3(2)) \times Q(-\kappa_2^3(2))\} + \{Q(-\kappa_1^4(2)) \times Q(-\kappa_2^4(2))\}, \tag{4.39}$$

where

$$\kappa_1^i(a) = \frac{|V(K)|(D^i(1) + \mu_{i1,i2,i3,i4,K}[1,d] - a)}{\sigma\sqrt{1 + \frac{\nu_{i1,i2,i3,i4,K}[d]}{2\sigma^2}}},$$
$$\kappa_2^i(a) = \frac{|V(K)|(D^i(2) + \mu_{i1,i2,i3,i4,K}[2,d] - a)}{\sigma\sqrt{1 + \frac{\nu_{i1,i2,i3,i4,K}[d]}{2\sigma^2}}}, \tag{4.40}$$

$\mathbf{D}^1 = (1\ \ 1)^T$, $\mathbf{D}^2 = (1\ \ 3)^T$, $\mathbf{D}^3 = (3\ \ 1)^T$, and $\mathbf{D}^4 = (3\ \ 3)^T$. $\nu_{i1,i2,i3,i4,K}[d] = E_d \boldsymbol{C}_{\bar{\boldsymbol{V}}|V(K)} E_d^*$ where $E_d = \mathbf{E}\mathbf{e}_d$ and $\mathbf{E} = (\mathbf{e}_{i1}\ 2\mathbf{e}_{i2}\ \mathbf{e}_{i3}\ 2\mathbf{e}_{i4})$. Also, $[\mu_{i1,i2,i3,i4,K}]_{2\times 1} = \mathbf{M}_K \mathbf{e}_d$ where $\mathbf{M}_K = (\mathbf{M}_{A,K}\mathbf{e}_{i1}\ 2\mathbf{M}_{A,K}\mathbf{e}_{i2}\ \mathbf{M}_{B,K}\mathbf{e}_{i3}\ 2\mathbf{M}_{B,K}\mathbf{e}_{i4})$,

$$[\mathbf{M}_{A,K}] = C_{V(K)V(K)}^{-1} \left(\Re(\mathbf{C}_{\bar{\boldsymbol{V}}V(K)})\ \Im(\mathbf{C}_{\bar{\boldsymbol{V}}V(K)})\right)^T, \text{and}$$
$$[\mathbf{M}_{B,K}] = C_{V(K)V(K)}^{-1} \left(\Im(\mathbf{C}_{\bar{\boldsymbol{V}}V(K)})\ -\Re(\mathbf{C}_{\bar{\boldsymbol{V}}V(K)})\right)^T.$$

As in the QPSK case, the SER can be evaluated by averaging (4.39) using (3.27) with $\sigma_R^2 = C_{V(K)V(K)}/2$. Therefore, the SER of OFDM systems employing 16-QAM for transmission

over frequency-selective Rayleigh fading channels can be obtained as

$$\begin{aligned}
\bar{P}_s = \frac{3}{4} - \frac{1}{4N \times 2^{4M+1}} \sum_{K=0}^{N-1} \sum_{i1=1}^{2^{M-1}} \sum_{i2=1}^{2^{M-1}} \sum_{i3=1}^{2^{M-1}} \sum_{i4=1}^{2^{M-1}} \sum_{d=1}^{16} \\
\left\{\Delta_1^1(0) \cdot \psi_1^1(0) \cdot g(\Delta_1^1(0) \cdot \psi_2^1(0)) + \Delta_2^1(0) \cdot \psi_2^1(0) \cdot g(\Delta_2^1(0) \cdot \psi_1^1(0))\right\} \\
- \left\{\Delta_1^1(0) \cdot \psi_1^1(0) \cdot g(\Delta_1^1(0) \cdot \psi_2^1(2)) + \Delta_2^1(2) \cdot \psi_2^1(2) \cdot g(\Delta_2^1(2) \cdot \psi_1^1(0))\right\} \\
- \left\{\Delta_1^1(2) \cdot \psi_1^1(2) \cdot g(\Delta_1^1(2) \cdot \psi_2^1(0)) + \Delta_2^1(0) \cdot \psi_2^1(0) \cdot g(\Delta_2^1(0) \cdot \psi_1^1(2))\right\} \\
+ \left\{\Delta_1^1(2) \cdot \psi_1^1(2) \cdot g(\Delta_1^1(2) \cdot \psi_2^1(2)) + \Delta_2^1(2) \cdot \psi_2^1(2) \cdot g(\Delta_2^1(2) \cdot \psi_1^1(2))\right\} \\
+ \left\{\Delta_1^2(0) \cdot \psi_1^2(0) \cdot g(\Delta_1^2(0) \cdot \psi_2^2(2)) + \Delta_2^2(2) \cdot \psi_2^2(2) \cdot g(\Delta_2^2(2) \cdot \psi_1^2(0))\right\} \\
- \left\{\Delta_1^2(2) \cdot \psi_1^2(2) \cdot g(\Delta_1^2(2) \cdot \psi_2^1(2)) + \Delta_2^2(2) \cdot \psi_2^2(2) \cdot g(\Delta_2^2(2) \cdot \psi_1^2(2))\right\} \\
+ \left\{\Delta_1^3(2) \cdot \psi_1^3(2) \cdot g(\Delta_1^3(2) \cdot \psi_2^3(0)) + \Delta_2^3(0) \cdot \psi_2^3(0) \cdot g(\Delta_2^3(0) \cdot \psi_1^3(2))\right\} \\
- \left\{\Delta_1^3(2) \cdot \psi_1^3(2) \cdot g(\Delta_1^3(2) \cdot \psi_2^3(2)) + \Delta_2^3(2) \cdot \psi_2^3(2) \cdot g(\Delta_2^3(2) \cdot \psi_1^3(2))\right\} \\
+ \left\{\Delta_1^4(2) \cdot \psi_1^4(2) \cdot g(\Delta_1^4(2) \cdot \psi_2^4(2)) + \Delta_2^4(2) \cdot \psi_2^4(2) \cdot g(\Delta_2^4(2) \cdot \psi_1^4(2))\right\}, \qquad (4.41)
\end{aligned}$$

where $\psi_1^i(a) = D^i(1) + \mu_{i1,i2,i3,i4,K}[1,d] - a$, $\psi_2^i(a) = D^i(2) + \mu_{i1,i2,i3,i4,K}[2,d] - a$,

$$\Delta_1^i(a) = \sqrt{\frac{\sigma_R^2 \bar{\eta}_s/5}{1 + \sigma_R^2 \bar{\eta}_s (\psi_1^i(a))^2/5 + \nu_{i1,i2,i3,i4,K}[d]\bar{\eta}_s/5}},$$

and

$$\Delta_2^i(a) = \sqrt{\frac{\sigma_R^2 \bar{\eta}_s/5}{1 + \sigma_R^2 \bar{\eta}_s (\psi_2^i(a))^2/5 + \nu_{i1,i2,i3,i4,K}[d]\bar{\eta}_s/5}}.$$

In case of flat fading channels, it can be noted that (4.34), (4.38), and (4.41) can be reduced easily to (3.21), (3.28), and (3.35), respectively. This can be explained by noting that in the case of flat fading channels, the frequency-domain channel covariance matrix $\boldsymbol{C} = \mathbf{F}_L \boldsymbol{C}_h \mathbf{F}_L^H$ is a matrix of all ones and hence the covariance matrix in (4.32) will be $\boldsymbol{C}_V = \boldsymbol{H}\boldsymbol{C}\boldsymbol{H}^H$. This results in the conditional covariance matrix $\boldsymbol{C}_{\bar{\boldsymbol{V}}|V(K)}$ in (4.31) being a matrix of all zeros and hence both $\nu_{i,K}$ and $\nu_{i1,i2,K}[m]$ in (4.34) and (4.38) are equal to zero, respectively.

4.3 Approximate Method for BER/SER Evaluation in Frequency-Selective Rayleigh Fading Channels

The same approach employed in Section 3.3 can be used for frequency-selective fading channels, but the way that is used to approximate the discarded coefficients is different because of the correlation introduced by frequency-selective fading. In this case, instead of computing the power of the discarded coefficients and adding it to the noise power, a compensation term is computed. The compensation term is computed in a way that assures that the product of the cosines of all the interfering coefficients have the same value as the product of the cosines of the chosen coefficients multiplied by the cosine of the compensation term. The evaluation is performed using the following computational algorithm.

Computational Algorithm:

- Compute the same function $F_1(l)$ used in the AWGN case, but using coefficients $S_K(l) = V^*(K)\bar{\boldsymbol{V}}^T$, $(l = 1, 2, ..., M)$, where $\boldsymbol{V} = \boldsymbol{H}\boldsymbol{\lambda}$ and $\boldsymbol{\lambda} = \mathbf{F}_L\mathbf{h}$. As an approximation, $\mathbf{h}$ is assumed to be equal to the square-root of the channel power delay profile $(\sigma_h(0)\ \sigma_h(1)\ ...\ \sigma_h(L-1))^T$.
- let $\bar{\boldsymbol{H}}$ be the matrix $\boldsymbol{H}$ defined in (4.25), but without the row K.
- Sort the coefficients $S_K(l)$ and the rows of the matrix $\bar{\boldsymbol{H}}$ in ascending order according to the value of $F_1(l)$: $S_K(l) \rightarrow \widehat{S}_K(l)$ and $\boldsymbol{H} \rightarrow \hat{\bar{\boldsymbol{H}}}$.
- Determine the number of coefficients that will be used in the evaluation of the BER/SER (N_a).
- Compute the same function $F_1(l)$ but for each of the sorted coefficients $(\widehat{S}_K(l))$, $(l = 1, 2, ..., N_a - 1)$ and let the result equal $F_2(l)$.
- Compute the following two product terms:
  For BPSK: $P_1 = \cos(|V(K)|^2) \cdot \Pi_{l=1}^{M} F_1(l)$, $P_2 = \cos(|V(K)|^2) \cdot \Pi_{l=1}^{N_a-1} F_2(l)$,
  For QPSK: $P_1 = \cos^2(|V(K)|^2) \cdot \Pi_{l=1}^{M} F_1(l)$, $P_2 = \cos^2(|V(K)|^2) \cdot \Pi_{l=1}^{N_a-1} F_2(l)$,
  For 16-QAM: $P_1 = (2\cos^3(|V(K)|^2) - \cos(|V(K)|^2))^2 \cdot \Pi_{l=1}^{M} F_1(l)$, $P_2 = (2\cos^3(|V(K)|^2) - \cos(|V(K)|^2))^2 \cdot \Pi_{l=1}^{N_a-1} F_2(l)$.

- Compute a correction factor that compensates for the effect of the discarded coefficients:
  For BPSK: $CF = \arccos(P_1/P_2)$,
  For QPSK: $CF = (\arccos(P_1/P_2))/2 + 1j(\arccos(P_1/P_2))/2$,
  For 16-QAM: The compensation factor can be computed by assuming that the real and imaginary components of it are equal, and solving the cubic equation $2\cos^3(2\Re(CF)) - \cos(2\Re(CF)) = P_1/P_2$. Without elaborating the details, the compensation factor equals $CF = (\arccos(\sqrt{(y+1)/2})) + 1j(\arccos(\sqrt{(y+1)/2}))$ where

$$y = \begin{cases} M_1 + N_1, & D \geq 0 \\ 2 \cdot \sqrt{-A/3} \cdot \frac{\sqrt{B^2/4}}{-A^3/27}, & D < 0 \end{cases}$$

  and $A = -1/2$, $B = -(P_1/P_2)/2$, $D = A^3/27 + B^2/4$, $M_1 = (-B/2 + \sqrt{D})^{1/3}$, and $N_1 = (-B/2 - \sqrt{D})^{1/3}$.

- Compute a correction row that compensates for the effect of the discarded rows of the matrix $\boldsymbol{H}$: $[\hat{\bar{H}}]_{N_a-1,n} = CF/\Re(\sum_{l=0}^{N-1} V^*(K)\lambda(l)), \quad 0 \leq n \leq N-1$.

- Define the matrix $\hat{\bar{\boldsymbol{H}}}$ as follows:
  $\hat{\bar{H}}_{0,n} = H_{K,n}$ and $\hat{\bar{H}}_{m+1,n} = \hat{H}_{m,n}, \quad 0 \leq m \leq Na-1, 0 \leq n \leq N-1$.

- Therefore, $\hat{\boldsymbol{V}} = \hat{\bar{\boldsymbol{H}}}\boldsymbol{\lambda}$, and $\boldsymbol{C}_{\hat{V}} = (\hat{\bar{\boldsymbol{H}}}\mathbf{F}_L)\boldsymbol{C}_h(\hat{\bar{\boldsymbol{H}}}\mathbf{F}_L)^H$.

- Then the BER can be computed from (4.34), and the SER from (4.38) by replacing M by N_a, $C^{-1}_{V(K)V(K)}$ by $C^{-1}_{\hat{V}(0)\hat{V}(0)}$, $\boldsymbol{C}_{\bar{\boldsymbol{V}}V(K)}$ by $\boldsymbol{C}_{\hat{\bar{\boldsymbol{V}}}\hat{V}(0)}$, and $\boldsymbol{C}_{\bar{\boldsymbol{V}}|V(K)}$ by $\boldsymbol{C}_{\hat{\bar{\boldsymbol{V}}}|\hat{V}(0)}$.

4.4 Numerical Results

In Fig. 4.1, the case when the delay spread is larger than the CP length in the absence of both the integer time and frequency offsets, is considered. The performance is shown for different frequency-selective fading channels. It can be seen that when the delay spread is equal to or less than the CP, the performance is similar to the flat fading case ($L = 1$).

Next, in Fig. 4.2, the exact evaluation of the BER is investigated when the time offset is negative (to the left) and with normalized frequency offset equals 0.01. In general, it can be seen that for negative time offsets, the CP alleviates the degradation in the performance. For instance, when the sum of the time offset and the delay spread is less than or equal to

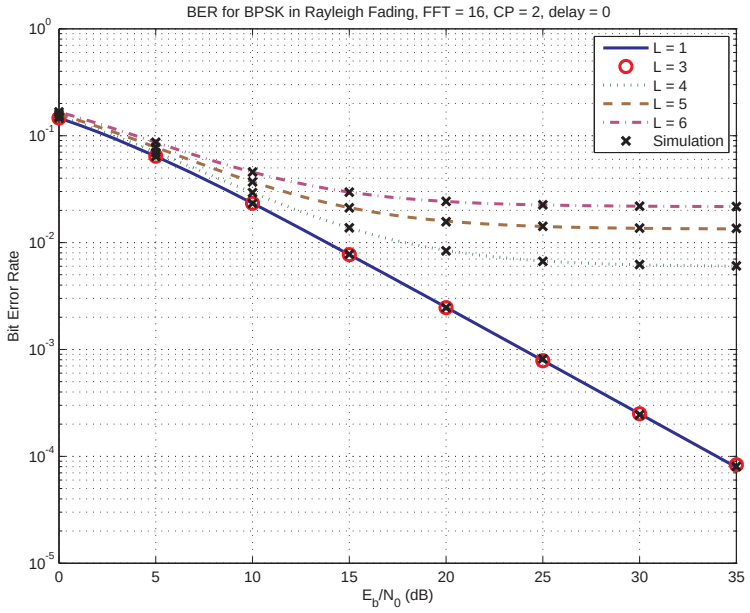

Figure 4.1: Exact BER performance of BPSK OFDM for Rayleigh fading channels when the delay equals zero.

the length of the CP, the performance is similar to the case of flat fading and degradation appears when this sum is larger than the CP length.

Fig. 4.3 shows the approximate SER for QPSK and 16-QAM OFDM when $N = 256$, $N_{CP} = 16$ and $L = 5$ when the time offset equals one sample to the right and the normalized frequency offset equals 0.01. The results are obtained using the proposed method for approximating the performance with a smaller number of coefficients ($N_a = 7$ for QPSK and $N_a = 4$ for 16-QAM). It can be seen that if the sum of the time offset and the delay spread is larger than zero, even if it is less than the CP length, there is performance degradation. It can also be seen that the results from the proposed method approximated very well the simulation results.

Finally, the performance of OFDM systems with CFO only is investigated for QPSK and 16-QAM in Fig. 4.4 and Fig. 4.5, respectively. The matching between the analytical and simulation results can be seen.

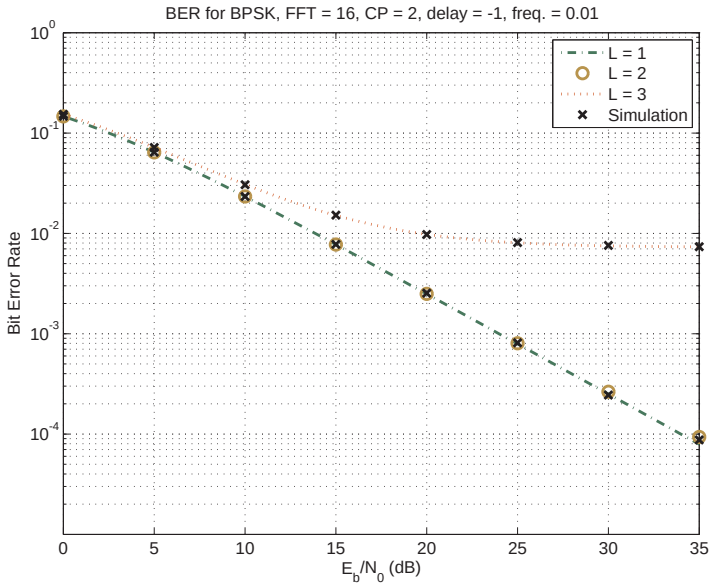

Figure 4.2: Exact BER performance of BPSK OFDM with negative integer time and frequency offsets.

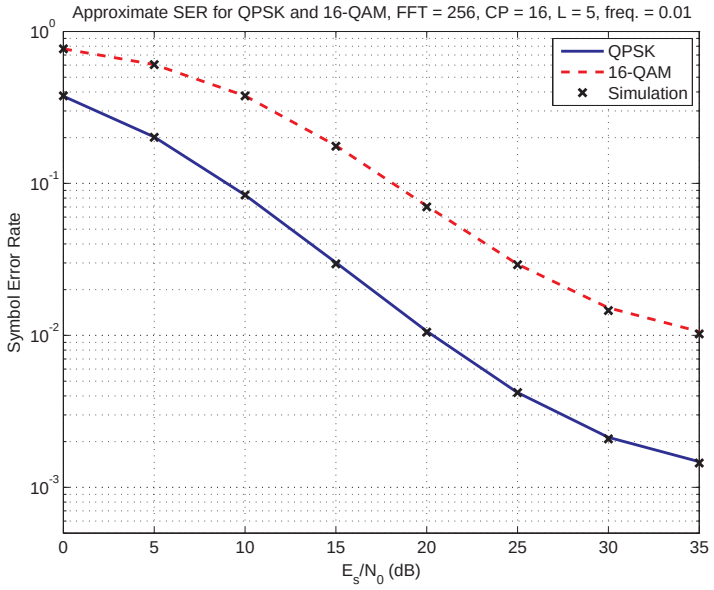

Figure 4.3: Approximate SER Performance of QPSK and 16-QAM OFDM in frequency-selective fading channel when time offset is positive.

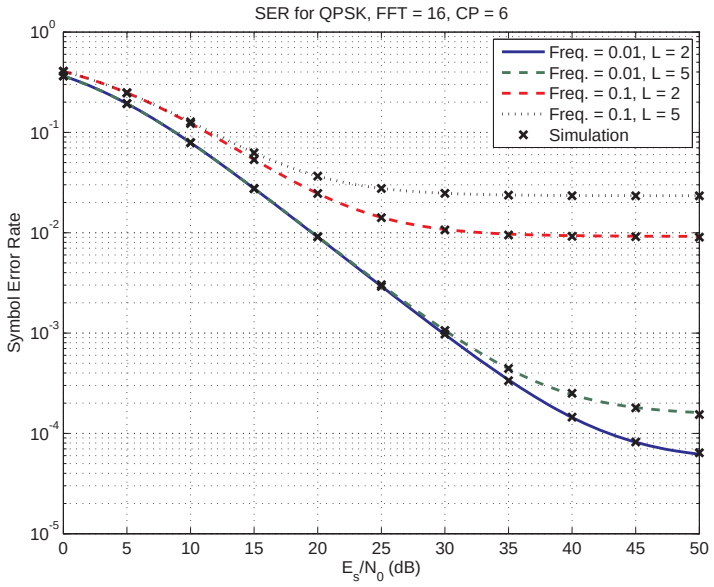

Figure 4.4: Exact SER performance of QPSK OFDM with frequency offset only.

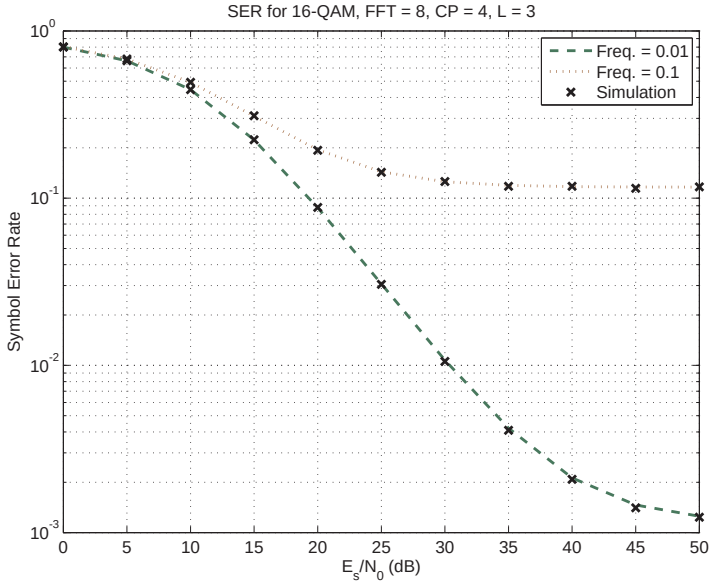

Figure 4.5: Exact SER performance of 16-QAM OFDM with frequency offset only.

Chapter 5

Timing Limitations on CoMP Operation

5.1 System Model

Consider an UL CoMP system with U UEs and B BSs, as shown in Fig. 5.1. The BSs are connected through fast backhaul links that enable the sharing of the baseband signals and CSI. Refereing to the deployment scenarios in Section 2.1.2, this model resembles the second deployment scenario. Joint processing (JP) is employed by the BSs to decode the received signals from UEs which share the same time and frequency resources. We consider a frequency reuse factor of one which is adopted by most of the modern cellular networks and assume that the number of users that share the same time and frequency resources is less than or equal to the number of BSs' antennas that are used to receive these signals. It is also assumed that the UEs in the same cell as the serving BS are synchronized in time with respect to this BS and their transmission powers are adjusted using automatic gain control so the signals received from them at this BS are not affected by path loss, which are practical assumptions.

In case of normal TA adjustment, the signals received at the BSs can be expressed as

$$r_m^b(n) = \sum_u \sum_{l=1}^{L} (h^{b,u}(l) \cdot x_m^u(n - l - \theta^{b,u} - mN_T)) + w_m^b(n), \tag{5.1}$$

where b, u, m are the BS, UE, and symbol indices, respectively. Therefore, $r_m^b(n)$ is the total received signal at BS b on symbol m, and $x_m^u(n)$ is the transmitted signal from UE u

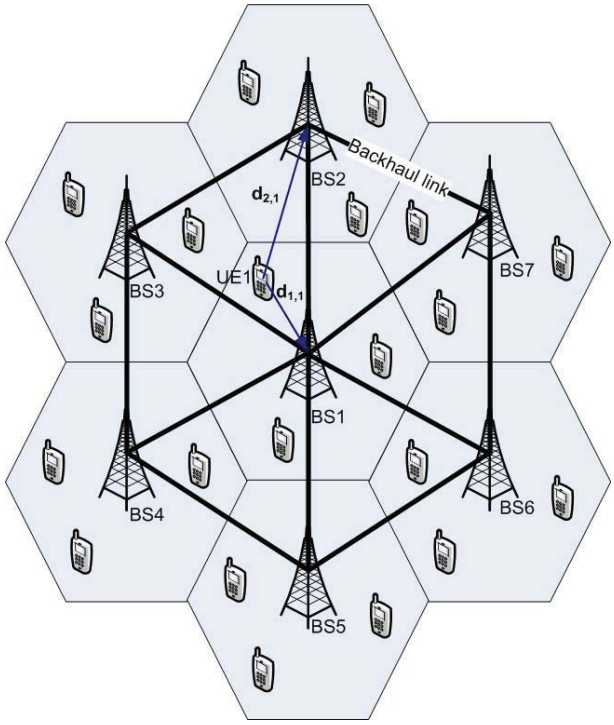

Figure 5.1: CoMP system model.

on symbol m. $h^{b,u}(l)$ is the CIR of the link from UE u to BS b. We assume a quasi-static channel with its taps $h^{b,u}(l), l = 0, 1, 2, ..., L-1$, where $\tau^{b,u}_{\max} = L-1$ is the maximum delay spread. The channel taps are modeled as complex Gaussian random variables with zero mean and variance equal to $(\psi^{b,u} \cdot \sigma^2_{b,u}(l))$, where $\sum_{l=0}^{L-1} \sigma^2_{b,u}(l) = 1$ and $\psi^{b,u}$ is a distance-dependent path loss defined as

$$\psi^{b,u} = \left(\frac{d_{b,u}}{d_0}\right)^{-\upsilon}, \tag{5.2}$$

where d_0 is the reference distance and υ is the path loss exponent. $w^b_m(n)$ is the AWGN at BS b on symbol m with zero mean and variance $\sigma^2_{w,b}$. Finally, $\theta^{b,u}$ is the delay in samples of the signal of user u when it is received at BS b, which is equal to $(d_{b,u} - d_{0,u})/(c \cdot T_s)$ where $d_{0,u}$ is the distance between the UE and its serving BS.

At each BS receiver, and after removing the CP, the received signal in the frequency domain can be expressed as

$$R^b_m(K) = \sum_u \alpha^{b,u} \lambda^{b,u}(K) \cdot X^u_m(K) \cdot e^{-j2\pi K \theta^{b,u}/N} + \sum_u V^{b,u}_m(K) + W^b_m(K), \tag{5.3}$$

where $X_m^u(K)$ and $W_m^b(K)$ are the samples of the DFTs of $x_m^u(n)$ and $w_m^b(n)$, respectively. Also, $\lambda^{b,u}(K)$ is the K-th subcarrier of the channel frequency response $\boldsymbol{\lambda}^{b,u}$ which equals $\boldsymbol{F}_L \boldsymbol{h}^{b,u}$, where $\boldsymbol{h}^{b,u} = (h^{b,u}(0)\ h^{b,u}(1)\ ...\ h^{b,u}(L-1))^T$ and $\boldsymbol{F}_L$ are the first L columns of the unitary FFT matrix given by $F_L(K,n) = \exp\{-j2\pi Kn/N\}, K, n = 0, 1, ..., N-1$. $\alpha^{b,u}$ is an attenuation factor applied to the signal received at BS b from user u if its delay does not satisfy the condition in (2.9) and $V_m^{b,u}(K)$ is an interference term that accounts for the asynchronous interference that occurs in this case. This asynchronous interference is in the form of ICI and IBI in case of AWGN channel. In case of frequency-selective fading channels, the asynchronous interference includes ISI in addition to the ICI and IBI.

In this chapter, two approaches are used to investigate the limitations caused by timing requirements of the JP CoMP. The areas that can be covered by normal CoMP operation and the BSs which are involved in this cooperation are determined. The first approach is geometrical, depending only on the distances between the UEs and the cooperating BSs in the system. The second approach is analytical, where the cooperation areas and the BSs are selected based on an optimization that aims to minimize the average probability of error (APE).

A best-condition scenario is adopted in this analysis to set an upper limit of the areas that can benefit from JP CoMP operation when no compensation scheme is applied to avoid the synchronization problem. We consider only one UE in the central cell, which is decoded by B BSs as shown in Fig. 5.1. In this scenario, there is no multiple user interference (MUI) and only asynchronous interference due to violation of the condition in (2.9) being taken into consideration. Also, the evaluation is carried out under AWGN channel conditions.

5.2 Geometrical Approach

In order for an UE to be covered by a CoMP operation, the condition in (2.9) must be satisfied (i.e., TDOAs from the UE location to the cooperating BSs must satisfy the condition in (2.9)). To start the analysis, consider two BSs that cooperate to decode the signal of a UE that is located exactly at the borders of the cooperation area between them. Then the TDOA of this UE signal at any of the BSs satisfies the following condition (neglecting the maximum delay spread $\tau_{\max}^{m,u}$):

$$(d_{b_2,u} - d_{b_1,u}) = cT_{CP}, \tag{5.4}$$

where $d_{b_1,u}$ and $d_{b_2,u}$ are the distances between user u and the two BSs. By definition, the locus of points satisfying (5.4) is a hyperbola which can be represented by the standard

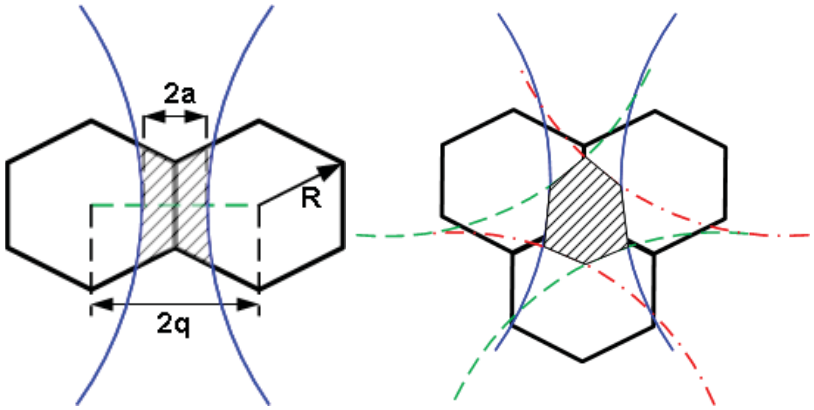

(a) (b)

Figure 5.2: (a) Locus of the points satisfying the synchronization condition; (b) the cooperation area of 3 BSs.

formula in (5.5) [90] and shown in Fig. 5.2(a):

$$\frac{(x-x_0)^2}{a^2} - \frac{(y-y_0)^2}{g^2} = 1,$$
$$q^2 = a^2 + g^2 \tag{5.5}$$

where $2a = cT_{CP}$, $2q$ is the inter-site distance between two BSs which equals $\sqrt{3}R$, and R is the cell radius.

All the users inside the shaded area in Fig. 5.2(a) satisfy the condition in (2.9). In general, for any number of cooperating BSs, the cooperation areas are formed by the intersection of hyperbolas that satisfy the synchronization condition between each pair of neighboring cells. For example, the shaded area in Fig. 5.2(b) is the cooperation area among 3 BSs. The same approach is used in [35] for the formation of clusters while taking the timing requirements into consideration.

In Fig. 5.3, the effect of the cell radius on the cooperation areas for an UE in the central cell is shown. The cells are numbered from 1 to 7, and the numbers inside each bracket indicate the BSs cooperating to serve this area (e.g., (1,2,3) denotes that BSs 1, 2, and 3 cooperate to serve this area). The area which is not covered by cooperation increases with increasing cell radius, and can be approximated by a circle with a radius equal to $\frac{\sqrt{3}}{2}R - a$ and when $R \gg a$ can be approximated with a hexagon with radius equal to $R - a$. Hence, the probability of cooperation P_c can be approximated as follows.

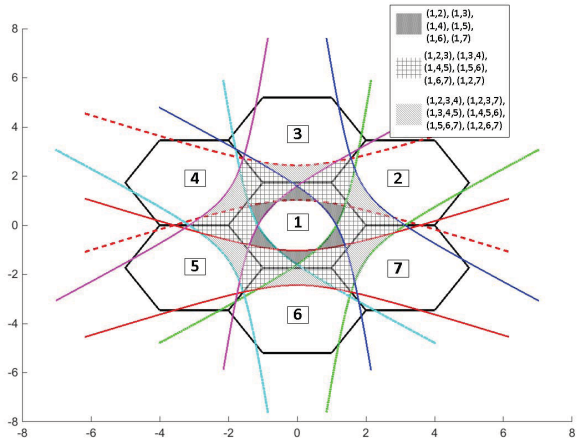

(a)

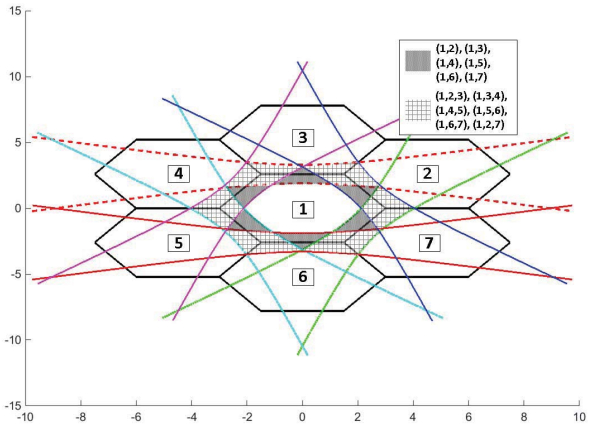

(b)

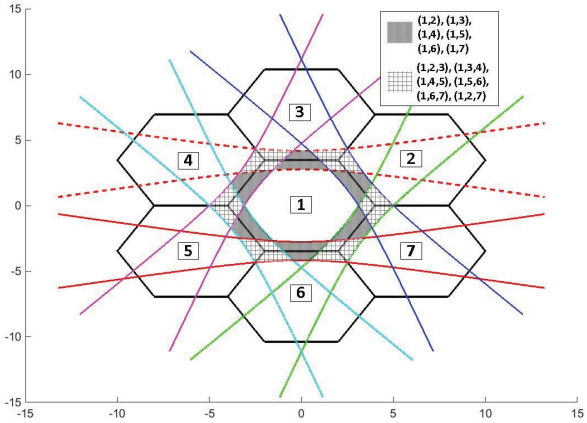

(c)

Figure 5.3: The possible cooperation areas for a user in a central cell with radius: (a) 2 km; (b) 3 km; (c) 4 km. The distance corresponding to the CP length equals 0.7 km.

$$
\begin{aligned}
P_c &= 1 - P_{\text{no coop}} \\
&= 1 - \frac{\text{No cooperation area}}{\text{Cell area}}
\end{aligned} \tag{5.6}
$$

where the no cooperation area equals $\pi * (\frac{\sqrt{3}}{2}R - a)^2$ in case of a circular approximation and equals $\frac{3\sqrt{3}}{2}(R-a)^2$ in case of a hexagonal approximation. It can be seen from (5.6) that the probability of an area to be covered by cooperation decreases with an increase in the radius of the cell. It can be noted that when $R \gg a$, the $P_{\text{no coop}} \approx 1$ which implies that in large-area cells there is no advantage of using cooperation without some compensation scheme for mitigating the asynchronous interference. This conclusion will be verified by numerical results later.

5.3 Analytical Approach

Although the geometrical approach is simple and has low complexity, it does not capture the effect of channel conditions and the receiver type at the BSs. Therefore, an analytical approach that takes into consideration these factors is proposed. In this approach, an optimization problem with objective function of minimizing the average probability of error (APE) is solved. For each point in the cell, the APE is computed for all possible combinations of BSs. The combination with the minimum APE is selected for this point, and this point is considered to be a part of the cooperation area covered by this selection of BSs.

In the following, we evaluate the APE for a point (UE1) in the central cell when its signal is jointly decoded by B BSs under AWGN channel. By employing the result in (3.8) with $\epsilon = 0$ and taking into consideration the path loss, the received signal in frequency domain at any of the BSs can be expressed as

$$
\begin{aligned}
R_m^b(K) = \frac{(N-\theta_{CP}^{b,1})}{N}\sqrt{\psi^{b,1}}X_m(K)e^{\frac{j2\pi K\theta^{b,1}}{N}} + \frac{\sqrt{\psi^{b,1}}}{N}\sum_{q=1}^{N-1}X_m((K-q)_N)e^{\frac{j2\pi\theta^{b,1}(K-q)}{N}}\cdot\Gamma_1^{b,1}(q) \\
+ \frac{\sqrt{\psi^{b,1}}}{N}\sum_{q=0}^{N-1}X_{m-1}((K-q)_N)e^{\frac{j2\pi(\theta^{b,1}+N_{CP})(K-q)}{N}}\cdot\Gamma_2^{b,1}(q) + W_m^b(K),
\end{aligned} \tag{5.7}
$$

where

$$
\Gamma_1^{b,1}(q) = \begin{cases} N-\theta_{CP}^{b,1}, & q=0 \\ \frac{(e^{-j2\pi q\theta_{CP}^{b,1}/N}-1)}{(1-e^{-j2\pi q/N})}, & q\neq 0 \end{cases}, \tag{5.8}
$$

$$\Gamma_2^{b,1}(q) = \begin{cases} \theta_{CP}^{b,1}, & q = 0 \\ \frac{1-e^{-j2\pi q\theta_{CP}^{b,1}/N}}{(1-e^{-j2\pi q/N})}, & q \neq 0 \end{cases}, \tag{5.9}$$

and $\theta_{CP}^{b,1} = \max(-\theta^{b,1} - N_{CP}, 0)$. Note that, since the signal will reach any BS (other than the serving one) late, the time offset $\theta^{m,1}$ is to the left and its value should be substituted by a negative value. The ICI ($C_K^{b,1}(q)$) and IBI ($G_K^{b,1}(q)$) coefficients are given in (5.10).

$$\begin{aligned} C_K^{b,1}(q) &= \frac{\sqrt{\psi^{b,1}}}{N} \cdot e^{\frac{j2\pi\theta^{b,1}(K-q)}{N}} \cdot \Gamma_1^{b,1}(q), \quad 0 \leq q \leq N-1, \\ G_K^{b,1}(q) &= \frac{\sqrt{\psi^{b,1}}}{N} \cdot e^{\frac{j2\pi(\theta^{b,1}+N_{CP})(K-q)}{N}} \cdot \Gamma_2^{b,1}(q), \quad 0 \leq q \leq N-1. \end{aligned} \tag{5.10}$$

In case of an EGC receiver, the total received signal on subcarrier K can be expressed as

$$R_m(K) = \sum_{b=1}^{B} R_m^b(K) e^{\frac{-j2\pi K\theta^{b,1}}{N}}, \tag{5.11}$$

and in case of an MRC receiver, the received signal can be expressed as

$$R_m(K) = \frac{\sum_{b=1}^{B} R_m^b(K) \left(C_K^{b,1}(0)\right)^*}{\sum_{b=1}^{B} |C_K^{b,1}(0)|^2}. \tag{5.12}$$

Employing the results in (3.18), (3.22) and (3.34), the APE can be computed for the different modulation techniques. Note that in the SIMO case σ_W^2 equals $\sum_{b=1}^{B} \sigma_{W,b}^2$ in case of an EGC receiver and in case of an MRC receiver equals $\frac{\sum_{b=1}^{B} \sigma_{W,b}^2 |C_K^{b,1}(0)|^2}{(\sum_{b=1}^{B} |C_K^{b,1}(0)|^2)^2}$. Also, the vector of the concatenated ICI and IBI coefficients can be computed as follows:

$$S_K(l) = \begin{cases} \sum_{b=1}^{B} C_K^{b,1}(l), & 0 \leq l \leq N-1, \\ \sum_{b=1}^{B} G_K^{b,1}(l-N), & N \leq l \leq M. \end{cases} \tag{5.13}$$

In the numerical results section, comparisons between the performance of the two receiver types (EGC and MRC receivers) in addition to comparisons between the geometrical and analytical approaches are demonstrated.

5.4 Numerical Results

To demonstrate the accuracy of the derived closed-form expressions for the probability of error of SIMO OFDM systems with integer time offsets, Fig. 5.4 shows the APE for BPSK

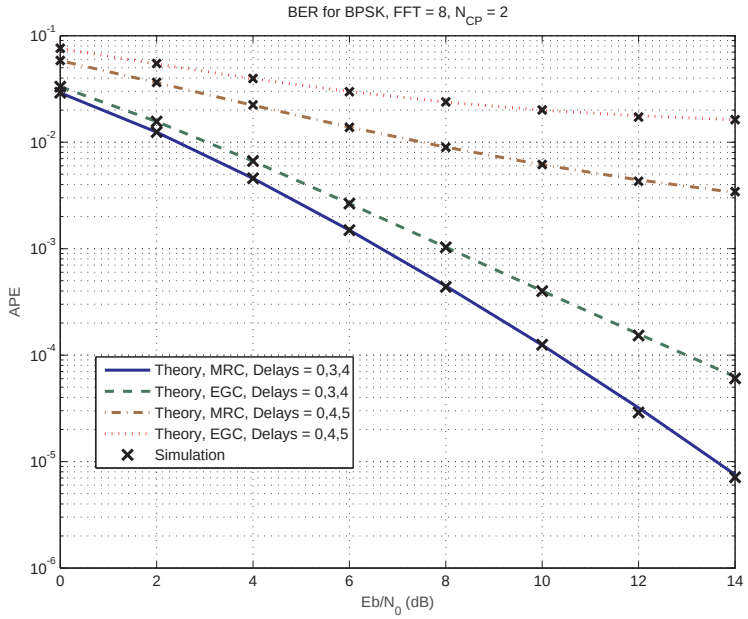

Figure 5.4: Average probability of error for 1×3 SIMO OFDM system in AWGN channel.

1×3 OFDM system with $N = 8$ subcarriers and $N_{CP} = 2$ samples in AWGN channel. The performance is investigated using different set of delays when MRC and EGC receivers are used for decoding the signals. This imitates a scenario where 3 BSs cooperate to decode the signals of one UE. Since the UE is at the same cell as one of the BSs, one of the integer delay values is zero. The other two integer delay values represent the distances between this UE and the other two BSs. In the simulation, we assume that the 3 BSs are connected and the received signals are decoded using a typical 1×3 SIMO receiver. It can be seen that the analytical results agree with the simulation results.

Next, the limitations of the CoMP system due to timing synchronization requirements are investigated. The APE performance of a randomly-located user inside the central cell is investigated, assuming equal noise power at each BS. In this simulation, the location of the user is uniformly distributed across a hexagonal cell. Also, we limited the maximum number of cooperating BSs to 3 in order to avoid extra overhead due to the additional signaling and exchanging of data needed among the BSs through the backhaul. In the analytical approach, the received signal at each BS is converted to the frequency domain by DFT operation; then the total received signals of all the combinations of one, two, and three BSs' signals are computed using both the EGC and MRC receivers. The combination that gives the minimum APE is selected (number of combinations $= \binom{6}{0} + \binom{6}{1} + \binom{6}{2} = 22$

given that the serving BS is chosen in any combination). The combinations are numbered from 1 to 22, wherein 1 denotes the combination that includes BS1 only (no cooperation) and combination 22 includes BSs 1, 6, and 7.

Fig. 5.5 shows the selection of BS combinations for 50 random locations using simulation and the analytical derived expressions. The FFT size of the UL signal is chosen to be 8 subcarriers (for higher FFT sizes, approximate expressions in Section 3.3 can be used). Other parameters are sampling frequency $1/T_s = 0.6$ MHz , cell radius ($R = 3$ km), $N_{CP} = 2$ samples which is equivalent to 1 km distance, path loss exponent ($\upsilon = 3.5$), and $1/\sigma^2_{W,b}$ equals 0 dB at each BS. The performance is investigated for transmission over AWGN channel and again we assume that the BSs are connected so typical SIMO receivers are used. The simulation results are produced by first generating a random location inside the central cell. Based on this location the distances to the BSs and the corresponding delays and path loss attenuation factors are computed. It is worth mentioning that the delay to the serving BS is considered to be zero and the path loss attenuation factor is one because these factors are adjusted through feedback messaging between the UE and the serving BS. The path loss attenuation factors between the UE and the other BSs is normalized with respect to the one with the serving BS. After that, a random signal with the parameters mentioned above is generated and using Monte Carlo simulation with 10000 frames the APE is computed for every combination of BSs (22 combinations) and the one with minimum APE is selected. In the analytical approach, instead of using Monte Carlo simulation, our derived expressions for finding the APE of OFDM SIMO systems are used to find the combination of BSs that has minimum APE.

As it can be seen from Fig. 5.5, while for most of the locations no cooperation is needed when EGC receiver is used, for MRC receiver the opposite is true. This is because in case of decoding using EGC receiver, the degradation due to asynchronous interference exceeds the gain obtained from diversity. On the other hand, since MRC receivers have better performance (in terms of probability of error) when compared to EGC receivers, this makes them able to benefit from diversity even with the existence of asynchronous interference. Also, it can be seen that BSs' combinations selected by the analytical expressions and simulation are similar which shows the accuracy of the analytical approach.

In the geometrical approach, the distances from the UE's location (point) to the BSs in the 6 adjacent cells are computed, and the BSs which satisfy the TDOA condition are considered to be the cooperating BSs for this location. Finally, if all the distances to the adjacent cells do not satisfy the TDOA condition, this leads to the signals of the user in this location being decoded by the serving BS only. Using the same parameters but for 1000 random locations, which are shown in Fig. 5.6, and with $1/\sigma^2_{W,b} = 5$ dB, Table 5.1 shows the probability of cooperation, with both the analytical and geometrical approaches

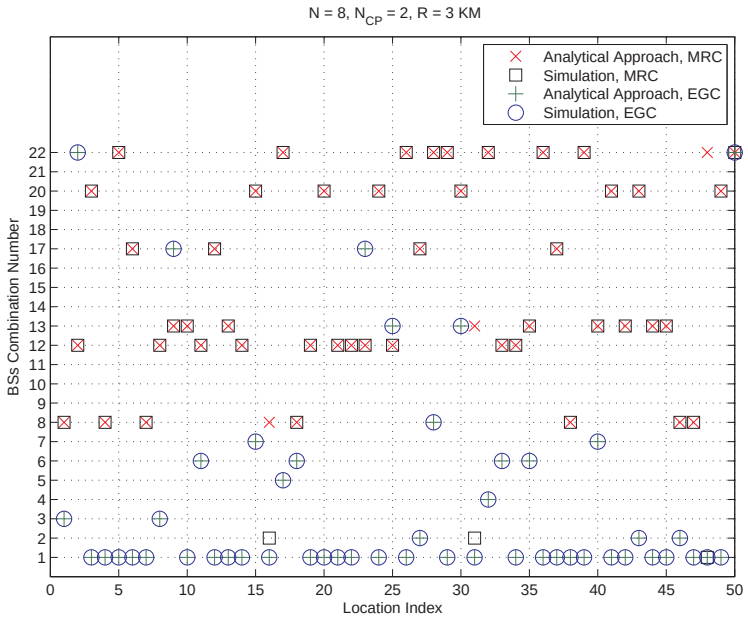

Figure 5.5: Selection of BSs combinations for 50 random locations inside the central cell.

at different cell radii. The geometrical results are obtained using simulation in addition to the approximate expressions in (5.6). Several notes can be inferred from the table as follows. First, in general, increasing the cell radius leads to decreasing the probability of cooperation, as expected. Second, again we can note that compared to the EGC receiver, using an MRC receiver increases significantly the probability of cooperation and hence increases the percentage of area that could benefit from BS cooperation. It can be seen that when R/a is not large, almost all the cell area could benefit from cooperation when MRC receiver is used. On the other hand, when EGC receiver is used, any increase in the cell radius leads to a decrease in the percentage of cooperation areas. Third, the circular approximation is better than the hexagonal one when R/a is not large and vice versa, as expected. Finally, the results obtained using the EGC receiver match the results obtained using the geometrical approach. This confirm our expectation that the main reason for performance degradation when using EGC receiver is due to the asynchronous interference and suggests that EGC receivers should be used only when the TDOA among received signals is less than the CP length (i.e., when there is no asynchronous interference).

Table 5.2 shows the probability of cooperation for different values of noise power at the BSs. The table is generated using the same parameters as before with cell radius equals 3 km. Once more, the matching between the results obtained using the EGC

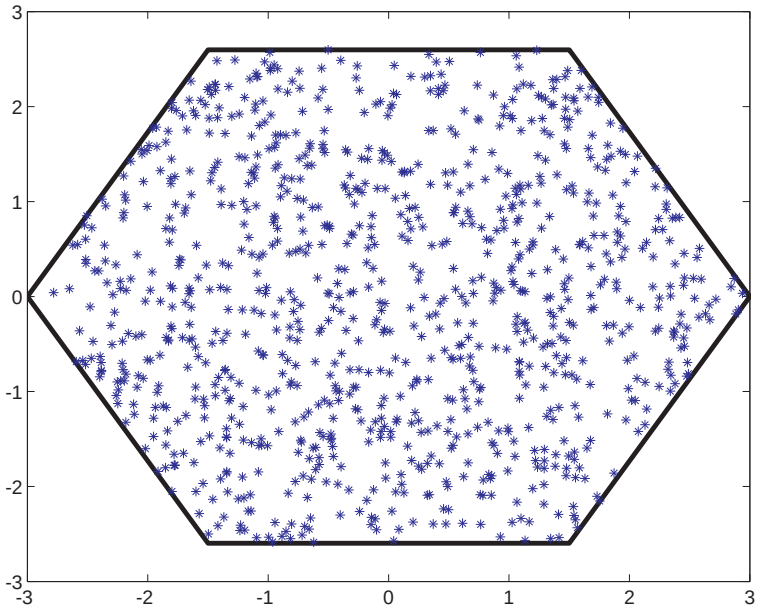

Figure 5.6: Uniform distribution of 1000 random user locations.

Table 5.1: Probability of cooperation at different radii

Radius (km)	5	6	7	8	9	10	20	30	40	50
P_c (analytical, MRC)	1	1	1	1	1	1	0.87	0.48	0.30	0.19
P_c (analytical, EGC)	0.33	0.32	0.28	0.25	0.23	0.21	0.10	0.07	0.05	0.04
P_c (geometrical, simulation)	0.28	0.24	0.21	0.18	0.16	0.14	0.07	0.05	0.04	0.03
P_c (geometrical, circular approx.)	0.29	0.26	0.24	0.22	0.21	0.19	0.14	0.13	0.12	0.11
P_c (geometrical, hexagonal approx.)	0.22	0.18	0.16	0.14	0.12	0.11	0.06	0.03	0.03	0.02

receiver and the geometrical results can be noted. Also, the superior performance of the MRC receiver when compared to the EGC receiver is clear. Finally, the percentage of cooperation is almost zero when the noise power is very small. The reason is that the cooperation could not enhance the performance of the users any more compared to the direct communication with the serving BS, and hence direct communication is preferable in these cases. Fig. 5.7 shows a normalized histogram for the probability of occurrence of the selected BSs combinations using the geometrical approach. As it can be seen, the probability of cooperation is $(1 - 0.579 = 0.421)$ which is similar to the probability of cooperation using the analytical approach for the EGC receiver in the range $1/\sigma^2_{W,b} < 25$ dB. Furthermore, the probability of cooperation using the circular approximation is 0.41 which is close to the one from the geometrical approach as anticipated.

Table 5.2: Probability of cooperation at different values of noise power

$1/\sigma^2_{W,b}$ (dB)	0	5	10	15	20	25	30	35	40
P_c (analytical, MRC)	0.99	0.99	0.99	0.99	0.98	0.64	0	0	0
P_c (analytical, EGC)	0.42	0.42	0.42	0.42	0.42	0.42	0	0	0

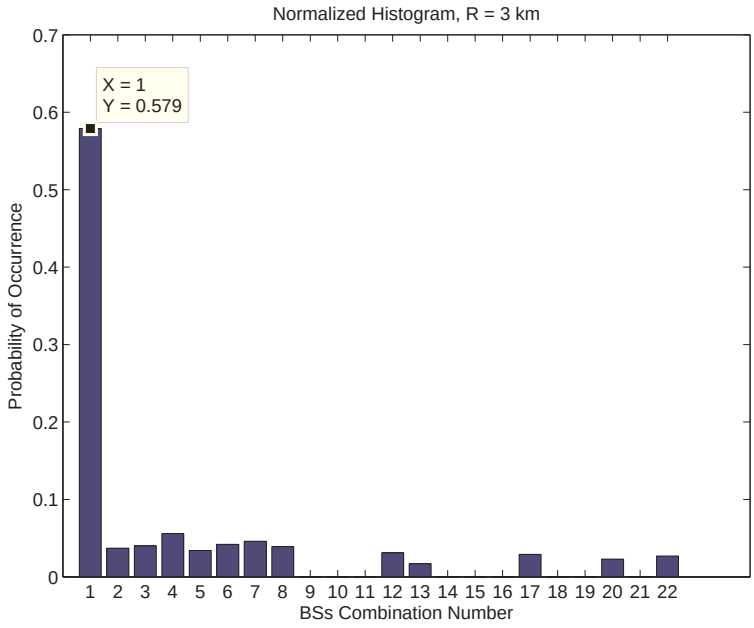

Figure 5.7: Probability of occurrence of the different BSs combinations for 1000 different locations inside the central cell.

Chapter 6

Asynchronous Interference Mitigation

As shown in the previous chapter, the timing requirements restrict the applicability of CoMP to small areas that decrease as the cell radius increases. In this chapter, using the same system parameters as the previous chapter, we propose a method that enables the detection and decoding of the signals in asynchronous UL CoMP systems, with both perfect and imperfect knowledge of delays and CSI.

6.1 Perfect Knowledge of Delays and CSI

Our approach depends on the full characterization of the asynchronous interference in the frequency domain. This characterization is carried on frequency-selective fading channels. In Chapter 4, a suitable model is derived for interference in the case of SISO OFDM systems. A generalization of this model to MIMO systems is given below. Employing the result in (4.22) for SISO OFDM systems and assuming BS b and UE u, the frequency domain of the received signal on subcarrier K at BS b when the time offset is negative (to the left) can be expressed as

$$R_m^b(K) = (\boldsymbol{H}_{\text{des}}^{b,u}\boldsymbol{\lambda}^{b,u})^T \boldsymbol{X}_m^u + (\boldsymbol{H}_{\text{int}}^{b,u}\boldsymbol{\lambda}^{b,u})^T \boldsymbol{X}_{m-1}^u + W_m^b(K), \tag{6.1}$$

where $\boldsymbol{H}_{\text{des}}^{b,u}$ and $\boldsymbol{H}_{\text{int}}^{b,u}$ are the same as $\boldsymbol{H}_{\text{des}}$ and $\boldsymbol{H}_{\text{int}}$ which are defined in (4.23) but with adding the superscripts b, u. Noting that the old symbol $\boldsymbol{X}_{m-1}^u$ is known, since it is already

decoded and assuming perfect knowledge of delays and CSI, the signal in (4.22) can be simplified to

$$R_m^b(K) = (\boldsymbol{a}_K^{b,u})^T \boldsymbol{X}_m^u + b_m^u(K) + W_m^b(K), \tag{6.2}$$

where $\boldsymbol{a}_K^{b,u} = \boldsymbol{H}_{\text{des}}^{b,u}\boldsymbol{\lambda}^{b,u}$ and $b_m^u(K) = (\boldsymbol{H}_{\text{int}}^{b,u}\boldsymbol{\lambda}^{b,u})^T \boldsymbol{X}_{i-1}^u$. $\boldsymbol{\lambda}^{b,u}$ is the channel frequency response of the link between BS b and UE u.

Now, in order to generalize the model to MIMO, let $\boldsymbol{R}_m = [R_m^1(0), R_m^1(1), R_m^1(2), R_m^1(N), R_m^2(0), ...R_m^2(N), ...R_m^M(N)]$ be a vector of all signals received at B BSs on the N subcarriers, $\boldsymbol{X}_m = [(\boldsymbol{X}_m^1)^T(\boldsymbol{X}_m^2)^T...(\boldsymbol{X}_m^U)^T]$ be a vector of all signals transmitted from U UEs on the N subcarriers, $\boldsymbol{b}_m$ be a vector of all IBI/ISI from all users and $\boldsymbol{W}_m$ be a vector of AWGN samples at all the BSs. Then the received signals from all UEs on all subcarriers can be modeled as

$$\boldsymbol{R}_m = \boldsymbol{A}^T \boldsymbol{X}_m + \boldsymbol{b}_m + \boldsymbol{W}_m, \tag{6.3}$$

where $\boldsymbol{A}$ is a matrix consisting of the sub-matrices $\boldsymbol{a}^{b,u}$. For instance, for a CoMP system with 2 BSs and 2 UEs, the system can be modeled as

$$\begin{bmatrix} \boldsymbol{R}_m^1 \\ \boldsymbol{R}_m^2 \end{bmatrix} = \begin{bmatrix} \boldsymbol{a}^{11} & \boldsymbol{a}^{12} \\ \boldsymbol{a}^{21} & \boldsymbol{a}^{22} \end{bmatrix} \begin{bmatrix} \boldsymbol{X}_m^1 \\ \boldsymbol{X}_m^2 \end{bmatrix} + \begin{bmatrix} \boldsymbol{b}_m^1 \\ \boldsymbol{b}_m^2 \end{bmatrix} + \begin{bmatrix} \boldsymbol{W}_m^1 \\ \boldsymbol{W}_m^2 \end{bmatrix} \tag{6.4}$$

Using the MMSE equalizer, and assuming that the noise variance is equal at all the BSs, the transmitted signals can be obtained as follows.

$$\hat{\boldsymbol{X}}_m = [\boldsymbol{A}^{\boldsymbol{H}}\boldsymbol{A} + \sigma_W^2 \boldsymbol{I}]^{-1} \boldsymbol{A}^{\boldsymbol{H}}(\boldsymbol{R}_m - \boldsymbol{b}_m), \tag{6.5}$$

where $\boldsymbol{I}$ denotes the identity matrix and σ_W^2 is the noise power which is, for simplicity, assumed to be equal at all the BSs. Since the estimation of the current symbol $\hat{\boldsymbol{X}}_m$ needs the computation of $\boldsymbol{b}_m$ which depends on the estimated old symbol, this could lead to error propagation in case the old symbol is wrongly decoded. In the numerical results shown later, this effect is taken into consideration.

6.2 Imperfect Knowledge of Delays and CSI

In the previous section, we have provided the analysis assuming perfect knowledge of delays and CSI. In order to study the impact of imperfect knowledge of these parameters on the performance of our detection method, we employ a joint delay and channel estimation

method, similar to the one used in [25] for the UL of an LTE system. In the LTE standard, a preamble called physical random access channel (PRACH) is employed in the UL for the initial uplink time synchronization and initial network access [91]. The preamble consists of a constant amplitude zero autocorrelation sequence, called Zadoff-Chu (ZC). This sequence was first proposed in [92, 93], and it is employed by the LTE and the LTE-A for both UL and DL synchronization tasks [94]. The ZC sequence's ideal correlation properties have led to its widespread use in new wireless standards. The ZC sequence is defined as

$$f(n) = \begin{cases} e^{j\pi r n^2/N_s}, & N_s \text{ is even} \\ e^{j\pi r n(n+1)/N_s}, & N_s \text{ is odd} \end{cases},$$

where N_s is the sequence length and r is the root sequence index which is typically chosen to be relatively prime to N_s. One of the great features of the ZC sequence is that the periodic correlation of a sequence with a cyclically shifted version of itself produces a Kronecker delta function which peaks at the lag instant and zero elsewhere. This feature can be utilized in our system model, by letting the UEs which transmit at the same time and frequency resources use the same ZC sequence (i.e., same root sequence index) but with different cyclic shifts. This achieves orthogonality among the transmitted preambles from different UEs which is needed to avoid cross interference. The second advantage of this feature is that correlating with the base ZC sequence (i.e., the one with zero shift) in each BS leads to estimating all the delays and CIRs of all the UEs received by this BS at once [25]. The number of samples of the cyclic shift N_{CS} is a parameter that needs to be selected carefully. This number should be large enough to accommodate the maximum expected TDOA, plus the maximum expected delay spread $\tau_{\max}^{\exp}$. We choose this number to equal (N_s/U), where U is the number of UEs that use the same sequence.

Given the aforementioned properties of the ZC sequence, the joint delay and channel estimation method can be described as follows. Each UE u from the set that uses the same time and frequency resources sends the same ZC sequence but with different shift $(u-1) * N_{CS}$, where $u = 1, 2, ..., U$. The assignment of N_{CS} to each UE could be through control messages sent from the BSs to the UEs in the downlink. At each cooperating BS b, $b = 1, 2, ..., B$, a periodic correlation between the total received signal and a local copy of the preamble used in this cell (e.g., for BS b the preamble is the same ZC sequence with shift $(b-1) * N_{CS}$) is performed in the frequency domain as follows:

$$y^b(n) = \frac{1}{N_s} \sum_{K=0}^{N_s-1} R^b(K) F_b^*(K) e^{\frac{j2\pi Kn}{N_s}}, \quad 0 \le n \le N_s - 1, \tag{6.6}$$

where $F_b(K)$ is the DFT of the ZC sequence used at BS b, and $y^b(n)$ is the correlation output. Then the magnitude of the correlation output $|y^b(n)|$ is searched for all peaks

above a given threshold that depends on the received SNR multiplied by the mean of the samples of $|y^b(n)|$, $0 \leq n \leq N_s - 1$. For instance, at BS1, the index of the first peak $t^{1,1}$ is the delay of UE1 ($\theta^{1,1}$) and samples of $y^b(n)$ from $t^{1,1}$ to the peak index that has value less than $t^{1,1} + \tau_{\max}^{\exp}$ are considered as the CIR of the channel between UE1 and BS1. The first peak that has index $t^{1,2}$ larger than $t^{11} + \tau_{\max}^{\exp}$ is the first tap of the channel between UE2 and BS1. Samples of $y^b(n)$ from $t^{1,2}$ to the peak index that has value less than $t^{1,2} + \tau_{\max}^{\exp}$ are considered the CIR of the channel between UE2 and BS1. The delay of UE2 equals $t^{1,2} - (u-1) * N_{CS}$ where $u = 2$ for UE2. The same is applied for the remaining UEs received by BS1. The same steps are applied for each BS to estimate all the delays and all the CIRs. For instance, Fig. 6.1 shows a block diagram for the channel and delay estimation at BS1. The algorithm at the BSs can be summarized as follows:

Algorithm 1 Joint Delay and Channel Estimation Algorithm

1: **for** BS index $b = 1$ to B **do**
2: Compute the periodic correlation $y^b(n)$.
3: Search $|y^b(n)|$ for all peaks above a given threshold.
4: **for** UE index $u = 1$ to U **do**
5: $\theta^{b,u} = t^{b,u} - (u-1) * N_{CS}$ where $t^{b,u}$ is the first peak index that is larger than $t^{b,u-1} + \tau_{\max}^{\exp}$ and $t^{b,1}$ is the first peak index.
6: The CIR between UE u and BS b is the samples from $t^{b,u}$ to the peak index that is less than $t^{b,u} + \tau_{\max}^{\exp}$.
7: **end for**
8: **end for**

It is worth mentioning that, although the detection method does not impose any restrictions on the delays, this joint method for delay and channel estimation restricts the delays to be less than $(N_{CS} - \tau_{\max}^{\exp})$.

6.3 Iterative Method for Asynchronous Interference Mitigation

As it can be seen from (6.5), the MMSE receiver needs an inverse operation which would have complexity of the order $O(n^3)$ [95] when solved by direct methods like Gaussian elimination, where $n = B \cdot N$ assuming the number of BSs B equals to the number of users U and N is the number of subcarriers. The system in (6.3), ignoring the AWGN term, can be considered as a system of linear equations which can be solved iteratively. For the

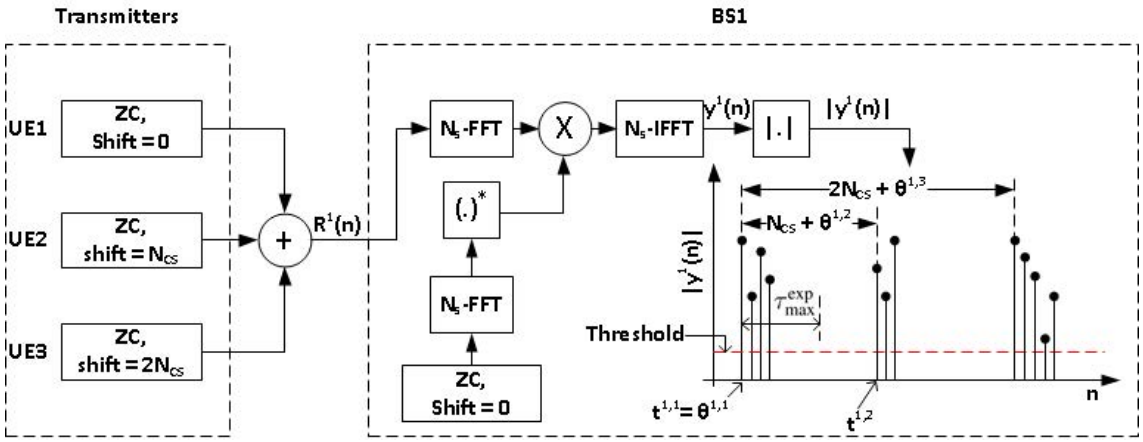

Figure 6.1: Block diagram of the channel and delay estimation at BS1 in a CoMP system of 3 UEs and 3BSs.

simplicity of the analysis, we consider a system like the one in (6.4) with 2 BSs and 2 UEs in AWGN channel. This system, ignoring the AWGN, can be modeled as

$$\begin{bmatrix} \bar{\boldsymbol{R}}^1 \\ \bar{\boldsymbol{R}}^2 \end{bmatrix} = \begin{bmatrix} \boldsymbol{I} & \boldsymbol{C}^{1,2} \\ \boldsymbol{C}^{2,1} & \boldsymbol{I} \end{bmatrix} \begin{bmatrix} \boldsymbol{X}^1 \\ \boldsymbol{X}^2 \end{bmatrix}, \tag{6.7}$$

where we dropped the symbol index m for clarity and $\bar{\boldsymbol{R}}^b = \boldsymbol{R}^b_m - \boldsymbol{b}^u_m$. $\boldsymbol{I}$ is the identity matrix and $\boldsymbol{C}^{b,u}$ is the ICI coefficients matrix with its elements can be inferred from (3.6) and (4.24) as follows:

$$[C_N]^{b,u}_{K,q} = \frac{1}{N}\Gamma_1^{b,u}((K-q)_N)e^{j2\pi\theta^{b,u}q/N}, \quad 0 \leq K, q \leq N-1, \tag{6.8}$$

where

$$\Gamma_1^{b,u}(q) = \begin{cases} N - \theta^{b,u}_{CP}, & q = 0 \\ \frac{(e^{-j2\pi q\theta^{b,u}_{CP}/N} - 1)}{(1-e^{-j2\pi q/N})}, & q \neq 0 \end{cases}. \tag{6.9}$$

Note that $\boldsymbol{C}^{1,1}$ and $\boldsymbol{C}^{2,2}$ in (6.7) are equal to the identity matrix $\boldsymbol{I}$ since users in the same cell as the serving BS are synchronized and hence there is no ICI (i.e., ICI coefficient matrix equal to $\boldsymbol{I}$).

Let us denote the matrix in (6.7) by $\boldsymbol{A}$. It is clear that this matrix is sparse, so iterative methods for sparse matrices [96] can be used to solve this system of linear equations in an

efficient way. Generally, the complexity of these methods is in the order of $O(i \cdot z \cdot n)$ where i is the number of iterations and z is the number of non-zero elements. If the matrix is dense, the order would be $O(i \cdot n^2)$ since in each iteration a matrix-vector multiplication with order $O(n^2)$ is needed. In the following, we demonstrate how one of the basic iterative methods can be employed to solve the system in (6.7). Then and based on the structure of the matrix $\boldsymbol{A}$, we propose further simplifications to reduce the complexity needed to solve this system of linear equations.

Jacobi method is one of the most basic iterative methods to solve systems of linear equations [96]. In this method, $\boldsymbol{A}$ is decomposed into 3 matrices where $\boldsymbol{A} = \boldsymbol{D} - \boldsymbol{E} - \boldsymbol{F}$. $\boldsymbol{D}$ is a diagonal matrix with its diagonal equal to the diagonal of $\boldsymbol{A}$ and $-\boldsymbol{E}$ and $-\boldsymbol{F}$ are the lower and upper triangular matrices, respectively, but with replacing the diagonal elements with zeros. The Jacobi iteration can be expressed as [96]

$$\begin{bmatrix} \boldsymbol{X}^1 \\ \boldsymbol{X}^2 \end{bmatrix}_{k+1} = \boldsymbol{D}^{-1}(\boldsymbol{E} + \boldsymbol{F}) \begin{bmatrix} \boldsymbol{X}^1 \\ \boldsymbol{X}^2 \end{bmatrix}_{k} + \boldsymbol{D}^{-1} \begin{bmatrix} \bar{\boldsymbol{R}}^1 \\ \bar{\boldsymbol{R}}^2 \end{bmatrix}, \tag{6.10}$$

where k is the iteration index. In the following, we provide further simplifications based on the special structure of the matrix $\boldsymbol{A}$.

- The matrix $\boldsymbol{D}$ and its inverse can be removed from the computations since in our system model $\boldsymbol{D}$ is simply the identity matrix $\boldsymbol{I}$. As a result, the iteration can be expressed as

$$\begin{bmatrix} \boldsymbol{X}^1 \\ \boldsymbol{X}^2 \end{bmatrix}_{k+1} = \bar{\boldsymbol{A}} \begin{bmatrix} \boldsymbol{X}^1 \\ \boldsymbol{X}^2 \end{bmatrix}_{k} + \begin{bmatrix} \bar{\boldsymbol{R}}^1 \\ \bar{\boldsymbol{R}}^2 \end{bmatrix}, \tag{6.11}$$

  where

$$\bar{\boldsymbol{A}} = \boldsymbol{E} + \boldsymbol{F} = \begin{bmatrix} \boldsymbol{0}_{N\times N} & -\boldsymbol{C}^{1,2} \\ -\boldsymbol{C}^{2,1} & \boldsymbol{0}_{N\times N} \end{bmatrix}. \tag{6.12}$$

- Due to the zero matrices in $\bar{\boldsymbol{A}}$, the iteration can be simplified to

$$\begin{bmatrix} \boldsymbol{X}^1 \\ \boldsymbol{X}^2 \end{bmatrix}_{k+1} = \begin{bmatrix} -\boldsymbol{C}^{1,2}\boldsymbol{X}^2_k \\ -\boldsymbol{C}^{2,1}\boldsymbol{X}^1_k \end{bmatrix} + \begin{bmatrix} \bar{\boldsymbol{R}}^1 \\ \bar{\boldsymbol{R}}^2 \end{bmatrix}. \tag{6.13}$$

- It can be seen from (6.8) that the matrix $\boldsymbol{C}^{b,u}$ can be decomposed into circulant matrix $\Gamma_1^{b,u}((K-q)_N)$ and a constant vector $e^{j2\pi\theta^{b,u}q/N}$ that does not change with

changing the row number K. Therefore, the matrix-vector multiplication $\boldsymbol{C}^{b,u}\boldsymbol{X}_k^u$ in (6.13) can be computed by FFT [97] as follows:

$$\begin{bmatrix} \boldsymbol{X}^1 \\ \boldsymbol{X}^2 \end{bmatrix}_{k+1} = \begin{bmatrix} -\text{ifft}\left\{\text{fft}(\Gamma_1^{1,2}(-q)_N) \circ \text{fft}(\boldsymbol{X}_k^2 \circ e^{j2\pi\theta^{1,2}q/N})\right\} \\ -\text{ifft}\left\{\text{fft}(\Gamma_1^{2,1}(-q)_N) \circ \text{fft}(\boldsymbol{X}_k^1 \circ e^{j2\pi\theta^{2,1}q/N})\right\} \end{bmatrix} + \begin{bmatrix} \bar{\boldsymbol{R}}^1 \\ \bar{\boldsymbol{R}}^2 \end{bmatrix}, \quad 0 \le q \le N-1. \tag{6.14}$$

- From the properties of the DFT, the Hadamard product $\boldsymbol{X}_k^u \circ e^{j2\pi\theta^{b,u}q/N}$ can be replaced by circular shift as follows:

$$\begin{bmatrix} \boldsymbol{X}^1 \\ \boldsymbol{X}^2 \end{bmatrix}_{k+1} = \begin{bmatrix} -\text{ifft}\left\{\text{fft}(\Gamma_1^{1,2}(-q)_N) \circ \text{fft}(x_k^2(n-\theta^{1,2})_N)\right\} \\ -\text{ifft}\left\{\text{fft}(\Gamma_1^{2,1}(-q)_N) \circ \text{fft}(x_k^1(n-\theta^{2,1})_N)\right\} \end{bmatrix} + \begin{bmatrix} \bar{\boldsymbol{R}}^1 \\ \bar{\boldsymbol{R}}^2 \end{bmatrix}, \quad 0 \le n, q \le N-1, \tag{6.15}$$

  where $x(n)$ is the n-th element of $\text{fft}(\boldsymbol{X})$.

With these simplifications, the complexity of the iterative method is reduced to be in the order of $O(i \cdot n \log n)$ instead of $O(i \cdot n^2)$.

The previous iterative procedure assumes that the matrix in (6.7) has an inverse, but this is not guaranteed. Sometimes the matrix in (6.7) is not invertible since the sub-matrices that form this matrix are not full rank. This is the reason that a zero-forcing equalizer is not a good option for estimating the transmitted signals in (6.4). Moreover, this suggests that for systems with more BSs and UEs or when the channel is frequency-selective, it is better to use a more robust iterative method from the Krylov subspace category [96] with a coefficient matrix equals to $\boldsymbol{A}^{\boldsymbol{H}}\boldsymbol{A} + \sigma_W^2\boldsymbol{I}$ and nonhomogeneous term equals to $\boldsymbol{A}^{\boldsymbol{H}}(\boldsymbol{R}_m - \boldsymbol{b}_m)$. In our numerical results, we have used the quasi-minimal residual (QMR) method which is an iterative method to solve non-Hermitian linear systems [98]. It has been proved that the QMR method is an efficient method for matrices where the identity matrix is dominating [99].

6.4 Numerical Results

The performance of our proposed scheme, to mitigate the asynchronous interference, is investigated in Fig. 6.2 which shows the performance of a CoMP system with 2 BSs and 2 UEs, each with one antenna. The 2 UEs have symmetrical positions with respect to

the BSs and they are using the same time and frequency resources. The FFT size is 128 subcarriers and the CP length is 9 samples. A turbo encoder with a rate of $\frac{1}{2}$ is used and the bits are mapped using the 16-QAM modulation. The performance is evaluated under a frequency-selective fading channel with a uniform power delay profile. The maximum delay spread is 5 samples and the path loss exponent equals 3.5. Finally, the parameters used for the joint channel and delay estimation are as follows. The ZC sequence length is 512 samples and the root sequence index is 25. A cyclic prefix is appended to the ZC sequence, with a length larger than the maximum delay spread (6 samples). The maximum expected delay spread is $\tau_{\max}^{\exp} = 22$ and the threshold values for each SNR which are used to find the peaks of the magnitude of the correlation output are determined by simulations.

It can be observed from Fig. 6.2 that there is an improvement in performance when the 2 BSs cooperate to decode the signals (CoMP, delays = 0), compared to the case in which each BS decodes only the signal of the UE in the same cell and considers the signal from the UE in the other cell as interference (no cooperation, delays = 0). Also, it can be seen that this improvement is lost when the delays are larger than the CP length (CoMP, delays = 25). Finally, the results show that our method retrieves the gains achieved by the CoMP operation, even when the delays are larger than the CP length.

The performance of more general scenarios is shown in Fig. 6.3 where two, three, and four BSs cooperate to decode the signals of UEs. The delay between each UE and BS is uniformly distributed in the closed interval [10,25] samples. Also, the number of channel taps for the link between each UE and BS is uniformly distributed in the closed interval [2,5] taps. Like the previous figure, turbo channel coding with rate $\frac{1}{2}$ and 16-QAM modulation are used. Also, the path loss exponent equals 3.5. The figure shows the case when the CP length is larger than the delay plus the maximum delay spread ($N_{CP} = 32$) and compares it to the case when the system uses the normal length of CP that is used in LTE standard ($N_{CP} = 9$) but with our method used for compensation. First, it can be seen that our method of compensation cancels most of the asynchronous interference and it gives performance close to the case when there is no asynchronous interference. Also, the larger the number of BSs that cooperate to decode the UEs' signals, the better the performance, as can be expected. This is not the case when we employ channel and delay estimation and as it can be seen when the number of BSs is fewer the performance is better. This can be explained by the fact that increasing the number of BSs increases the number of delays and channel links that need to be estimated and hence increases the probability of error due to the accumulation of estimation errors from different links.

Finally, the performance of the iterative methods is shown in Fig. 6.4. For the QMR method, we used the function provided by MATLAB. In both iterative methods, the QMR and the proposed one, the maximum allowable number of iterations is $N = 128$ which is

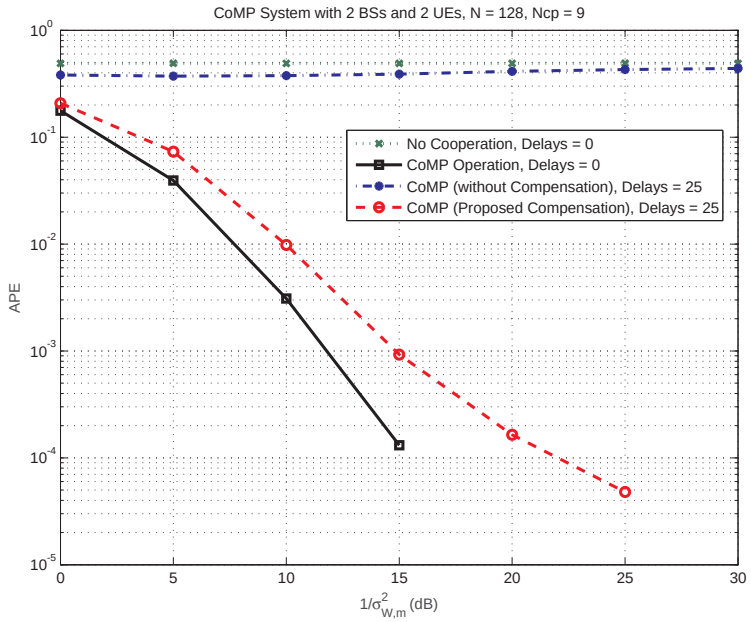

Figure 6.2: APE performance of our proposed mitigation method with channel and delay estimation in symmetrical CoMP scenario.

one half of the matrix size ($2N \times 2N$). Also, the tolerance of both methods was set to 10^{-6}, so whenever the difference between the estimated vector and the previous estimated one is less than or equal 10^{-6}, the algorithm stops and returns the current estimated vector. In our proposed iterative method, if the desired tolerance is not achieved within the maximum allowable number of iterations, an MMSE equalizer is used to estimate the transmitted signals. It can be seen from the figure that the performance of the QMR is similar to the performance of the MMSE equalizer and this is because the inputs to the QMR method are: coefficient matrix equals to $\boldsymbol{A}^{\boldsymbol{H}}\boldsymbol{A} + \sigma_W^2\boldsymbol{I}$ and nonhomogeneous term equals to $\boldsymbol{A}^{\boldsymbol{H}}(\boldsymbol{R}_m - \boldsymbol{b}_m)$. Although our proposed iterative method has slightly worse performance than the QMR method but as indicated in Section 6.3, it is less complex. Also, it is worth mentioning that our proposed method could not find a solution (when $\boldsymbol{A}$ is not invertible) and used an MMSE equalizer in only 2.43% of the total number of simulated frames (10000 frames).

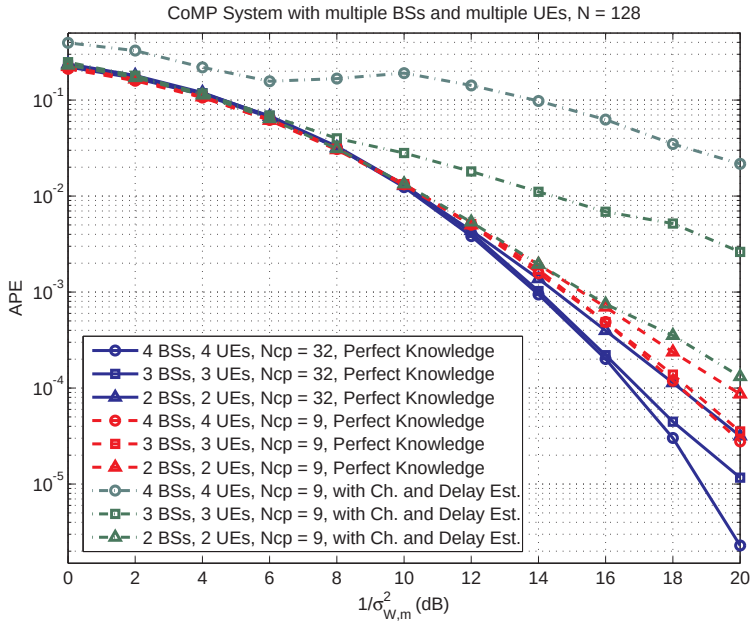

Figure 6.3: APE performance of our proposed mitigation method in general CoMP scenario with multiple BSs and multiple UEs.

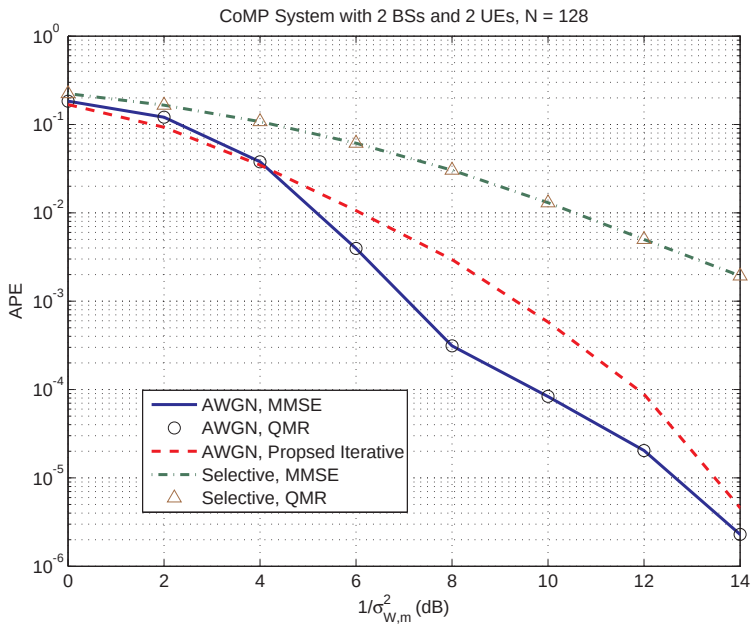

Figure 6.4: APE performance of iterative methods in CoMP scenario with 2 BSs and 2 UEs.

Chapter 7

Concluding Remarks and Future Work

7.1 Concluding Remarks

In the first part of the thesis, we first have provided a complete analysis for the asynchronous interference that results from the frequency and integer time offsets in OFDM systems. In particular, it has been shown that integer time offsets result in three types of interference: ICI, IBI, and ISI. The latter appears in frequency-selective fading channels. Also, our analysis and simulation showed that, due to the existence of the CP, the different subcarriers in OFDM systems with integer time offset do not have the same performance. Closed-form expressions and an approximate method for evaluating the BER/SER of BPSK, QPSK and 16-QAM under both AWGN and Rayleigh fading channels were provided. Simulation results showed that our expressions are accurate and that the approximation works well.

In the second part, we have shown the effect of asynchronous interference on UL CoMP systems when the TDOAs of UEs' signals are larger than the CP length. An upper bound for the percentage of areas that can be covered by cooperation was set using geometrical and analytical approaches. The effect of cell radius on this percentage was demonstrated, and increasing this radius without using compensation algorithms was found to result in the percentage of BS cooperation decreasing. Therefore, a robust method that eliminates asynchronous interference was proposed to solve this problem. An MMSE equalizer, preceded by joint channel and delay estimation, was used to eliminate the MUI in addition to the asynchronous interference. Although an UL system with a single antenna was con-

sidered in both the UEs and the BSs, the proposed method can be applied to any system with any number of antennas given that the number of the received signals is larger than or equal to the number of signals that need to be decoded. Finally, numerical results were provided to show the accuracy of the derived expressions and the good performance of the proposed method.

7.2 Future Work

The main objective of this research was to propose a method for mitigating the asynchronous interference that results from the timing synchronization problem in CoMP systems. In our analysis, we have taken into consideration the effect of imperfect knowledge of delays and CSI. Nevertheless, and as an extension to our work the effect of the following factors should be investigated.

- **Channel Estimation:** In our research, we used a dedicated one OFDM symbol of successive subcarriers (preamble) for channel estimation. The effect of using scattered pilots within the data symbols for channel estimation should be investigated. The advantage of using pilots for channel estimation is to track the changes in channel gains over time. Also, this should reduce the overhead in terms of the resources needed for channel estimation.

- **Carrier Frequency Offset:** The effect of CFO on channel and delay estimation needs to be investigated. Integer CFO could leads to wrong delay estimation results. This will affect the performance of the interference mitigation method.

- **Multiple User Interference:** In our analysis, we considered only the users that employ the same time and frequency resources. The effect of interference caused by other users in the system should be investigated. Also, it is desirable to evaluate the performance of our proposed method by system level simulations where multiple users and BSs use different time and frequency resources.

- **Iterative Procedure:** In our analysis, we have provided customized iterative procedure for the interference mitigation method when the number of BSs and UEs is two and for transmission over AWGN channel. For systems with more BSs and UEs or for transmission over frequency-selective fading channels the standard QMR method is used. A customization for this method based on the signal model of the CoMP system could reduce the complexity more.

Appendix A

In evaluating the integral in (3.26), we need to use the error function and some identities related to it. The error function can be defined as shown in (1).

$$\text{erf}(ax) = \frac{2}{\sqrt{\pi}} \int_0^{ax} e^{-t^2} dt. \tag{1}$$

From the definition, it can be concluded that:

$$\frac{d}{dx}\text{erf}(ax) = \frac{2a}{\sqrt{\pi}} e^{-a^2x^2}, \tag{2}$$

and

$$\int e^{-a^2x^2} dx = \frac{\sqrt{\pi}}{2a}\text{erf}(ax). \tag{3}$$

An important integral that will be used in the evaluation of (3.26) is the one shown in (4).

$$II = \int_0^{\infty} e^{-b^2x^2}\text{erf}(ax)dx. \tag{4}$$

The result of this integral can be found in [100, eq. 4.3.2], but the reported result is valid only when a is positive. In the following, we derive a result that is valid for positive and negative values of a. The proof starts by differentiating (4) with respect to a using (2) as shown in (5).

$$\frac{d}{da}II = \frac{2}{\sqrt{\pi}} \int_0^{\infty} xe^{-a^2x^2} e^{-b^2x^2} dx. \tag{5}$$

Then computing the integral in (5) with respect to x as shown in (6).

$$\frac{d}{da}II = \frac{1}{\sqrt{\pi}} \frac{1}{a^2 + b^2}. \tag{6}$$

Finally, integrating the result in (6) leads to the final result shown in (7).

$$II = II(0) + \int_0^a \frac{1}{\sqrt{\pi}} \frac{1}{x^2 + b^2} dx. = \frac{1}{\sqrt{\pi} b} \arctan(\frac{a}{b}). \tag{7}$$

Now, the integral in (3.26) can be represented by

$$I = \frac{1}{2\pi} \int_0^\infty \frac{r}{\sigma^2} e^{\frac{-r^2}{2\sigma^2}} \int_{x_1 = rA_1}^\infty e^{\frac{-x_1^2}{2}} dx_1 \int_{x_2 = rA_2}^\infty e^{\frac{-x_2^2}{2}} dx_2 \; dr. \tag{8}$$

Using the identity in (3), the integral in (8) can be represented by

$$\begin{aligned} I &= \frac{1}{4} \int_0^\infty \frac{r}{\sigma^2} e^{\frac{-r^2}{2\sigma^2}} [1 - \text{erf}(\frac{rA_1}{\sqrt{2}})][1 - \text{erf}(\frac{rA_2}{\sqrt{2}})] dr \\ &= I_1 - I_2 - I_3 + I_4, \end{aligned} \tag{9}$$

where

$$I_1 = \frac{1}{4} \int_0^\infty \frac{r}{\sigma^2} e^{\frac{-r^2}{2\sigma^2}} dr = \frac{1}{4}, \tag{10}$$

and

$$I_2 = \frac{1}{4} \int_0^\infty \frac{r}{\sigma^2} e^{\frac{-r^2}{2\sigma^2}} \text{erf}(\frac{rA_1}{\sqrt{2}}) dr. \tag{11}$$

Integrating (11) by parts with the aid of (2) and (3) leads to the result

$$I_2 = \frac{1}{4} \frac{A_1 \sigma}{\sqrt{1 + \sigma^2 A_1^2}}. \tag{12}$$

Similarly, but with replacing A_1 with A_2:

$$I_3 = \frac{1}{4} \frac{A_2 \sigma}{\sqrt{1 + \sigma^2 A_2^2}}. \tag{13}$$

Finally, I_4 can be represented as follows:

$$I_4 = \frac{1}{4} \int_0^\infty \frac{r}{\sigma^2} e^{\frac{-r^2}{2\sigma^2}} \text{erf}(\frac{rA_1}{\sqrt{2}}) \text{erf}(\frac{rA_2}{\sqrt{2}}) dr. \tag{14}$$

The integral in (14) can be evaluated as shown in (15) using integration by parts with the aid of the identity in (2).

$$I_4 = \frac{A_1}{2\sqrt{2\pi}} \int_0^\infty e^{-\frac{1+\sigma^2 A_1^2}{2\sigma^2} r^2} \text{erf}(\frac{rA_2}{\sqrt{2}}) dr + \frac{A_2}{2\sqrt{2\pi}} \int_0^\infty e^{-\frac{1+\sigma^2 A_2^2}{2\sigma^2} r^2} \text{erf}(\frac{rA_1}{\sqrt{2}}) dr. \tag{15}$$

The two integrals in the right hand side of (15) are in the form of (4). Therefore, the result of the integral in (15) can be represented as shown in (16).

$$I_4 = \frac{1}{2\pi} \frac{A_1\sigma}{\sqrt{1+\sigma^2 A_1^2}} \text{arctan} \frac{A_2\sigma}{\sqrt{1+\sigma^2 A_1^2}} + \frac{1}{2\pi} \frac{A_2\sigma}{\sqrt{1+\sigma^2 A_2^2}} \text{arctan} \frac{A_1\sigma}{\sqrt{1+\sigma^2 A_2^2}}. \tag{16}$$

Combining the results in (10), (12), (13), and (16) according to (9) leads to the final result shown in (3.27).

References

[1] G. Wunder, P. Jung, M. Kasparick, T. Wild, F. Schaich, Y. Chen, S. ten Brink, I. Gaspar, N. Michailow, A. Festag, *et al.*, "5GNOW: non-orthogonal, asynchronous waveforms for future mobile applications," *IEEE Communications Magazine*, vol. 52, no. 2, pp. 97–105, 2014.

[2] I. F. Akyildiz, D. M. Gutierrez-Estevez, R. Balakrishnan, and E. Chavarria-Reyes, "LTE-Advanced and the evolution to beyond 4G (B4G) systems," *Physical Communication*, vol. 10, pp. 31–60, 2014.

[3] W. Nam, D. Bai, J. Lee, and I. Kang, "Advanced interference management for 5G cellular networks," *IEEE Communications Magazine*, vol. 52, no. 5, pp. 52–60, 2014.

[4] S. Chen and J. Zhao, "The requirements, challenges, and technologies for 5G of terrestrial mobile telecommunication," *IEEE Communications Magazine*, vol. 52, no. 5, pp. 36–43, 2014.

[5] A. Osseiran, F. Boccardi, V. Braun, K. Kusume, P. Marsch, M. Maternia, O. Queseth, M. Schellmann, H. Schotten, H. Taoka, *et al.*, "Scenarios for 5G mobile and wireless communications: the vision of the METIS project," *IEEE Communications Magazine*, vol. 52, no. 5, pp. 26–35, 2014.

[6] J. F. Monserrat, G. Mange, V. Braun, H. Tullberg, G. Zimmermann, and Ö. Bulakci, "METIS research advances towards the 5G mobile and wireless system definition," *EURASIP Journal on Wireless Communications and Networking*, vol. 2015, no. 1, pp. 1–16, 2015.

[7] N. S. Networks, "LTE-Advanced: The advanced LTE toolbox for more efficient delivery of better user experience," *White Paper*, 2011.

[8] D. H. Nguyen and T. Le-Ngoc, *Wireless Coordinated Multicell Systems: Architectures and Precoding Designs*. Springer, 2014.

[9] N. Networks, "LTE release 12 and beyond," *White Paper*, 2014.

[10] 4G Americas, "Understanding 3GPP release 12 standards for HSPA+ and LTE-advanced enhancements." 2015.

[11] D. Gesbert, S. Hanly, H. Huang, S. Shamai Shitz, O. Simeone, and W. Yu, "Multi-cell MIMO cooperative networks: A new look at interference," *IEEE Journal on Selected Areas in Communications*, vol. 28, no. 9, pp. 1380–1408, 2010.

[12] R. Irmer, H. Droste, P. Marsch, M. Grieger, G. Fettweis, S. Brueck, H. Mayer, L. Thiele, and V. Jungnickel, "Coordinated multipoint: Concepts, performance, and field trial results," *IEEE Communications Magazine*, vol. 49, no. 2, pp. 102–111, 2011.

[13] P. Marsch and G. Fettweis, *Coordinated Multi-Point in Mobile Communications: from theory to practice*. Cambridge Univ Pr, 2011.

[14] V. Jungnickel, K. Manolakis, W. Zirwas, B. Panzner, V. Braun, M. Lossow, M. Sternad, T. Svensson, *et al.*, "The role of small cells, coordinated multipoint, and massive MIMO in 5G," *IEEE Communications Magazine*, vol. 52, no. 5, pp. 44–51, 2014.

[15] S. Sun, Q. Gao, Y. Peng, Y. Wang, and L. Song, "Interference management through CoMP in 3GPP LTE-advanced networks," *IEEE Wireless Communications*, vol. 20, no. 1, pp. 59–66, 2013.

[16] M. Ding and H. Luo, "Coordinated multipoint system," in *Multi-point Cooperative Communication Systems: Theory and Applications*, pp. 217–243, Springer, 2013.

[17] Q. Cui, H. Wang, P. Hu, X. Tao, P. Zhang, J. Hamalainen, and L. Xia, "Evolution of limited-feedback CoMP systems from 4G to 5G: CoMP features and limited-feedback approaches," *IEEE Vehicular Technology Magazine*, vol. 9, no. 3, pp. 94–103, 2014.

[18] D. Lee, H. Seo, B. Clerckx, E. Hardouin, D. Mazzarese, S. Nagata, and K. Sayana, "Coordinated multipoint transmission and reception in LTE-advanced: deployment scenarios and operational challenges," *IEEE Communications Magazine*, vol. 50, no. 2, pp. 148–155, 2012.

[19] C. Yang, S. Han, X. Hou, and A. F. Molisch, "How do we design CoMP to achieve its promised potential?," *IEEE Wireless Communications*, vol. 20, no. 1, pp. 67–74, 2013.

[20] X. Tao, X. Xu, and Q. Cui, "An overview of cooperative communications," *IEEE Communications Magazine*, vol. 50, no. 6, pp. 65–71, 2012.

[21] Q. Wang, G. Ren, and J. Wu, "A centralized multiuser detection bsed random access scheme for LTE CoMP transmission," *IEEE Transactions on Vehicular Technology*, 2015. to appear url:ieeexplore.ieee.org/iel7/25/4356907/07031449.pdf?arnumber=7031449.

[22] V. Kotzsch and G. Fettweis, "On synchronization requirements and performance limitations for CoMP systems in large cells," in *Proceedings of International Workshop on Multi-Carrier Systems & Solutions (MC-SS'11)*, pp. 1–5, 2011.

[23] A. M. Hamza and J. W. Mark, "A timing synchronization scheme in coordinated base-stations cooperative communications," in *Proceedings of International Conference on Wireless Communications & Signal Processing (WCSP'12)*, pp. 1–6, 2012.

[24] Huawei, CMCC, RITT, and CATT, "Analysis on uplink/downlink time delay issue for distributed antenna system," *R1-084336, 3GPP TSG RAN WG1 #55*, 2008.

[25] S. Sesia, I. Toufik, and M. Baker, *LTE: the UMTS Long Term Evolution: from theory to practice*. Wiley Online Library, 2009.

[26] L. Zhao, K. Liang, G. Cao, R. Qian, and D. Lopez-Perez, "An enhanced signal-timing-offset compensation algorithm for coordinated multipoint-to-multiuser systems," *IEEE Communications Letters*, vol. 18, no. 6, pp. 983–986, 2014.

[27] R. K. Martin, K. Vanbleu, M. Ding, G. Ysebaert, M. Milosevic, B. L. Evans, M. Moonen, and C. R. Johnson, "Unification and evaluation of equalization structures and design algorithms for discrete multitone modulation systems," *IEEE Transactions on Signal Processing*, vol. 53, no. 10, pp. 3880–3894, 2005.

[28] A. M. Hamza and J. W. Mark, "Closed form SER expressions for QPSK OFDM systems with frequency offset in Rayleigh fading channels," *IEEE Communications Letters*, vol. 18, no. 10, pp. 1687–1690, 2014.

[29] N. C. Beaulieu, "A useful integral for wireless communication theory and its application to rectangular signaling constellation error rates," *IEEE Transactions on Communications*, vol. 54, no. 5, pp. 802–805, 2006.

[30] A. Jeffrey and D. Zwillinger, *Table of integrals, series, and products*. Access Online via Elsevier, 2007.

[31] S. Nadarajah, "A simpler derivation for an integral useful in wireless communication theory," *Signal Processing*, vol. 88, no. 4, pp. 1069–1070, 2008.

[32] A. M. Hamza and J. W. Mark, "Closed-form expressions for the BER/SER of OFDM systems with an integer time offset," *IEEE Transactions on Communications*, vol. 63, pp. 4461–4473, Nov 2015.

[33] P. Dharmawansa, N. Rajatheva, and H. Minn, "An exact error probability analysis of OFDM systems with frequency offset," *IEEE Transactions on Communications*, vol. 57, no. 1, pp. 26–31, 2009.

[34] A. M. Hamza, J. W. Mark, and E. A. Sourour, "Asynchronous interference mitigation in OFDM CoMP systems," submitted to IEEE Transactions on Wireless Communications.

[35] A. M. Hamza and J. W. Mark, "A clustering scheme based on timing requirements in coordinated base-stations cooperative communications," in *Proceedings of IEEE Wireless Communications and Networking Conference (WCNC'13)*, pp. 3764–3769, 2013.

[36] S. Shabdanov, P. Mitran, and C. Rosenberg, "Achieving optimal throughput in cooperative wireless multihop networks with rate adaptation and continuous power control," *IEEE Transactions on Wireless Communications*, vol. 13, no. 7, pp. 3880–3891, 2014.

[37] S. Shabdanov, P. Mitran, and C. Rosenberg, "On cooperative wireless relaying: A joint routing and scheduling flow-based framework," in *Proceedings of IEEE Global Telecommunications Conference (GLOBECOM'12)*, pp. 4641–4646, 2012.

[38] S. Hanly and P. Whiting, "Information-theoretic capacity of multi-receiver networks," *Telecommunication Systems*, vol. 1, no. 1, pp. 1–42, 1993.

[39] A. D. Wyner, "Shannon-theoretic approach to a Gaussian cellular multiple-access channel," *IEEE Transactions on Information Theory*, vol. 40, no. 6, pp. 1713–1727, 1994.

[40] H. Zhang, H. Dai, and Q. Zhou, "Base station cooperation for multiuser MIMO: Joint transmission and BS selection," in *Proceedings of Conference on information sciences and systems*, 2004.

[41] S. Shamai and B. Zaidel, "Enhancing the cellular downlink capacity via co-processing at the transmitting end," in *Proceedings of IEEE Vehicular Technology Conference (VTC'01 Spring)*, vol. 3, pp. 1745–1749, 2001.

[42] A. Goldsmith, S. A. Jafar, N. Jindal, and S. Vishwanath, "Capacity limits of MIMO channels," *IEEE Journal on Selected Areas in Communications*, vol. 21, no. 5, pp. 684–702, 2003.

[43] X. Chu, D. Lopez-Perez, Y. Yang, and F. Gunnarsson, *Heterogeneous Cellular Networks: Theory, Simulation and Deployment*. Cambridge University Press, 2013.

[44] E. Hossain, D. Kim, and V. Bhargava, *Cooperative Cellular Wireless Networks*. Cambridge Univ Pr, 2011.

[45] IEEE P802.16m/D10, "IEEE Draft Amendment Standard for Local and Metropolitan Area Networks - Part 16: Air Interface for Broadband Wireless Access Systems - Advanced Air Interface." 2010.

[46] 4G Americas, "Mobile broadband evolution: 3GPP release 11 & release 12 and beyond," *White Paper*, 2014.

[47] 3GPP TR 36.819 V11.2.0, "Coordinated multi-point operation for LTE physical layer aspects." 2013.

[48] P. Marsch, *Coordinated multi-point under a constrained backhaul and imperfect channel knowledge*. PhD thesis, Technische Universitat Dresden, 2010.

[49] J. Zhang, R. Chen, J. Andrews, A. Ghosh, and R. Heath, "Networked MIMO with clustered linear precoding," *IEEE Transactions on Wireless Communications*, vol. 8, no. 4, pp. 1910–1921, 2009.

[50] A. Papadogiannis, D. Gesbert, and E. Hardouin, "A dynamic clustering approach in wireless networks with multi-cell cooperative processing," in *Proceedings of IEEE International Conference on Communications (ICC'08)*, pp. 4033–4037, 2008.

[51] P. Marsch and G. Fettweis, "A decentralized optimization approach to backhaul-constrained distributed antenna systems," in *Proceedings of IST Mobile and Wireless Communications Summit (IST'07)*, pp. 1–5, 2007.

[52] S. Venkatesan, "Coordinating base stations for greater uplink spectral efficiency in a cellular network," in *Proceedings of IEEE International Symposium on Personal, Indoor and Mobile Radio Communications (PIMRC'07)*, pp. 1–5, 2007.

[53] F. Boccardi and H. Huang, "Limited downlink network coordination in cellular networks," in *Proceedings of IEEE International Symposium on Personal, Indoor and Mobile Radio Communications (PIMRC'07)*, pp. 1–5, 2007.

[54] V. Jungnickel, T. Wirth, M. Schellmann, T. Haustein, and W. Zirwas, "Synchronization of cooperative base stations," in *Proceedings of IEEE International Symposium on Wireless Communication Systems (ISWCS'08)*, pp. 329–334, 2008.

[55] K. Manolakis, C. Oberli, and V. Jungnickel, "Synchronization requirements for OFDM-based cellular networks with coordinated base stations: Preliminary results," in *Proceedings of International OFDM Workshop (InOWo'10)*, 2010.

[56] B. Zarikoff and J. Cavers, "Coordinated multi-cell systems: carrier frequency offset estimation and correction," *IEEE Journal on Selected Areas in Communications*, vol. 28, no. 9, pp. 1490–1501, 2010.

[57] V. Jungnickel, A. Forck, S. Jaeckel, F. Bauermeister, S. Schiffermueller, S. Schubert, S. Wahls, L. Thiele, T. Haustein, W. Kreher, *et al.*, "Field trials using coordinated multi-point transmission in the downlink," *in Proceedings of IEEE International Symposium on Personal, Indoor and Mobile Radio Communications Workshops (PIMRC'10)*, 2010.

[58] M. Konstantinos, A. Adamis, and P. Constantinou, "SNR degradation due to timing and frequency synchronization errors for OFDMA systems with subband carrier allocation," in *Proceedings of European Wireless Conference (EW'08)*, pp. 1–6, 2008.

[59] Y. Mostofi and D. Cox, "Mathematical analysis of the impact of timing synchronization errors on the performance of an OFDM system," *IEEE Transactions on Communications*, vol. 54, no. 2, pp. 226–230, 2006.

[60] M. Morelli, C. Kuo, and M. Pun, "Synchronization techniques for orthogonal frequency division multiple access (OFDMA): A tutorial review," *Proceedings of the IEEE*, vol. 95, no. 7, pp. 1394–1427, 2007.

[61] M. Speth, S. Fechtel, G. Fock, and H. Meyr, "Optimum receiver design for wireless broad-band systems using OFDM. I," *IEEE Transactions on Communications*, vol. 47, no. 11, pp. 1668–1677, 1999.

[62] J. G. Andrews, A. Ghosh, and R. Muhamed, *Fundamentals of WiMAX: understanding broadband wireless networking*. Pearson Education, 2007.

[63] L. Rugini and P. Banelli, "BER of OFDM systems impaired by carrier frequency offset in multipath fading channels," *IEEE Transactions on Wireless Communications*, vol. 4, no. 5, pp. 2279–2288, 2005.

[64] K. Sathananthan and C. Tellambura, "Probability of error calculation of OFDM systems with frequency offset," *IEEE Transactions on Communications*, vol. 49, no. 11, pp. 1884–1888, 2001.

[65] J. L. Seoane, S. K. Wilson, and S. Gelfand, "Analysis of intertone and interblock interference in OFDM when the length of the cyclic prefix is shorter than the length of the impulse response of the channel," in *Proceedings of IEEE Global Telecommunications Conference (GLOBECOM'97)*, pp. 32–36, 1997.

[66] S. Chen and C. Zhu, "ICI and ISI analysis and mitigation for OFDM systems with insufficient cyclic prefix in time-varying channels," *IEEE Transactions on Consumer Electronics*, vol. 50, no. 1, pp. 78–83, 2004.

[67] M. Park, K. Ko, H. Yoo, and D. Hong, "Performance analysis of OFDMA uplink systems with symbol timing misalignment," *IEEE Communications Letters*, vol. 7, no. 8, pp. 376–378, 2003.

[68] K. A. Hamdi, "Precise interference analysis of OFDMA time-asynchronous wireless ad-hoc networks," *IEEE Transactions on Wireless Communications*, vol. 9, no. 1, pp. 134–144, 2010.

[69] J. I. Montojo and L. B. Milstein, "Effects of imperfections on the performance of OFDM systems," *IEEE Transactions on Communications*, vol. 57, no. 7, pp. 2060–2070, 2009.

[70] R. U. Mahesh and A. K. Chaturvedi, "Closed form BER expressions for BPSK OFDM systems with frequency offset," *IEEE Communications Letters*, vol. 14, no. 8, pp. 731–733, 2010.

[71] C. R. Athaudage, "BER sensitivity of OFDM systems to time synchronization error," in *Proceedings of the 8th International Conference on Communication Systems (ICCS'02)*, pp. 42–46, 2002.

[72] Y. Han, H. Huh, and J. V. Krogmeier, "Comparison of error probability for OFDM and SC-FDE," in *Proceedings of the Thirty-Seventh Asilomar Conference on Signals, Systems and Computers (ACSSC'03)*, vol. 1, pp. 497–501, 2003.

[73] Y. Wang, Z. Zhang, and Y. Chen, "BER analysis of BPSK OFDM systems with residual frequency and timing offsets over frequency selective rayleigh fading channels," *Journal of Computational Information Systems*, vol. 8, no. 24, pp. 10349–10357, 2012.

[74] T. Keller and L. Hanzo, "Adaptive multicarrier modulation: a convenient framework for time-frequency processing in wireless communications," *Proceedings of the IEEE*, vol. 88, pp. 611–640, May 2000.

[75] C. Wang and J. Kim, "On the symbol error probability of 16-QAM based OFDM systems impaired by carrier frequency offset," in *Proceeding of the 25th IEEE Canadian Conference on Electrical Computer Engineering (CCECE'12)*, pp. 1–4, 2012.

[76] K. Raghunath, Y. U. Itankar, A. Chockalingam, and R. K. Mallik, "BER analysis of uplink OFDMA in the presence of carrier frequency and timing offsets on rician fading channels," *IEEE Transactions on Vehicular Technology*, vol. 60, no. 9, pp. 4392–4402, 2011.

[77] L. Campbell and P. Wittke, "Mathematical problems in error calculations for interference," *IEEE Transactions on Communications*, vol. 45, pp. 1527–1528, Dec 1997.

[78] P. Zhou, M. Jiang, C. Zhao, and W. Xu, "Error probability of OFDM systems impaired by carrier frequency offset in frequency selective Rayleigh fading channels," in *Proceedings of IEEE International Conference on Communications (ICC'07)*, pp. 1065–1070, June 2007.

[79] M. Baker, "LTE-Advanced physical layer," *IMT-Advanced Evaluation Workshop*, 2009.

[80] T. Koivisto and V. Koivunen, "Impact of time and frequency offsets on cooperative multi-user MIMO-OFDM systems," in *Proceedings of International Symposium on Personal Indoor and Mobile Radio Communications (PIMRC'09)*, pp. 3119–3123, 2009.

[81] V. Kotzsch, C. Jandura, W. Rave, and G. Fettweis, "On timing constraints and OFDM parameter design for cooperating base stations," in *Proceedings of International ITG Workshop on Smart Antennas (WSA'10)*, pp. 169–176, 2010.

[82] H. Zhang, N. B. Mehta, A. F. Molisch, J. Zhang, and H. Dai, "Asynchronous interference mitigation in cooperative base station systems," *IEEE Transactions on Wireless Communications*, vol. 7, no. 1, pp. 155–165, 2008.

[83] S. Iwelski, B. Badic, Z. Bai, R. Balraj, C. Kuo, E. Majeed, T. Scholand, G. Bruck, and P. Jung, "Feedback generation for CoMP transmission in unsynchronized networks with timing offset," *IEEE Communications Letters*, vol. 18, no. 5, pp. 725–728, 2014.

[84] Y. Liu, Y. Li, D. Li, and H. Zhang, "Space-time coding for time and frequency asynchronous CoMP transmissions," in *Proceedings of IEEE Wireless Communications and Networking Conference (WCNC'13)*, pp. 2632–2637, 2013.

[85] C.-C. Cheng, S. Sezginer, H. Sari, and Y. Su, "Linear interference suppression with covariance mismatches in MIMO-OFDM systems," *IEEE Transactions on Wireless Communications*, vol. 13, no. 12, pp. 7086–7097, 2014.

[86] K. Ishihara, Y. Takatori, S. Kubota, and F. Adachi, "Multiuser detection for asynchronous broadband single-carrier transmission systems," *IEEE Transactions on Vehicular Technology*, vol. 58, no. 6, pp. 3066–3071, 2009.

[87] V. Kotzsch, W. Rave, and G. Fettweis, "Interference cancellation and suppression in asynchronous cooperating base station systems," in *Proceedings of International ITG Workshop on Smart Antennas (WSA'12)*, pp. 78–85, 2012.

[88] A. Prudnikov, Y. Brychkov, and O. Marichev, *Integrals and Series, volume 2: Special Functions*. Gordon and Breach Science Publishers, 1986.

[89] S. M. Kay, *Fundamentals of statistical signal processing, volume I: Estimation theory*. Prentice Hall, 1993.

[90] A. Belyaev, "Plane and space curves. Curvature. Curvature-based features," *Max–Planck–Institut für Informatik*, 2004.

[91] X. Yang and A. O. Fapojuwo, "Enhanced preamble detection for PRACH in LTE," in *proceedings of IEEE Wireless Communications and Networking Conference (WCNC'13)*, pp. 3306–3311, 2013.

[92] R. Frank, S. Zadoff, and R. Heimiller, "Phase shift pulse codes with good periodic correlation properties," *IRE Transactions on Information Theory*, vol. 8, no. 6, pp. 381–382, 1962.

[93] D. Chu, "Polyphase codes with good periodic correlation properties," *IEEE Transactions on information theory*, pp. 531–532, 1972.

[94] M. M. U. Gul, S. Lee, and X. Ma, "Robust synchronization for OFDM employing Zadoff-Chu sequence," in *Proceedings of 46th Annual Conference on Information Sciences and Systems (CISS'12)*, pp. 1–6, 2012.

[95] Y. Saad and H. A. Van Der Vorst, "Iterative solution of linear systems in the 20th century," *Journal of Computational and Applied Mathematics*, vol. 123, no. 1, pp. 1–33, 2000.

[96] Y. Saad, *Iterative methods for sparse linear systems*. SIAM, 2003.

[97] G. H. Golub and C. F. Van Loan, *Matrix computations*, vol. 3. JHU Press, 2012.

[98] R. W. Freund and N. M. Nachtigal, "QMR: a quasi-minimal residual method for non-Hermitian linear systems," *Numerische mathematik*, vol. 60, no. 1, pp. 315–339, 1991.

[99] O. Axelsson, M. Neytcheva, and B. Ahmad, "A comparison of iterative methods to solve complex valued linear algebraic systems," *Numerical Algorithms*, vol. 66, no. 4, pp. 811–841, 2014.

[100] E. W. Ng and M. Geller, "A table of integrals of the error functions," *Journal of Research of the National Bureau of Standards B*, vol. 73, pp. 1–20, 1969.